UNIVERSIDAD DE CÓRDOBA
DEPARTAMENTO DE AGRONOMÍA

Programa de doctorado

Biociencias y ciencias agroalimentarias

TESIS DOCTORAL

Estimación de radiación interceptada en cultivos discontinuos mediante teledetección y modelos de transferencia radiativa

Estimation of intercepted radiation on row-structured orchards with remote sensing and radiative transfer models

Autora
Mª Luz Guillén Climent

Dirigida por
Dr. Pablo J. Zarco Tejada
Dr. Francisco J. Villalobos Martín

Tesis financiada por el programa JAEpre-CSIC (cofinanciado por Fondos Sociales Europeos)

Instituto de Agricultura Sostenible-CSIC

Dicen que un rey tenía un anillo con una frase mágica y llena de sabiduría. El mensaje era "Esto también pasará". La reflexión servía tanto a momentos de agotamiento y desesperación, como los de éxito y abundancia. Y aunque de todo hay; escribiendo estas líneas y pensando en tantos momentos vividos durante estos años en mi paso por el IAS, sinceramente sólo tengo palabras de cariño y agradecimiento para todas las personas que de una forma u otra me han acompañado en este camino, y que sin su ayuda, su apoyo y colaboración no habría conseguido finalizar este trabajo.

Me gustaría empezar expresando mi agradecimiento a mis directores Francisco Villalobos por transmitirme su amplio conocimiento sobre la arquitectura de la vegetación y la radiación PAR interceptada, a sus propuestas y mejoras continuas del trabajo. Y a Pablo Zarco, porque para mi es todo un referente. Por su profesionalidad en la labor de director de tesis, de investigador y experto en teledetección, por estar siempre a mi lado para darme palabras de motivación y celebrar todos los pasitos dados hasta conseguir la meta propuesta. Con quién aprendí que el trabajo acompañado de optimismo finalmente da sus frutos, y principalmente porque nunca dejó de confiar en mí. Me siento muy afortunada de haber trabajado contigo.

A todos mis compañer@s y amig@s del IAS, porque tantas horas en el laboratorio y de trabajo de campo en verano (en Córdoba y en Agosto) siempre se hacen más frescas y llevaderas gracias a quienes te rodean: Guada, Vic, Berni, Lola, Jesús, Manoli, David, Alberto sabéis bien de lo que hablo, muchas gracias por todo vuestro apoyo. Rafa y Alberto, muchas gracias por todo vuestro trabajo y la ayuda que me habéis prestado siempre que os he necesitado, esos mosaicos y demás figuras que ahora aparecen tan bonitas en la tesis llevan vuestra firma. A Óscar, Marga, Manuel, Carmen Ruz, Auxi porque formáis parte del equipo de personas importantes gracias al que he disfrutado de mi trabajo en el instituto y además haber tenido la suerte de teneros desde el principio. A Luca, Ignacio, Jose Luis, Rafa por prestarme vuestra ayuda en los comienzos, que siempre anda una un poco perdida. Y a gente que he ido conociendo más recientemente, pero que también han sido un apoyo importante dentro y fuera del IAS, esas cervecitas después del duro día son siempre necesarias Ana, Inian, Omar, Inma, Pato, Eva, Yesi, Cecilia, Clemen. Rocío Hernández, Manolo, Pepa, muchas gracias por vuestro cariño.

Además, parte de esta tesis se llevó a cabo en Swansea, gracias a Peter North por acogerme esos dos meses en su grupo y enseñarme el uso de FLIGHT. Y a Benny, Laura, Johny, Adam, Peter, Nick, Tim por hacerme sentir como en casa desde el principio. También a Frederic Baret y Raúl López por permitirme trabajar y aprender con vosotros en mi estancia en el INRA en Avignon. Alexis, Marie Joe merçi beacoup.

A mis amig@s, que siguen ahí siempre, nos veamos en unas temporadas más, y en otras menos, pero a quienes siempre siento cerca por el cariño y apoyo que me dan Inma, Isa, Fran, Juanlu, Juan Carlos, Sandra, Rafa Calero, Fran Enríquez. Sole, Pili, Teresa, Amelia, gracias por vuestras palabras siempre cariñosas y fortalecedoras.

A quienes han sido una familia para mi, Ana, Isa, Lucía, Mamen, Martin, Peter, Pedrito, porque siempre me han arrancado una sonrisa cuando l@s he necesitad@, porque la convivencia con ell@s en este año ultimo final de tesis me ha aportado muchísimo, gracias de corazón por haber podido contar con vosotr@s.

Y como se suele decir… por último, pero no por ello menos importante, de hecho los más importantes. Porque su amor es incondicional, porque son quienes mejor me conocen, me han dado su mano para levantarme una y otra vez y porque no hay palabras para mostrarles todo mi agradecimiento, orgullo y felicidad por tener una madre, un padre y una hermana tan maravillosos, os dedico este trabajo, porque habéis disfrutado y sufrido parte de él a través mía. Os adoro.

Table of contents

List of figures

List of tables

List of abbreviations

Anth	*Anthocianins*
AOD	*Aerial Optical Depth*
APAR	*Absorbed photosynthetic active radiation*
BFS	*Beam Fraction Sensor*
CR	*Canopy Reflectance*
fAPAR	*Fraction of absorebed active radiation*
fIPAR	*Fraction of intercepted active radiation*
FLIGHT	*Forest Light interaction model*
fr_{shs}	*Fraction of shaded soil*
FWHM	*Full width at half maximum*
I_0	*Incident PAR*
IPAR	*Intercepted photosynthetic active radiation*
L	*Length of central nerve of the leaf*
LADF	*Leaf angle distribution function*
LAI	*Leaf Area Index*
LUT	*Look Up Table*
MCRM	*Markov canopy reflectance model*
NDVI	*Normalized Difference Vegetation Index*
NIR	*Near Infrared*
NPV	*Non photosynthetic vegetation*
ORIM	*Orchard radiation intercepted model*
OSAVI	*Optimized Soil-Adjusted Vegetation Index*
PAR	*Photosynthetic Active Radiation*
PRI	*Photochemical reflectance index*
RAMI	*Radiation Model Intercomparison*
Rc	*PAR flux density reflected by canopy*
rfl_{PARss}	*Reflectance of sunlit soil*
rfl_{PARshs}	*Reflectance of shaded soil*
RMSE	*Root mean squared error*
rRMSE	*relative root mean squared error*
Rs	*PAR flux density reflected by soil*
RTM	*Radiative Transfer Models*
Rx	*Crown radius in x axis*
Ry	*Crown radius in y axis*
SA	*Solar azimuth*
SAIL	*Scattering by Arbitrary Inclined Leaves*

SVI	*Spectral vegetation index*
SZ	*Solar zenith*
Tc	*Transmittance of the canopy*
TCARI	*Transformed Chlorophyll Absorption in Reflectance Index*
TOW	*Take off weight*
UAV	*Unmanned aerial vehicle*
VIS	*Visible region*

Summary

The light energy absorbed by plant leaves drives fundamental physiological processes such as photosynthesis. The absorption of light occurs within the 400-700 nm spectral region, so it is called Photosynthetic Active Radiation, PAR. Thus, the fraction of intercepted PAR is called fIPAR. This thesis studies the estimation of fIPAR with high spatial resolution sensors and radiative transfer models in heterogeneous orchards. The objective is to obtain maps showing the spatial variability of fIPAR within the field. In previous works, relationships between spectral vegetation indices (SVI) and fIPAR have been obtained for homogeneous crops. However, studies were lacking where these kind of relationships were explored for heterogeneous orchards. The heterogeneous orchards are more structurally complex than homogeneous crops; therefore previous relationships might not be applicable in a general way. This work explored these relationships in heterogeneous canopies. This study required extensive field measurements of architecture of the canopy, fIPAR as well as analysis of airborne imagery acquired by a sensor on board and unmaned aerial vehicle (UAV). The different studied canopies were orange, peach, olive and vineyard orchards. Moreover, the use of radiativa transfer models allowed the evaluation of the influence of different parameters such as, solar geometry or row orientation on SVI, fIPAR as well as on the relation between them.

Resumen

La radiación solar interceptada por un cultivo es un factor determinante en numerosos procesos de importancia para la planta como lo es la fotosíntesis. La energía absorbida por el cultivo para llevar a cabo estos procesos es la comprendida en la región del espectro 400 – 700 nm, y se denomina radiación fotosintéticamente activa o de su traducción al inglés radiación PAR. Así, la fracción de radiación PAR interceptada es llamada fIPAR. En este trabajo se aborda la estimación de fIPAR en cultivos discontinuos, como árboles frutales, mediante sensores de alta resolución espacial y modelos de transferencia radiativa. El objetivo es crear mapas de variabilidad espacial de fIPAR útiles para el manejo del cultivo en agricultura de precisión. En trabajos previos se han obtenido índices de vegetación (IV) mediante teledetección demostrando su relación con fIPAR en cultivos homogéneos. Sin embargo no existen muchos trabajos donde se investiguen este tipo relaciones en cultivos heterogéneos, cuya estructura más compleja hace que relaciones obtenidas en estos trabajos anteriores, puedan no ser aplicables de forma general. Para estudiar estas relaciones en este tipo de cubiertas se llevaron a cabo medidas estructurales y de radiación interceptada en fincas de naranjo, melocotón, olivar y viñedo. El procesamiento y análisis de imágenes se llevó a cabo mediante métodos innovadores basados en vehículos aéreos no tripulados (UAVs). Con el fin de evaluar la estimación de radiación interceptada se usaron modelos de transferencia radiativa. Estos modelos permitieron simular distintos escenarios de plantación y estudiar de qué manera parámetros, como la posición del sol, la orientación del cultivo o el tipo de suelo, influyen a la variación de índices de vegetación, fIPAR, y la relación entre ellos.

1. General Introduction

1.1 Introduction

Biomass production and therefore crop yield is directly related to the capacity of plants to convert the intercepted solar radiation in the accumulation of crop mass (Monsi & Saeki, 1953; Monteith, 1969, 1972, 1977). The light energy absorbed by plant leaves drives fundamental physiological processes such as photosynthesis. The absorption of light occurs within the 400-700 nm spectral region, so it is called Photosynthetic Active Radiation, PAR. Absorbed radiation influences plant secondary processes such as plant growth, the vertical structure and crown shape, leaf morphology, and the uptake and emission of trace gases involved in biogeochemical cycles and atmospheric chemistry (Baldocchi & Collineau, 1994; Larcher, 1995).

The first attempts to study the light levels on crops related with physiological process and mass accumulation are dated in the late 1950s, with works of De Wit in (1959), and Loomis and Williams in (1963). It was in 1972 when John Monteith published a paper establishing experimental and theoretical ground for the relationship between accumulated crop dry matter and intercepted solar radiation. Several studies followed, which focused on the estimations of intercepted radiation as related to growth of herbaceous crops (Gallagher & Biscoe, 1978; Gosse et al., 1986; Dalezios et al., 2001) as well as fruit trees (Palmer & Jackson, 1977; Jackson, 1980; Green et al., 2003). The supply of PAR sets a limit to the potential production, which is determined by the incident radiation conditions as well as by the optical and architectural properties of the stand (Ross, 1981). This assumption boosted the research of models to study the response between photosynthetic response of leaves and the distribution of radiation on these

phytoelements. A review of models of radiation attenuation in homogeneous canopies can be found in Myneni et al. (1989). Discontinuous canopies, such as row structured orchards, present not only a more complex architecture, but also exhibit the influence of the background between the rows among other factors. As such, homogeneous canopy models are not directly applicable for this kind of crops. Mariscal et al. (2000) reviewed models suitable for such row structured orchards, and proposed a model to estimate the fraction of intercepted PAR (fIPAR) in olive trees. None or little work has been found on heterogeneous canopies such as the row-structured open-tree canopies; some examples are Friday & Fowness (2001); Annadale et al. (2004); Oyarzun et al. (2007), and recently Casadesus et al. (2011).

In the following sections, the differences regarding the fIPAR estimation on homogeneous and heterogeneous canopies is explained. Examples showing the structure of different crop canopies mentioned above are shown in Figure 1.1.

a) 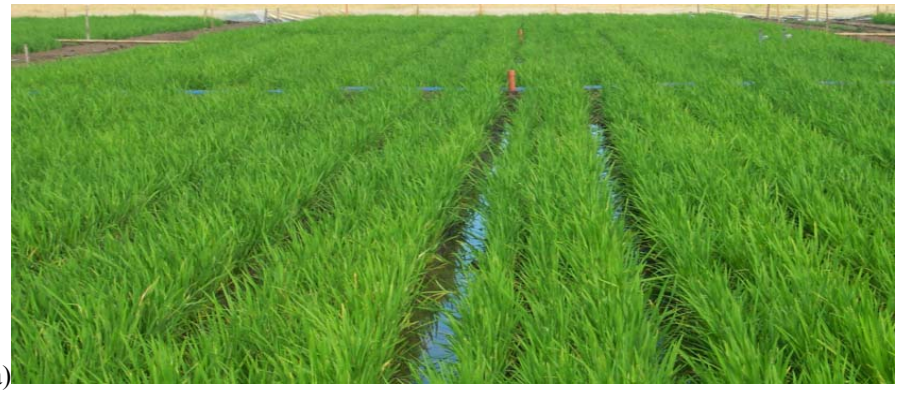

b) 

c) 

Figure 1.1. Architectural differences of herbaceous crops (homogeneous canopy) (a), citrus (b) and vineyards (c) orchards, showing the orchard and row-structured canopies.

Continuous vs row-structured canopies for radiation interception estimation

In continuous canopies, the amount of intercepted radiation is usually estimated based on the leaf area index (LAI) (Asrar et al., 1984, Clevers, 1997). In contrast, orchard systems grow as discontinuous canopies leaving stripes of bare soil between rows, and the leaves are located within an envelope that is distributed in the space according to a planting pattern and row orientation. These issues make a direct measurement of LAI difficult and often not feasible (Villalobos et al., 1995; Mariscal et al., 2000). A revision about devices used in the field to measure fIPAR in orchards may be found in Jackson (1980). An appropriate measurement of fIPAR may be performed using tube solarimeters beneath the canopy compared to the values above the canopy (Szeicz et al., 1964; Monteith, 1981). Alternatively, a pyranometer used for measuring the incident solar radiation and a sensing bar containing photodiodes installed above and below the canopy was the system used in Casadesus et al. (2011). The tube solarimeters measure total solar radiation. Other instruments, ceptometers, are available to measure the PAR region only (Wunsche et al., 1995, Cohen et al., 1997, Huemmrich, 2001). Figure 1.2 shows an example of ceptometer. Another device is based on hemispherical photographs to determine patterns of light penetration (Smart, 1973; Lopez-Lozano, 2009) from analyzing upward-looking fisheye photographs taken beneath the plant canopy. The photographs show the proportion of the sky which can be seen from any given point below the canopy and hence the size and frequency of canopy gaps.

a) 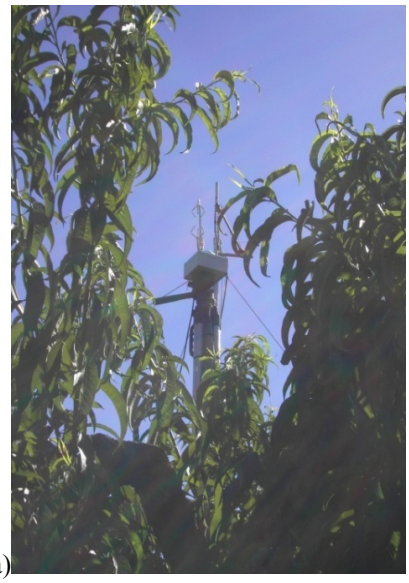 b) 

Figure 1.2. Sensor measuring PAR above the canopy (a), and a portable ceptometer device making spot measurements below the canopy (b).

The amount of solar energy intercepted by the crop is the difference between incident radiation above the canopy and the amount transmitted beneath the canopy. To calculate the solar energy absorbed, the radiation reflected from the ground towards the canopy, and the radiation reflected by the overall crop are also accounted for (Bonhomme, 2000).

The instruments can be used to measure the fraction of intercepted PAR (fIPAR) at canopy level at different locations within a crop field, therefore enabling the assessment of the spatial variability of intercepted radiation. Such within-field spatial variability is more easily measured on small plots for optimal management strategies (Robert et al., 1995; Stafford, 2000). At larger scales the use of such tools is impractical, as measurements of IPAR and/or the related fraction of intercepted PAR (fIPAR) can be time consuming when accounting for both spatial and temporal variability. In this context, remote sensing techniques may be useful, enabling the generation of

maps showing the spatial variability of fIPAR at the field level, at different times of the day as well as during the critical phenological stages of the growing season.

Remote sensing methods to estimate fIPAR

Maps of estimated fIPAR using remote sensing could be helpful for precision crop management (Moran et al., 1997). Several studies have investigated the use of optical vegetation indices obtained from remote sensing methods to estimate fIPAR. In particular, spectral vegetation indices (SVI) based on contrasting canopy reflectance in the red and near-infrared bands have been applied to assess fIPAR from the canopy-level up to the global scale, finding that the Normalized Difference Vegetation Index (NDVI) was the best correlated (Asrar et al., 1992; Myneni & Williams, 1994; North, 2002). Relationships between SVI and fIPAR have been obtained in homogeneous canopies, such as wheat, maize or soybean crops (e.g., Daughtry et al., 1983; Asrar et al., 1984; Moriondo et al., 2007) as well as in forest canopies (e.g., Zhang et al., 2009, Fensholt et al., 2004, Bacour et al., 2006). These studies were focused mainly on randomly distributed canopy elements and closed canopy forest areas, but have not yet been extended to discontinuous canopies, such as row-structured orchards. The relationships between fIPAR and SVI are more complex for discontinuous canopies than for homogeneous canopies because more parameters are required to define their architecture. The sunny and shaded soil proportions between rows contributes greatly to the canopy reflectance, and determined by row orientation, row structure, crop dimensions, viewing direction, and sun position Zhao et al., (2010). Huete (1989), Choudhury (1987) or Huemmrich & Goward (1997) have assessed the sensitivity of these fIPAR-

SVI relationships to changes in canopy architecture, the optical properties of the canopy elements and the background.

These relationships are too often considered as unique and constant (Bégué, 1993). In fact, studies such as Bacour et al. (2006) or Zhang et al. (2009) that worked with satellite images of coarse resolution cannot be applicable in a general way, since they present strong limitations due to the spatial resolution. High spatial resolution allows to separate pure crown from pure soil as well as sunny and shaded scene components. This separation is needed to study the influence of all these factors in the canopy reflectance, SVI calculated from the canopy reflectance, and on the measured fIPAR. In this sense, appropriate modeling strategies are required to simulate the row structure to account for the effects of canopy structure, dimensions, row orientation and soil and shadow effects on the canopy reflectance. Different types of canopy reflectance models are explained below.

Canopy reflectance models

The canopy radiation regime depends largely on canopy configuration, as well as solar incident radiation and the optical properties of vegetation and background (Goel, 1988). The link between canopy properties and sensor-measured radiation becomes more complex when we move from homogeneous to heterogeneous canopies. The mathematical and physical sophistication of the techniques used to understand these interactions have increased considerably. Canopy reflectance (CR) models can be classified into different categories depending upon the assumptions and theory used in its formulation:

(i) Turbid medium: the vegetation canopy is assumed to be a planar horizontally medium. The architecture of the canopy is defined by LAI and leaf angle distribution function (LADF), and no geometrical effects other than the leaf inclinations are considered. The Scattering by Arbitrarily Inclined Leaves (SAIL model) (Verhoef, 1984) is an example of turbid medium model widely used. These kinds of models are typically suitable for dense vegetation canopies. The emphasis is on one-dimensional, plane-parallel formulation, but three-dimensional cases and heterogeneous canopies are outlined.

(ii) Geometrical optical: the canopy here is designed with elements with known dimensions and shape, placed and distributed in different configurations. Geometric models are used primarily in non-dense canopies. Most of these models and their applications have been evaluated in the review of Chen et al. (2000).

(iii) Hybrid models: when the vegetation canopy does not totally fit into any of previous category, hybrid CR models better represent the canopy by combination of elements of both. Geometric shapes are taken into account; therefore the canopy is designed by elements with known size, relative positions and distances. Thus, these models include the row effects. Some example of this kind of CR models are Markov canopy reflectance model with addition of row effects (rowMCRM) used in Zarco-Tejada et al. (2005), and Meggio et al. (2008). It is assumed that the vegetation canopy along rows is formed by periodic rectangular prisms of plant material, with bare soil in between prisms. However, these row models stemmed from the classical theory of radiation transfer in turbid media.

(iv) Computer simulation models: these models simulate positions and orientation of the elements forming the vegetation in a very realistic way. The most common is to use Monte Carlo method to follow the trajectory of the photon. The trajectory is followed from its origin to its absorption or reflection and detection by the sensor. North (1996) calculated forest directional reflectance using the Monte Carlo radiative transfer theory, in the model FLIGHT. They are typically suitable for complex simulations for canopy radiation regimes as horizontally heterogeneous or discontinuous canopies such as row crops, or orchards with isolated tree crowns.

Therefore, the choice of approach to simulate the canopy must be considered carefully, bearing in mind the objectives of the study and the output variables (Louarn et al., 2008). It is also important to consider that the quality of remotely sensed fIPAR products requires ensuring a proper verification of the physically based radiative transfer model (RTM) that contribute to the retrieval of algorithms used to estimate these products (Widlowski, 2010). Real imagery and field data measurements are needed for a good validation of the models. To work with real imagery and to acquire good quality of imagery face several steps: calibration of the imagery, correction of the atmospheric effects, geometrically calibrate/orthorectify the imagery, as well as work conducted in the field to measure the structural parameters, such as dimensions, height, LAI and LADF. Modeling methods once validated will demonstrate the feasibility of parameter retrieval using model inversion or scaling up methods. In the different chapters of this thesis, these processes are discussed and methodologies to create maps showing the spatial variability of fIPAR for different row structured orchards is explained.

Mapping fIPAR variability from remote sensing imagery

The studies of light interception provide a scientific basis for the practical management of canopies. For homogeneous crops, optical remote sensing can provide information about fIPAR during growing season (Clevers, 1997). However, while methods for estimate fIPAR in homogeneous canopies are relatively mature, further research is needed for a robust estimation of fIPAR in open canopies, to understand the effect of row orientation, soil background or viewing geometry on remote sensing indices and canopy reflectance to estimate instantaneous fIPAR. This research deals with the understanding of the relationships between spectral vegetation indexes and fIPAR, and mapping the spatial variability of fIPAR in heterogeneous crop using remote sensing techniques together with modelling strategies. Field data measurements were collected in citrus, peach, olive and vineyard orchards to characterize different types of discontinuous row structured orchards. Peach and citrus orchards were selected to study row structured trees with overlapped crowns. The olive orchard is presented as isolated trees with a planting pattern of 7 m x 6 m and vineyards as a wall structure (3 m x 1.5 m). High spatial resolution airborne imagery (15-cm pixel size) and fIPAR measurements were acquired at different locations and sun geometries, obtaining a wide data base of spatial and temporal variability of fIPAR and canopy reflectance. The study areas were simulated with the RTMs to check their feasibility for modelling this kind of canopies. Different modelling approaches were used and compared in this thesis. For peach and orange orchards, the 3-D Forest Light interaction model, FLIGHT, (North, 1996), based on the Monte Carlo ray tracing theory was used. FLIGHT has as outputs canopy reflectance and fIPAR. For olive orchards, FLIGHT was used to simulate canopy reflectance and was coupled with a model to

simulate fIPAR in olive orchards, Orchard Radiation Intercepted Model ORIM, developed by Mariscal et al. (2000). In the case of vineyards, simulations of canopy reflectance were carried out with FLIGHT and compared with two hybrid models, the *Markov-Chain Canopy Reflectance Model* (MCRM) and the *Scattering by Arbitrary Inclined Leaves* (SAIL) model, both modified to simulate the row crop structure (rowMCRM and rowSAIL, respectively).

1.2. Objectives and outline of the thesis

The general objectives of this thesis are:

i) To study the relationships between SVI and fIPAR in row-structured orchards.

ii) To understand the effects of architectural and leaf optical parameters on the relationship previously defined, using RT models.

iii) To study alternative methodologies to estimate fIPAR from high spatial resolution imagery obtained from sensors on board unmanned platforms. The high spatial resolution allows the discrimination of the different component of the image.

iv) Mapping the spatial variability of instantaneous fIPAR in this kind of complex canopies, assessing the errors obtained for each crop and methodology used.

To achieve these objectives, the following tasks were conducted:

- Validation of RT models to simulate the studied crop canopies using field measurements

- Study area selection comprising a wide range of optical and structural properties, to enable a study of spatial variation of canopy reflectance and fIPAR

- Measurements of canopy reflectance and fIPAR to study the diurnal changes as a function of the architecture and row orientation.

The thesis is presented as chapters, each one dealing with the objectives previously described and focused on the different crops studied.

Chapter 2 describes the use of remote sensing data coupled with RT modelling approaches to estimate fIPAR in citrus and peach orchards using visible (VIS) and near infrared (NIR) bands, as well as to assess the effects of sun angle, row orientation, canopy architecture and background on the canopy reflectance and SVI used to estimate fIPAR.

Chapter 3 follows the same scheme for an olive orchard; this canopy is presented as individual crowns in contrast to the overlapped crowns in citrus and peach orchards.

Chapter 4 deals with vineyard canopies. A wide database which includes a range in row orientation, percentage of vegetation cover, and background was used to validate RT models in vineyards. The canopy reflectance was simulated using hybrid models and a more complex approach based on the Monte Carlo ray tracing method. Model simulations with both approaches were compared against 15-cm resolution imagery acquired with a multispectral sensor and 10-nm full width at half maximum (FWHM) bandset.

Chapter 5 focused on the estimation of fIPAR in vineyards using the high spatial resolution to separate areal fractions and pure reflectance from the different component of the image (vegetation, shaded and sunlit soil). This analysis was compared with a medium spatial resolution analysis. The SVI vs fIPAR relationships in vineyards using FLIGHT were applied for aggregated pixels.

References

Annandale, J. G., Jovanovic, N. Z., Campbell, G. S., Du Sautoy, N. & Lobit, P. (2004). Two-dimensional solar radiation interception model for hedgerow fruit trees. Agricultural and Forest Meteorology, 121, Issues 3-4, 207-225

Asrar, G., Fuchs, M., Kanemasu, E.T. & Hatfield, J.L.(1984). Estimating absorbed Photosynthetically active radiation and leaf area index from spectral reflectance in wheat. Agronomy Journal, 76, 300-306.

Asrar, G., Myneni, R.B. & Choudbhury, B.J. (1992). Spatial Heterogeneity in Vegetation Canopies and Remote Sensing of Absorbed Photosynthetically Active Radiation: A Modelling Study. Remote Sensing of Environment, 41, 85-103.

Bacour, C., Baret, F., Béal, D., Weiss, M. & Pavageau, K. (2006). Neural network estimation of LAI, fAPAR, fCover and LAIxC_{ab}, from top of canopy MERIS reflectance data:Principles and validation. Remote Sensing of Environment, 105, 313-325.

Baldocchi D. & Collineau S. (1994). The physical nature of solar light in heterogeneous canopies: spatial and temporal attributes. Exploitation of Environmental Heterogeneity by Plants. Academic Press, pp 21-71

Bégué, A. (1993). Leaf Area Index, Intercepted Photosynthetically Active Radiation, and Spectral Vegetation Indices: A Sensitivity Analysis for Regular-Clumped Canopies. Remote Sensing of Environment, 46, 45-59.

Bonhomme, F. (2000). Beware of comparing RUE values calculated from PAR vs solar radiation or absorbed vs intercepted radiation. Field crops research, 68, 3, 247-252.

Casadesus, J., Mata, M., Marsal J. & Girona, J. (2011). Automated irrigation of Apple tres based on measurements of light interception by the canopy. Biosystems engineering 108, 220-226.

Chen, J.M., Li, X., Nilson, T. & Strahler, A. (2000). Recent advances in geometrical optical modelling and its applications. Remote Sensing reviews, 18, 2-4.

Choudhury, B.J. (1987). Relationships between vegetation indices, radiation absorption, and net photosynthesis evaluated by a sensitivity analysis, Remote Sensing of Environment, 22, 209-233.

Clevers, J.G.P.W. (1997). A Simplified Approach for Yield Prediction of Sugar Beet Based on Optical Remote Sensing Data. Remote sensing of environment 61, 222-228.

Cohen, S., Rao, R. S., & Cohen, Y. (1997). Canopy transmittance inversion using a line quantum probe for a row crop. Agricultural and Forest Meteorology, 86, 225-234.

Dalezios, N. R., Domenikiotis, C., Loukas, A., Tzortzios S.T. & Kalaitzidis, C., (2001). Cotton yield estimation based on NOAA/AVHRR produced NDVI. Phys. Chem. Earth (B) 26(3), 247-251.

Daughtry, C.S.T., Gallo, K.P., & Bauer, M.E. (1983). Spectral estimates of solar radiation by corn canopies, Agronomy Journal, 75, 527-531.

De Wit, C.T. (1959). Potential photosynthesis of crop surfaces. Netherlands. The Journal of Agricultural Science, 7, 141-149.

Fensholt, R., Snadholt, I. & Rasmussen, M.S. (2004). Evaluation of MODIS LAI, fAPAR and the relation between fAPAR and NDVI in a semi-arid environment using in situ measurements. Remote Sensing of Environment, 91, 490-507.

Friday, J.B. & Fowness, J.H. (2001). A simulation model for hedgerow light interception and growth. Agricultural and Forest Meteorology, 108, 1, 29-43.

Gallagher, J.N. & P.V. Biscoe. (1978). Radiation absorption, growth and yield of cereals. Journal Agricultural Science Cambridge. 91:47-60.

Green, S., McNaughton, K., Wünsche, J.N. & Clothier, B. (2003). Modeling Light Interception and Transpiration of Apple Tree Canopies. Agronomy Journal, 95, 1380-1387.

Goel, N.S. (1988). Models of vegetation canopy reflectance and their use in estimation of biophysical parameters from reflectance data. Remote Sensing Reviews, vol. 4, issue 1. Harwood Academis Publishers, New York, London.

Gosse, G., C.Varlet-Grancher, R.Bonhomme, M.Chartier, J.M.Allirand and G.Lemaire. (1986). Production maximale de matiere seche et rayonnement solaire intercepté par un couvert vegetal. Agronomie 6:47-56.

Huemmrich, K.F. & Goward, S.N., (1997). Vegetation canopy PAR Absorptance and NDVI: An Assessment for Ten Species with SAIL model. Remote Sensing of Environment, 61, 254-269.

Huemmrich, K.F. (2001). The GeoSail model: a simple addition to the SAIL model to describe discontinuous canopy reflectance. Remote Sensing of Environment, 75, 423- 431.

Huete, A.R., Jackson, R.D. & Post, D.F. (1985). Spectral Response of a Plant Canopy with Different Soil Backgrounds. Remote Sensing of Environment, 17, 37-53.

Huete, A.R. (1989). Soil influences in remotely sensed vegetation canopy-spectra. Theory-Applications of Optical Remote Sensing (G.Asrar, Ed.), New York, Willey, 107-141.

Jackson, J.E. (1980). Light Interception and Utilization by Orchard Systems. Horticultural Reviews, 2, 208-267.

Larcher, W. (1995) Physiological Plant Ecology,3rd edn. Springer Verlag, Berlin.

Loomis, R.S. & Williams, W.A. (1963). Maximum crop productivity: An estimate. Crop Science 3, 67-72.

López-Lozano, R., Baret, F., García de Cortázar-Atauri, I., Bertrand, N. and Casterad, M.A. (2009). Optical geometric configuration and algorithms for LAI indirect estimates under row canopies: The case of vineyards. Agricultural and Forest Meteorology, 149, pp. 1307-1316.

Louarn, G., Dauzat, J., Lecoeur, J. & Lebon, E. (2008). Influence of trellis system and shoot positioning on light interception and distribution in two grapevine cultivars with different architectures: an original approach based on 3D canopy modeling. Australian Society of Viticulture and Oenology Inc., 14, 143-152.

Mariscal, M.J., Orgaz, F. & Villalobos, F.J. (2000). Modelling and measurement of radiation interception by olive canopies. Agricultural and Forest Meteorology, 100 (183-197).

Meggio, F., Zarco-Tejada, P.J., Miller, J.R., Martín, P., González, M.R., and Berjón, A. (2008). Row orientation and viewing geometry effects on row-structured vine crops for chlorophyll content estimation. Canadian Journal of Remote Sensing, Vol. 34, No. 3, pp. 220-234.

Moriondo, M., Maselli, F.& Bindi, M. (2007). A simple model of regional wheat yield based on NDVI data. European Journal of Agronomy, 26, 266–274.

Myneni, R.B., Ross, J. & Asrar, G., (1989). A review on the theory of photon transport in leaf canopies. Agric. For. Meteorol. 45, 1–153.

Myneni, R.B. & Williams, D.L. (1994). On the Relationships between FAPAR and NDVI. Remote Sensing of Environment, 49, 200-211.

Monteith, J.L. (1969). Light interception and radiative exchange in crops stands. Physiological aspect of crop yield. American Society of Agronomy, Madison, Wisc, 89-111.

Monteith, J.L., (1972). Solar radiation and productivity in tropical ecosystems. Journal of Applied Ecology. 9, 747-766.

Monteith, J.L. (1977). Climate and the efficiency of crop production in Britain. Philos. Trans. R.Soc. London B 281, 277-294.

Monteith, J.L. (1981). Does light limit crop production. C.B. Johnson (Ed.), Physiological Process Limiting Plant Productivity, Butterworths, London, pp. 23-38.

Monsi, M., & Saeki, T. (1953). Uber den Liechfaktor in den Pflanzengesellschaften und seine Bedeutung für die Stoffproduktion (*On the factor light in plant communities and its importance for matter production*). Japanese Journal of Botany. 14:22-52.

Moran, M.S., Inoue, Y. and Barnes, E.M. (1997). Opportunities and Limitations for Image-based Remote Sensing in Precision Crop Management. Remote Sensing of Environment, 61, 319-346.

Moriondo, M., Maselli, F.& Bindi, M. (2007). A simple model of regional wheat yield based on NDVI data. European Journal of Agronomy, 26, 266–274.

North, P.R.J. (1996). Three-Dimensional Forest Light Interaction Model Using a Monte Carlo Method. IEEE Transaction on Geoscience and Remote Sensing, 34, (4), 946-956.

North. P.R.J. (2002). Estimation of f_{APAR}, LAI, and vegetation fractional cover from ATSR-2 imagery. Remote Sensing of Environment, 80, 114-121.

Oyarzun, R.A., Stöckle,C.O. & Whiting, M.D. (2007). A simple approach to modeling radiation interception by fruit-tree orchards Agricultural and Forest Meteorology, 142, 1, 12-24

Palmer, J.W. & Jackson, J.E., (1977). Seasonal light interception and canopy development in hedgerow and bed system apple orchards. Journal of Applied Ecology, 14, 2, 539-549.

Robert, P. C., Rust, R. H. and Larson, W. E. (1995). Site-Specific Management for Agricultural Systems. Madison, Wis.: American Society of Agronomy, Crop Science Society of America, and Soil Science Society of America.

Smart, R.E., (1973). Sunlight interception by vineyards. Amer. J. ENol. Viticult., 24, 4, 141-147.

Stafford, J.V. (2000) Implementing Precision Agriculture in the 21st Century. J. agric. Engng Res, 76, 267-275.

Szeicz, G., Monteith, J.L. and Dos Santos, J.M. (1964) Tube solarimeters to measure radiation among plants. J. Appl. Ecol 1, 169-174.

Robert, P.C., Bust, R.H., & Larson, W.E. (1995). Site Specific Management for Agricultural Systems. American Society of Agronomy, Madison, WI.

Ross, J., (1981). The Radiation Regime and Architecture of Plant Stands. W. Junk, The Hague.

Verhoef, W. (1984). Light scattering by leaf layers with application to canopy reflectance modeling : The SAIL model. Remote Sensing of Environment 16:125-141.

Villalobos, F.J., Orgaz, F. & Mateos, L. (1995). Non-destructive measurement of leaf area in olive (Olea europaea L.) trees using a gap inversion method. Agricultural and Forest Meteorology, 73, 29-42.

Widlowski, J.L. (2010) On the bias of instantaneous FAPAR estimates in open-canopy forests. Agricultural and Forest Meteorology 150, 1501-1522.

Wunsche, J. N., Lakso, A. N., & Robinson, T. L. (1995). Comparison of four methods for estimating total light interception by apple trees of varying forms. HortScience, 30, 272-276.

Zarco-Tejada, P.J., Berjón, A., López-Lozano, R., Miller, J.R., Martín, P., Cachorro, V., González, M.R. & Frutos, A. (2005), Assessing Vineyard Condition with Hyperspectral Indices: Leaf & Canopy Reflectance Simulation in a Row-Structured Discontinuous Canopy. Remote Sensing of Environment, 99, 271-287.

Zhang, Q., Middleton, E.M., Margolis, H.A., Drolet, G.G., Barr, A.A. & Black, T.A. (2009). Can a satellite-derived estimate of the fraction of PAR absorbed by chlorophyll ($FAPAR_{chl}$) improve predictions of light-use efficiency and ecosystem photosynthesis for a boreal aspen forest? Remote Sensing of Environment, 113, 880-888.

Zhao, F., Gu, X., Verhoef, W., Wang, Q., Yu, T., Liu, Q., Huang, H., Qin, W., Chen, L. & Zhao, H. (2010). A spectral directional reflectance model of row crops. Remote Sensing of Environment, 114, 265-285.

2. Mapping radiation interception in peach and citrus orchards using a 3D simulation and high resolution airborne imagery.

Chapter 2

Mapping radiation interception in row-structured orchards using a 3D simulation and high resolution airborne imagery. The case of peach and citrus orchards.

Abstract

This study was conducted to model the fraction of intercepted photosynthetically active radiation (fIPAR) in heterogeneous row-structured orchards, and to develop methodologies for accurate mapping of the instantaneous fIPAR at field scale using remote sensing imagery. The generation of high-resolution maps delineating the spatial variation of the radiation interception is critical for precision agriculture purposes such as adjusting management actions and harvesting in homogeneous within-field areas. *Scaling-up* and model inversion methods were investigated to estimate fIPAR using the 3-D radiative transfer model FLIGHT. The model was tested against airborne and field measurements of canopy reflectance and fIPAR acquired on two commercial peach and citrus orchards, where study plots showing a gradient in the canopy structure were selected. High-resolution airborne multi-spectral imagery was acquired at 10 nm bandwidth and 15 cm spatial resolution using a miniaturized multi-spectral camera on board an unmanned aerial vehicle (UAV). In addition, simulations of the land surface bidirectional reflectance were conducted to understand the relationships between canopy architecture and fIPAR. Input parameters used for the canopy model, such as the leaf and soil optical properties, canopy architecture, and sun geometry were studied in order to assess the effect of these inputs on canopy reflectance, vegetation indices and fIPAR. The 3D canopy model approach used to simulate the discontinuous row-tree canopies yielded spectral RMSE values below 0.03 (visible region) and below 0.05 (NIR) when compared against airborne canopy reflectance imagery acquired over the sites under study. The FLIGHT model assessment conducted for fIPAR estimation against field measurements yielded RMSE values below 0.08. The simulations conducted suggested the usefulness of these modeling methods in heterogeneous row-structured orchards, and the high sensitivity of the *Normalized Difference Vegetation Index* (NDVI) and fIPAR to background, row orientation, percentage cover and sun geometry. Mapping fIPAR from high-resolution airborne imagery through *scaling-up* and model inversion methods conducted with the 3D model yielded RMSE

error values below 0.09 for the *scaling-up* approach, and below 0.10 for the model inversion conducted with a *look-up table* (LUT). The generation of intercepted radiation maps in row-structured tree orchards is demonstrated to be feasible using a miniaturized multi-spectral camera on board UAV platforms for precision agriculture purposes.

Keywords: fIPAR, NDVI, airborne imagery, row-structured tree canopies, radiative transfer model, *scaling-up*, model inversion.

2.1. Introduction

Intercepted photosynthetically active radiation (IPAR) by a crop canopy is the main factor determining dry matter production under non-limiting water and nutrients supply conditions (Gallagher & Biscoe, 1978 and Hunt, 1994). The influence of radiation levels on crop photosynthesis and biomass accumulation was proposed in the late 1950s by work developed by De Wit (1959) and Loomis & Williams (1963), which showed a close link between the amount of radiation received by a crop and its growth. It was Monteith (1972) who first distinguished the crop function in absorbing and transforming the intercepted solar energy into biomass. Further studies investigated the relationships between the incident solar radiation and the limiting factors determining the light interception in crop canopies, showing that leaf area index (LAI) is the dominant factor in the case of continuous canopies (e.g., Lang et al., 1985). Fruit tree orchards, however, are grown as discontinuous canopies, and the amount of PAR intercepted depends primarily on the orchard architecture, which varies with planting system, tree spacing, tree shape, tree height, alley width, row orientation as well as LAI (Jackson, 1980 and Robinson & Lakso, 1991). Examining within-field variability to optimize crop yield and production has been a target of precision agriculture in the early 80s. In this context, maps of fIPAR variability, crop yield or crop nutrient, derived from image-based remote sensing techniques, have been presented as potential benefits for precision crop management (Moran et al., 1997).

Several previous studies investigated the feasibility of estimating the fraction of intercepted photosynthetically active radiation (fIPAR) and absorbed (fAPAR) using methods based on optical remote sensing. Measurements of IPAR and/or the related fraction of intercepted PAR (fIPAR) can be time consuming because of the need to sample for spatial and temporal variability. In this context, remote sensing techniques are useful enabling the assessment of large areas. Spectral vegetation indices (SVI) based on contrasting canopy reflectance in the red and near-infrared bands were applied to assess fIPAR and fAPAR at canopy-level scales, finding that the Normalized Difference Vegetation Index (NDVI) was the best correlated (Asrar et al., 1992; North, 2002). Empirical and modeled relationships between SVI and fIPAR were obtained in homogeneous canopies, such as wheat, maize or soybean crops (e.g., Daughtry et al., 1983; Hall et al., 1992 and Moriondo et al., 2007) and forest canopies (e.g., Myneni & Williams, 1994; Huemmrich, 2001 and Zhang et al., 2009). Later, the sensitivity of these relationships between SVI and the fraction of PAR, absorbed or intercepted, was investigated using 3D models of radiative transfer in plant canopies. Work developed by Huete (1989), Choudhury (1987) and Huemmrich & Goward (1997) showed the sensitivity of these relationships with the canopy architecture, the optical properties of the canopy elements and the background. However, these studies were focused on randomly distributed canopy elements and closed canopy forestry areas. Only a limited number of studies have focused on heterogeneous canopies such as the row-structured open-tree canopies, therefore the application of such random-distribution scenarios on these relationships may not be valid. The effects due to the row orientation, soil background and the viewing geometry on remote sensing vegetation indices and canopy reflectance used

to estimate instantaneous fIPAR need appropriate modeling strategies. In particular, radiative transfer models that aim at deriving the amount and distribution of fIPAR by the crop canopy were reviewed by Mariscal et al. (2000) who developed a model to simulate fIPAR in non-homogeneous olive canopies. Later, the 3-D Forest Light Interaction Model (FLIGHT) (North, 1996) was used to estimate fAPAR in forest canopies (North, 2002; Prieto-Blanco et al., 2009), and model simulations showed the need for accounting for the row structure in orchard canopies (Kempeneers et al., 2008). While methods for modeling and estimating fIPAR in homogenous vegetation are relatively mature, further research is needed for a robust estimate of fIPAR in open canopies, in particular where the architecture of oriented row planting violates the common modeling assumption of angular invariance with respect to solar azimuth. In this research work, a dedicated remote sensing study aiming at assessing the estimation of radiation interception from high-resolution imagery was conducted using an unmanned aerial vehicle. The quality of remotely sensed fIPAR and fAPAR products requires ensuring a proper verification of the physically-based radiative transfer models that contribute to the retrieval of algorithms used to estimate these products (Pinty et al., 2002). Therefore, 3D radiative transfer models that allow the simulation of local radiation measurements in complex canopy architectures under realistic illumination and sampling conditions are needed (Widlowski, 2010). Thus, the objectives of this study were: (i) to use remote sensing data coupled with 3D modeling approaches (forward and inverse) to estimate fIPAR in heterogeneous row-tree canopies using visible (VIS) and near-infrared (NIR) bands acquired from a miniaturized multi-spectral camera on board an UAV platform in the context of precision agriculture; and (ii) to assess the effects of the sun angle, row orientation, canopy

architecture and background on the canopy reflectance and NDVI used to estimate fIPAR in discontinuous row-tree crop canopies.

2.2. Materials and Methods

2.2.1. Study area description and field data collection

The ground truth data and airborne imagery required for this study were acquired in 2007 and 2008 in a commercial peach (90-ha) and a citrus (80-ha) orchard located in southern Spain, Cordoba (37º 48'N, 4º 48'W) and Seville (37º 20'N, 5º 50'W), respectively. The area has a Mediterranean climate with approximately 600 mm average annual rainfall, mostly concentrated in the Autumn-Spring period.

The study in the *Prunus persica* (L.) Batsch orchard was conducted in nectarine (cv. Sweet Lady) and peach (cv. Babygold 8) plantations. The nectarine and peach trees were planted in 1990 at 6 m x 3.3 m (500 tree ha^{-1}) and in 1993 at 5 m x 3.3 m (600 tree ha^{-1}), respectively, on a deep alluvial soil of loam to clay-loam texture, with rows oriented in the north-south direction. Eight plots were selected from the peach orchard with trees covering a range of LAI from 2 to 4.2, tree height between 2.2 to 4 m, and horizontal crown diameters of 1.4 to 3.5 m. The study in the citrus orchard was conducted in sweet-orange (*Citrus sinensis* L. Osb cv. Navelina) and clementine-mandarin (*C. clementina* Hort. ex Tan. Cv. Orornules) plantations. The orange and mandarin trees were planted in 1997 at 7 m x 3 m (476 tree ha^{-1}) on a sandy-loam, with rows in east-west direction. Sixteen plots were selected with a range of LAI from 1 to 4, tree height between 1.5 and 4 m, and horizontal crown diameters ranging from 0.8 to 4.5 m. The field campaign was carried out in summer months. Peach trees were fully

dressed and had fruits. Orange trees were also fully dressed, as they are perennials, not having fruits at that period. None of them had flowers. In peach orchards, and in general in deciduous fruit orchards, the irrigation season coincides when the trees are fully dressed. Therefore, from an agronomic point of view, the determination of IPAR is critical at this period. The terms intercepted PAR and absorbed PAR are often used interchangeably in the literature; the intercepted PAR (IPAR) is understood as the difference in the PAR flux density above (I_o) and below the plant canopy (the transmittance, T_c). The difference between absorbed PAR and intercepted PAR is *Rs – Rc,* where *Rs* is the PAR flux density reflected by soil, and *Rc* the PAR flux density reflected by the canopy.

$$fIPAR = \frac{I_0 - T_c}{I_0} \qquad [2.1]$$

$$fAPAR = \frac{(I_0 + R_s) - (T_c + R_c)}{I_0} \qquad [2.2]$$

This difference is very small for full green canopies (Daughtry et al., 1992). In this study, IPAR and fIPAR were used. Ground measurements were conducted on these selected plots concurrent with the airborne over-flights. The interception of solar radiation by the orchard canopies at each time of day was estimated with a ceptometer (SunScan Canopy Analysis System, Delta-T Devices Ltd, Cambridge, UK). The instrument is composed of two units: (i) a probe, portable instrument 1-m long, for measuring the transmitted photosynthetically active radiation (PAR) flux beneath the canopy; and (ii) a beam fraction sensor (BFS) that measures PAR incident on the canopy at the same time. The BFS incorporates two photodiodes, one of

which can be shaded from direct solar radiation by the shade ring. This allows the direct and diffuse components of PAR to be separated. As expected, the fraction of intercepted PAR by a tree is influenced by the rest of the surrounding trees and background. In addition, the crowns are highly overlapped in row-structured tree crops. Therefore, the area comprising the 4 central trees of each study area was selected to conduct the field measurements of fIPAR. Figure 2.1a shows imagery acquired by the multi-spectral airborne sensor at 15 cm spatial resolution, representing two fields used in this study with extreme row orientation angles, and the block of 4-trees selected on each study site for field data collection of radiation interception. The high spatial resolution acquired enabled targeting pure scene components, such as pure soil and vegetation, separately as well as on aggregated pixels. The image reflectance extracted for a pure crown, bare soil and aggregated pixels are shown in Figure 2.1b. The measurements of transmitted PAR made within the area beneath the four central trees of each plot were in a 1 x 0.25 m grid, concurrent with the airborne over-flights (Figure 2.2). For the assessment of the spatial variation of fIPAR among the different selected plots with a gradient in structural parameters, measurements were conducted at 10.00 GMT (+/- half-hour). In addition, transmitted and incident PAR measurements were repeated every hour from dawn to noon in one plot per orchard, to assess the diurnal variation of interception solar radiation. The study area where the PAR measurements were conducted and the diurnal variation of interception solar radiation are shown in Figure 2.3. The airborne image in this figure shows the bands B: 530nm, G: 800nm and R: 670nm.

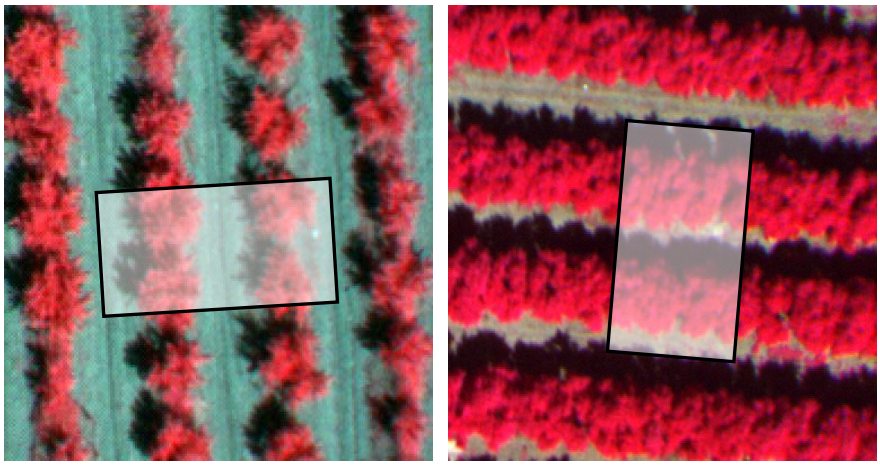

a)

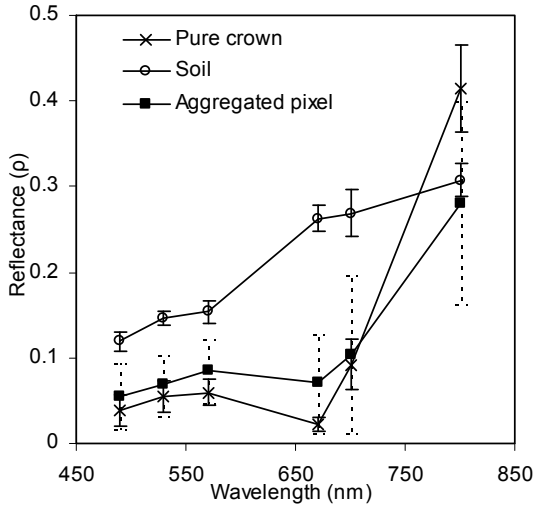

b)

Figure 2.1. Multi-spectral reflectance image acquired at 10 nm FWHM and 15 cm spatial resolution acquired from the UAV platform, showing the two fields used in the study, peach (a) and citrus (b). Canopy reflectance obtained from pure crowns and pure soil pixels, and by aggregating tree crowns, shadows and soil background (c).

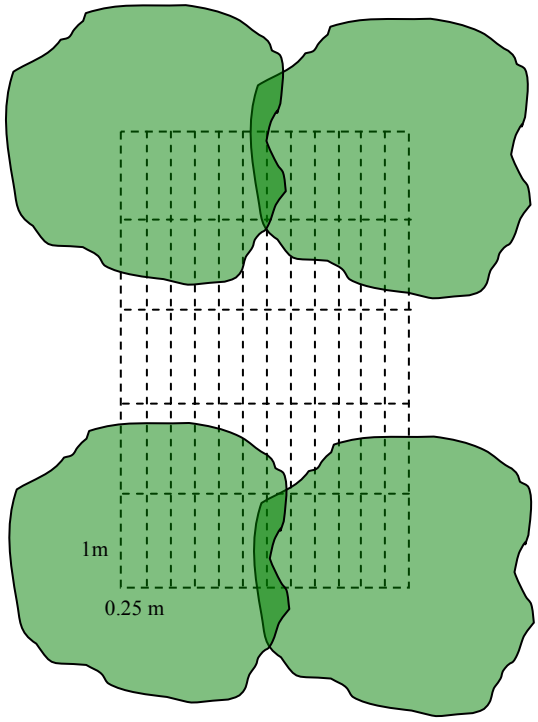

Figure 2.2. Schematic view of the grid (1 m x 0.25 m) used for field measurements made by the ceptometer between the four trees per plot (the instrument was orientated in such a way that user's shadow did not affect the measurements).

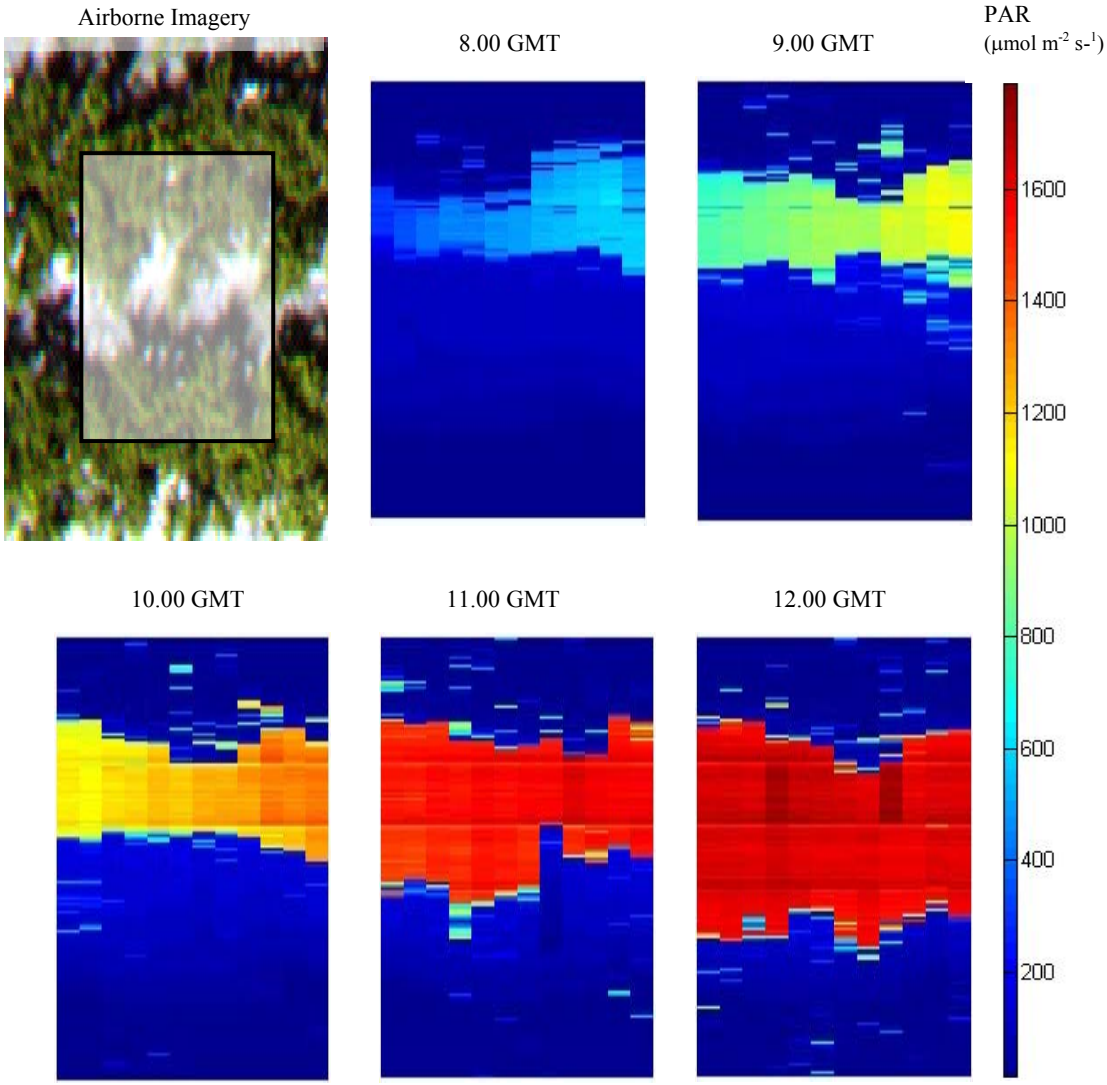

Figure 2.3. Airborne imagery acquired from the UAV platform showing one of the study sites (orange orchard, 2007, 14th August, the 3 bands are: B: 530nm G: 800nm R: 670nm). and diurnal variation of PAR measured by ceptometer at soil level (area shown is the same as in Figure 2.2).

Parameters used as input for the FLIGHT model were measured in the field at each study plot. Table 2.1 shows the input parameters required by the model. Single leaf reflectance and transmittance measurements were acquired on leaf samples using an Integrating Sphere (Li-Cor 1800-12, Inc., Lincoln, NE, USA), coupled with a 200-μm diameter single mode fibre to a spectrometer (Ocean Optics Inc. model USB2000, Dunedin, FL, USA). The single leaf values for reflectance (ρ) and transmittance (τ) were acquired as described in the manual of the Li-Cor 1800-12 system (Li-Cor Inc., 1984) and in Zarco-Tejada et al. (2005). More than 150 leaves of peach and orange trees were measured to characterize the leaf optical properties of each crop. Sunlit soil reflectance was extracted from the airborne imagery at the time of each flight. Figure 2.4 shows the mean leaf reflectance and transmittance measured on peach and orange leaves and used as input for the 3D canopy modeling conducted.

Table 2.1. Nominal values and range of parameters used for canopy modelling conducted with FLIGHT for the orchard study sites

FLIGHT input parameters	Description
Leaf optical and structural parameters	
Hemispherical reflectance and transmittance of green leaves	Integrating Sphere (see fig. 2.4)
Hemispherical reflectance and transmittance of senescent leaves	Not used
Leaf equivalent radius	0.025 m
Canopy layer and structural parameters	
Leaf area index of vegetation	m^2/m^2 (see Table 2.2)
Fractional cover	4 – 70 %
Leaf angle distribution function	9 parameters (see fig. 2.5)
Fraction green leaves	1
Fraction senescent leaves	0
Fraction of bark	0
Hemispherical reflectance and transmittance of bark	Not used
Number of stands and position coordinates	Coordinates (m)
Crown shape	Elliptical
Crown height and radius	m (see table 2.2)
Trunk height and radius	m
Background and viewing geometry	
Solar zenith and azimuth angles	Degrees (see table 2.2)
Sensor zenith and azimuth angles	Degrees (see table 2.2)
Incident PAR	Measured by BFS
Soil reflectance	Image extracted
Soil roughness	0
Aerosol optical depth (AOD)	0.15

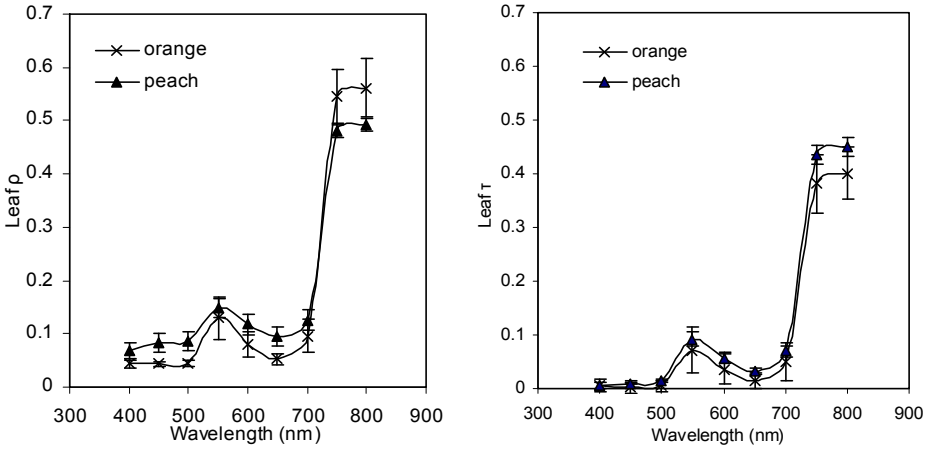

Figure 2.4. Reflectance and transmittance measured by integrating sphere for orange and peach leaves.

Leaf area index (*LAI*) was estimated from the equation (Lang, 1987):

$$LAI = -\frac{\cos(\theta) LnT(\theta)}{G(\theta)} \qquad [2.3]$$

where *G (θ),* named the *G*-function, is the mean projection of unit leaf area on a plane normal to the beam; *T (θ)* is the transmittance sunbeam, and θ is the solar zenith angle. Taking transmittance measurements with the ceptometer at the time where θ = 1- radian (57.3º), where *G*-function is close to 0.5 (Ross, 1981) the equation yields:

$$LAI = -1.1 \cdot LnT(1) \qquad [2.4]$$

The leaf angle distribution function for adult peach and orange trees was calculated according to Lemeur (1973). Random leaf azimuth was assumed. The leaf angle range (0º-90º) was split into 9 intervals of 10º each. The leaf angle distribution function (LADF), were obtained as the relative frequency

of leaves with angle α in each α interval (Figure 2.5). The leaf inclination was measured in the field with an inclinometer (Fisco Solatronic Inclinometer, Essex, UK), as the angle between the vertical and the normal vector to the upper leaf surface. For each crop, the number of measured leaves of peach and orange was 4000.

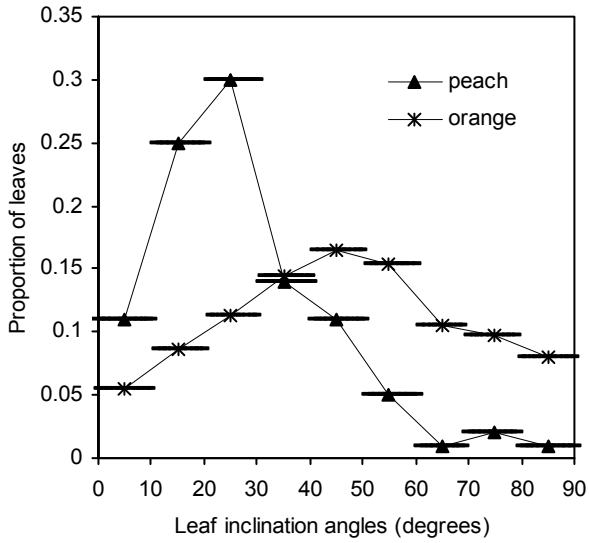

Figure 2.5. Leaf angle distribution function in 10º intervals measured for peach and orange trees.

The crown radius and shape, and the height of the fruit trees were measured using a scale pole. The architectural properties for the four central trees of each plot were measured. The trees were divided into its eight octants for measuring horizontal radii and shape (Figure 2.6a). In each octant, the tree silhouette was estimated by measuring the upper and the lower limits of the tree-crown with a vertical pole, which was systematically moved away from the tree-trunk in 0.2 m increments (Villalobos et al., 1995) as is shown in Figure 2.6b. Table 2.2 shows the mean values measured for each study plot. Table 2.2, and Figure 2.4 and Figure 2.5 show the field

measurements collected on each study site. These data are later used for the 3D canopy modeling assessment of aggregated reflectance and fIPAR estimation.

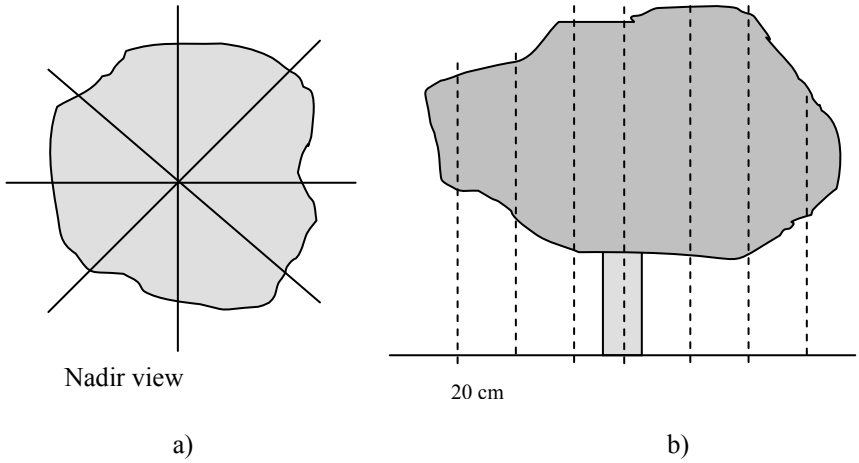

Figure 2.6. Schematic view of the nadir (a) and profile (b) view used to measure tree's silhouette.

Table 2.2. Main characteristics of peach and citrus orchard used for FLIGHT model validation: 14th August 2007 (peach), 16th September 2008 (citrus).

Plot	Time (GMT) and Solar angles at image acquisition (SZº-SAº)		Planting grid (m x m)	Rx (m)	Ry (m)	Tree height (m)
Peach orchard (Lat. 37º 49'N; Long 4º 53'W) Row orientation 20º NW-SE						
1	8.00	62.27º-87.36º	5 x 3.3	1.8	1.7	4
1	9.00	50.59º-77.06º	5 x 3.3	1.8	1.7	4
1	10.00	35.02º-69.5º	5 x 3.3	1.8	1.7	4
1	11.00	29.73º-44.51º	5 x 3.3	1.8	1.7	4
2	10.00	35.02º-69.5º	5 x 3.3	1.6	1.4	3.6
2	12.00	23.78º-14.68º	5 x 3.3	1.6	1.4	3.6
3	10.00	35.02º-69.5º	5 x 3.3	0.8	0.6	2.2
3	12.00	23.78º-14.68º	5 x 3.3	0.8	0.6	2.2
4	10.00	35.02º-69.5º	5 x 3.3	0.9	0.6	2.4
4	12.00	23.78º-14.68º	5 x 3.3	0.9	0.6	2.4
5	10.00	35.02º-69.5º	5 x 3.3	0.85	0.7	2.3
5	12.00	23.78º-14.68º	5 x 3.3	0.85	0.7	2.2
6	10.00	35.02º-69.5º	6 x 3.3	1.6	1.5	3.8
6	12.00	23.78º-14.68º	6 x 3.3	1.6	1.5	3.8
7	10.00	35.02º-69.5º	6 x 3.3	1.4	1.2	3
8	10.00	35.02º-69.5º	6 x 3.3	1.4	1.2	3
Orange orchard (Lat. 37º20'N; Long 5º48'W) Row orientation 70º NE-SW						
1	8.00	68.11º-76.39º	7 x 3	1.75	2.3	4
1	9.00	56.85º-65.21º	7 x 3	1.75	2.3	4
1	10.00	47º-49.2º	7 x 3	1.75	2.3	4
1	11.00	38.74º-32.31º	7 x 3	1.75	2.3	4
1	12.00	34.58º-8.05º	7 x 3	1.75	2.3	4
2	10.00	47º-49.2º	7 x 3	1.33	1.56	2.48
3	10.00	47º-49.2º	7 x 3	1.6	2.45	3.15
4	10.00	47º-49.2º	7 x 3	1.8	2.7	4
5	10.00	47º-49.2º	7 x 3	1.5	2.05	2.3
6	10.00	47º-49.2º	7 x 3	1.15	1.31	2.04
7	10.00	47º-49.2º	7 x 3	2	2.3	3.5
8	10.00	47º-49.2º	7 x 3	0.4	0.4	1.5
9	10.00	47º-49.2º	7 x 3	1.42	2.2	3.2
10	10.00	47º-49.2	7 x 3	1	0.9	1.8
11	10.00	47º-49.2º	7 x 3	1.5	1.5	2.56
12	10.00	47º-49.2º	7 x 3	1.26	2.1	3
13	10.00	47º-49.2º	7 x 3	1.6	1.6	2
14	10.00	47º-49.2º	7 x 3	1.8	1.6	2.6
15	10.00	47º-49.2º	7 x 3	1.8	1.8	3.4
16	10.00	47º-49.2º	7 x 3	2	1.7	3.8

Rx : crown radius in the row direction
Ry : crown radius between rows
SZ: solar zenith (degrees from the North)
SA: solar azimuth (degrees from South, clockwise negative)

2.2.2. Airborne campaigns

The sensor used in this study was a 6-band multi-spectral camera (MCA-6, Tetracam Inc., California, USA) used for biophysical parameter estimation over crops (Berni et al., 2009) and stress detection studies using chlorophyll and PRI bands (Suárez et al., 2009; 2010). An unmanned aerial vehicle (UAV) platform for remote sensing research carried the camera (details about the UAV operation can be found in Berni et al., 2009; Zarco-Tejada et al., 2008 and Zarco-Tejada et al., 2012). The UAV platform operated in this experiment consisted of a 2-m fixed-wing platform capable of carrying a 3.5 kg payload for 1 h endurance at 5.8 kg take-off weight (TOW) (mX SIGHT, UAV Services and Systems, Germany). The UAV was controlled by an autopilot (AP04, UAV Navigation, Madrid, Spain) for autonomous flight to follow a flight plan using waypoints. The camera consisted of 6 independent image sensors and optics with user-configurable spectral filters. The image resolution was 1280 x 1024 pixels with 10-bit radiometric resolution and optical focal length of 8.5 mm, yielding an angular field of view (FOV) of 42.8º x 34.7º and 15-cm pixel spatial resolution at 150-m flight altitude. High-resolution multi-spectral images acquired over the peach and citrus orchards enabled the identification of each study site used for field measurements of crop structure and fIPAR. The flight plan was designed to image each study plot at nadir. The plots were marked in the field using bright ground control points easily detectable on the imagery. The bandsets selected for this study comprised centre wavelengths at 670 and 800 nm with 10 nm full width at half maximum (FWHM) used for computing the *Normalized Difference Vegetation Index* (NDVI) and bands centered at 490, 530, 570 and 700 nm to compute other

spectral indices such as the *Photochemical Reflectance Index* (PRI) for stress detection studies, and the red edge for chlorophyll estimation.

Diurnal campaigns were conducted for both airborne imagery acquisition and intercepted PAR field measurements collected every hour from 8.00 to 12.00 GMT (8.00-12.00 GMT on citrus in 2007; 8.00-11.00 GMT on peach in 2008; 10.00 and 12.00 GMT on peach in 2007), thus a total of 11 airborne images were acquired over the selected plots for each orchard. The objective was to study the diurnal variation of the intercepted radiation over the course of the day as a function of the sun geometry. Additionally, to assess the effects of the variability of the intercepted solar radiation and reflectance bands as a function of orchard architecture, a total of 30 additional airborne images were collected over the study plots. Atmospheric correction and radiometric calibration methods were applied to the imagery to calculate the spectral reflectance. Radiometric calibration was conducted in the laboratory using coefficients derived from measurements made with a uniform calibration body (integrating sphere, CSTM-USS-2000C Uniform Source System, LabSphere, NH, USA) at four levels of illumination and eleven integration times. Radiance values were converted to reflectance using the total incoming irradiance simulated with SMARTS (Gueymard, 2005) using aerosol optical depth at 550 nm measured with Micro-Tops II sunphotometer (Solar LIGHT Co., Philadelphia, PA, USA) collected in the study areas at the time of the imagery acquisition. This radiative transfer model has been previously used in other studies such as Berni et al. (2009) and Suárez et al. (2010). The algorithms used by SMARTS were developed to match the output from the MODTRAN complex band models within 2%, but uses AOD (aerial optical depth) as input. The geometric calibration was

conducted using Bouguet's calibration method (Bouguet, 2001) in order to recover the intrinsic camera parameters (Berni et al., 2009).

2.2.3. 3D simulation of row-structured tree canopies

A detailed simulation of the land surface bidirectional reflectance was undertaken in order to understand the relationships between canopy architecture and the intercepted PAR as a function of the vegetation canopy structure, tree spatial distribution, and leaf and background optical properties. A 3-D model of light interaction with vegetation canopies (FLIGHT) was used for this study. FLIGHT was selected because it allowed simulation of row orientations, tree dimensions, soil background effects, and to generate 3D scenes to assess the effects of the architecture, crown structure and biochemical inputs. The FLIGHT model is based on the Monte Carlo ray tracing method as a tool to simulate the radiative transfer in a canopy structure (North, 1996). Monte Carlo simulation allows highly accurate estimation of light interception and bidirectional reflectance (Barton & North, 2001; Disney et al., 2000). The technique requires sampling of the photon free-path within a canopy representation, and simulation of the scattering event at each iteration. An accurate treatment of light interception and multiple scattering between foliage elements and the soil boundary is obtained by iteration (North, 2002). In addition to calculating absorbed or intercepted radiation, the model also allows direct calculation of canopy photosynthesis, accounting for structure and anisotropic down-welling radiation field (Alton et al., 2007). The FLIGHT model has been assessed with other three-dimensional codes as part of the *Radiation Model Intercomparison* (RAMI) project (Widlowski et al., 2007). The recent analysis within RAMI of six selected three-dimensional models, including

FLIGHT, showed dispersion within 1% over a large range of canopy descriptions (Widlowski et al., 2008).

2.2.3.1. Canopy model assessment for simulating row tree orchards

The FLIGHT model inputs consisted of: (i) geometric characteristics: crown shape, height, and radius, leaf angle distribution, LAI and location of each single crown in the scene, as well as trunk geometry, total scene size and vegetation coverage; (ii) optical properties: soil reflectance and green leaf reflectance and transmittance; (iii) sun and view azimuth and zenith angles; and (iv) other parameters such as soil roughness, aerosol optical thickness and the number of photons simulated. Table 2.1 shows the input parameters required to run the FLIGHT model for the scenes simulated in this study. The output of the model simulation is a 3D hyperspectral image with the same number of bands as the input leaf spectral signature and the estimated intercepted PAR (*IPAR*) for the scene.

A detailed simulation of the canopy reflectance was undertaken to assess the performance of the FLIGHT model for this type of row-tree structure canopy. Table 2.2 shows the selected plots used for the 3D canopy model assessment. The study areas were selected to assure spatial variability, showing a wide range in vegetation cover fraction: 9%-60% in peach, and 4%-75% in citrus orchards, as well as different row orientations (N-S; E-W) and tree heights (1.8-4 m). In addition, flights conducted at different times enabled the assessment of the diurnal evolution of canopy reflectance and fIPAR estimated by the 3D model. FLIGHT simulations were conducted with structural and optical measurements collected at each plot (see Figure 2.4 for the optical properties and Table 2.2 for the structural parameters used). Model assessment for the canopy reflectance simulations was

conducted by comparisons between the modeled reflectance and the airborne imagery reflectance acquired on each plot and flight time, calculating the RMSE.

Assumptions considered in the modeling work consisted of fixed leaf angle distribution for all trees on the scene. In addition, the trees in a 3D scene had the same shape, which corresponded to the mean value measured for the four central trees on each site. The woody material (NPV) was not considered as field measurements conducted indicated less than 8% NPV, and negligible effects were found on the reflectance and NDVI values used to relate with fIPAR. Fruits for peach trees were not considered in the simulations.

2.2.3.2 Scaling up and Model Inversion methods for fIPAR estimation

The FLIGHT model was tested to assess the accuracy of the simulations for fIPAR in row-structured tree canopy scenes. To assess the influence of the architecture on the canopy reflectance, on the aggregated NDVI and on fIPAR, the FLIGHT input parameters were varied and the simulated reflectance per plot was aggregated by the four central trees of the plot, including the soil between tree rows and shadows (see Figure 2.1a and Figure 2.1b). *Scaling-up* and model inversion methods were conducted to estimate the instantaneous fIPAR in the row-tree orchards using the airborne imagery acquired on each study site.

For the *scaling-up* method, the objective was to develop predictive relationships NDVI-fIPAR calculated under specific canopy assumptions. The predictive relationships for the peach and citrus orchards were obtained with input parameters fixed according to mean field measurements for each

orchard: leaf angle distribution function, leaf optical properties, row orientation and soil reflectance extracted from the airborne image, and the solar geometry depending on the time of flight. The methods used in this study are relevant for fully dressed peach trees and for the entire season in perennial citrus orchards. A specific set of input parameters for the FLIGHT model typical for these orchards to define the canopy structure were: 0.5 to 2 m in the case of crown radii, tree height ranged from 1.4 to 4 m, and LAI from 2 to 6. Table 2.3 shows a summary of all input parameters used for the *scaling-up* method. The modeled relationships NDVI vs fIPAR obtained for each orchard were then applied to the multi-spectral airborne imagery reflectance to estimate the instantaneous fIPAR for each flight time and study site. This methodology enabled the application of sensor-derived optical indices for scaled-up relationships NDVI-fIPAR that are a function of canopy structure, optical properties and the viewing geometry.

The estimation of fIPAR based on model inversion was conducted by using *look-up* tables (LUT) developed independently for each orchard type, using the specific leaf spectral properties, row orientation and sun geometry. The range of parameters used to define the canopy structure was the same as in the scaling-up methodology, while including the variability in the soil optical properties (Table 2.3). In our analysis, three different types of soil reflectance were considered, representing dark, medium and bright soils (Figure 2.7). A total of 1000 synthetic spectra were generated using the FLIGHT model with random input parameters within the ranges previously proposed. The 1000 synthetic spectra were composed of 9 bands with wavelength centres at 400, 450, 500, 570, 600, 670, 700, 750 and 800 nm to simulate the bands acquired by the airborne sensor. The FLIGHT model used for fIPAR estimation was first tested with synthetic spectra using a

numerical model inversion method. A subset of 500 synthetic spectra was used to build the LUT, and the remaining subset used for model inversion to assess the retrieval of fIPAR. This step was conducted to assess the robustness of the FLIGHT model for retrieving fIPAR. Next, the reflectance spectra obtained from the imagery for each study site were used as input for the model inversion method to estimate fIPAR for each study area. For this step, the 1000 synthetic spectra LUT was used, and the error calculation consisted of determining the set of reflectance spectra which minimized the merit function Δ^2, Equation [2.5].

$$\Delta^2 = \sum_n \left[r_m(\lambda_i) - r^*(\lambda_i) \right]^2 \qquad [2.5]$$

where $r_m(\lambda_i)$ is the canopy spectral reflectance from the LUT; $r^*(\lambda_i)$ is the canopy spectral reflectance inverted . In the present study, two methods were used in the inversion procedure, (i) using reflectance bands centred at wavelength 570, 670, 700 and 800 nm; and (ii) building the merit function based on the NDVI index. This methodology has been previously applied by Weiss et al. (2000) and Koetz et al. (2005) for LAI estimation.

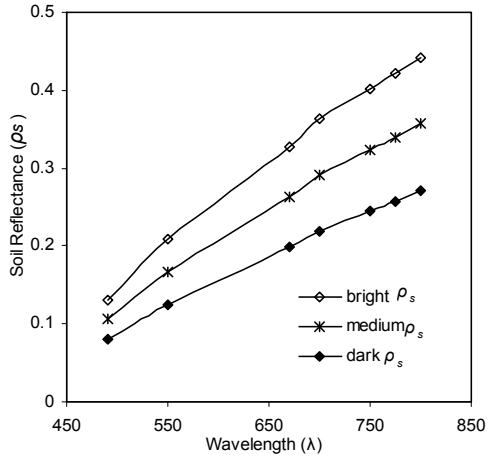

Figure 2.7. Spectral reflectance for three different soil brightness levels.

Table 2.3. Variables used to generate predictive relationships and look-up tables for the *scaling- up* and model inversion methods. Coefficients of determination and RMSE values obtained between the ground-measured fIPAR and the estimated fIPAR by *scaling-up* and model inversion for both peach and citrus orchards.

	Predictive relationship		**Model inversion *(LUT)***	
Fixed parameters	Leaf (ρ and τ)	See Figure 2.4	Leaf (ρ and τ)	See Figure 2.4
	LADF	See Figure 2.5	LADF	See Figure 2.5
	Row orientation	NS (peach) EW (orange)	Row orientation	NS (peach) EW (orange)
	Sun geometry	SZ:35.02º; SA:69.5º (peach) SZ: 47º; SA: 49.2º (orange)	Sun geometry	SZ:35.02º; SA:69.5º (peach) SZ: 47º; SA: 49.2º (orange)
	Soil (ρ_s)	Image extracted		
Variable parameters	Tree radius (m)	0.5 – 2	Soil (ρ_s)	See Figure 2.7
	Tree height (m)	1.4 – 5	Tree radius (m)	0.5 – 2
	LAI	2 – 6	Tree height (m)	1.4 – 5
			LAI	2 – 6
Results		*r^2 ;(RMSE)*		*r^2 ; RMSE*
NDVI	Peach	0.87; (0.08)	Peach	0.84; (0.12)
	Citrus	0.88; (0.09)	Citrus	0.85; (0.08)
4 bands (570, 670, 700 800 nm)	---	---	Peach	0.82; (0.11).
			Citrus	0.76; (0.08)

SZ: solar zenith (degrees from the North)
SA: solar azimuth (degrees from South, clockwise negative)

2.3. Results and Discussion

2.3.1 Using the FLIGHT model for row-structured tree canopies: canopy reflectance assessment.

A sample FLIGHT simulation scene corresponding to the orange orchard at different sun angles is shown in Figure 2.8a. Block spectra (Figure 2.1) were extracted from the airborne imagery and simulation scenes, and vegetation indices calculated. Reflectance spectra comparisons were made between model simulations and airborne imagery, assessing the canopy reflectance simulations for the visible and near-infrared (NIR) wavelengths. Figure 2.8 shows image-extracted and simulated canopy reflectance for the peach orchard (Figure 2.8b) and orange orchard (Figure 2.8c) at different times. Leaf optical properties and LADF data appear in Figure 2.4 and Figure 2.5, respectively. The image data used in this study were collected in 2 years. The multi-spectral sensor has configurable bandsets. Thus, during 2007, the selected wavelengths were 530,570,670,715,730 and 800 nm and, in 2008, the bands used were 530,550,570,670,700 and 800 nm. Both datasets had the bands required for NDVI calculation. The trend observed in the airborne imagery as a function of sun angle showed an increasing canopy reflectance with time due to the reduced shadow proportions, which were well captured by the model. This effect is more evident in N-S oriented orchards (Figure 2.8b), as the shaded contribution changes more significantly in this orientation than in E-W orientation (Figure 2.8c).

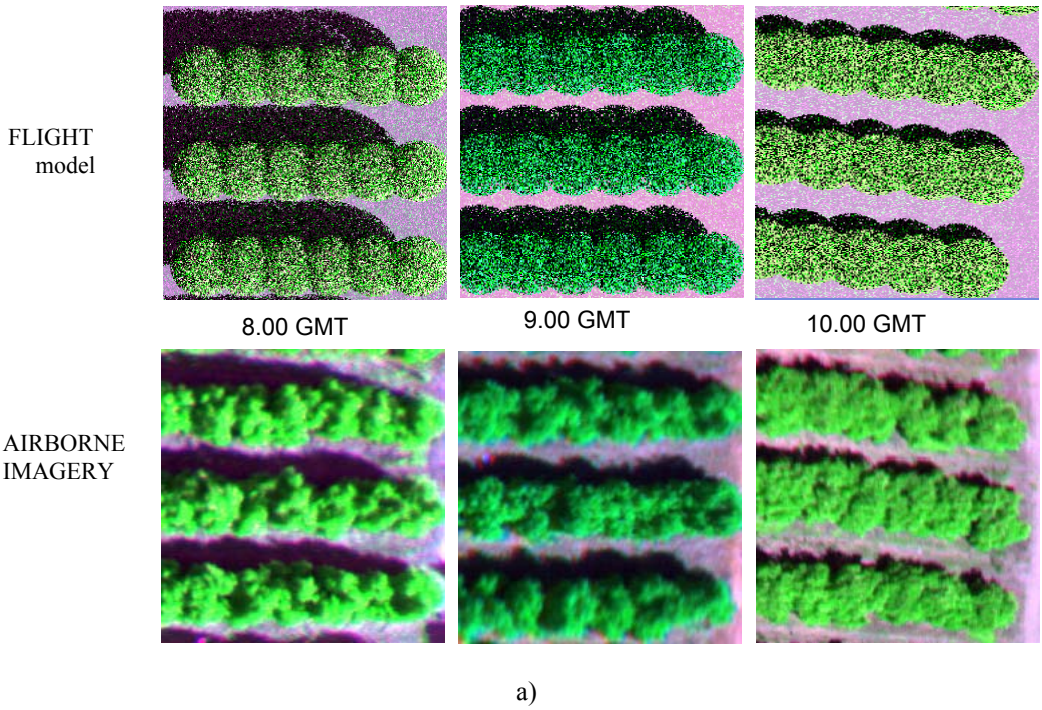

Figure 2.8. UAV airborne imagery acquired from one study site, and the corresponding simulations conducted with FLIGHT at 8.00, 9.00 and 10.00 GMT (a). Spectra obtained for aggregated vegetation-soil pixels: multispectral image spectra collected at 8.00 GMT and 12.00 GMT, and canopy simulations conducted with FLIGHT on peach (b) and orange (c) orchards.

The green (570 nm), red (670 nm) and NIR (800 nm) bands extracted from the imagery acquired over the study plots were compared against simulations conducted with the FLIGHT model (Figure 2.9a). The FLIGHT input parameters used were measured for each study site (Table 2.2, Figure 2.4-Figure 2.5). The simulations for the green spectral band (10 nm FWHM) yielded RMSE values of 0.011 and 0.024 for orange and peach, respectively; similar results were obtained for the red band (RMSE=0.017 and 0.031). For the NIR band, the errors increased slightly (RMSE~0.05). Higher errors were obtained for N-S orientation as compared to E-W due to higher changes in reflectance over the diurnal course. The RMSE values obtained for all bands in the visible were below 0.03, and below 0.05 in the NIR.

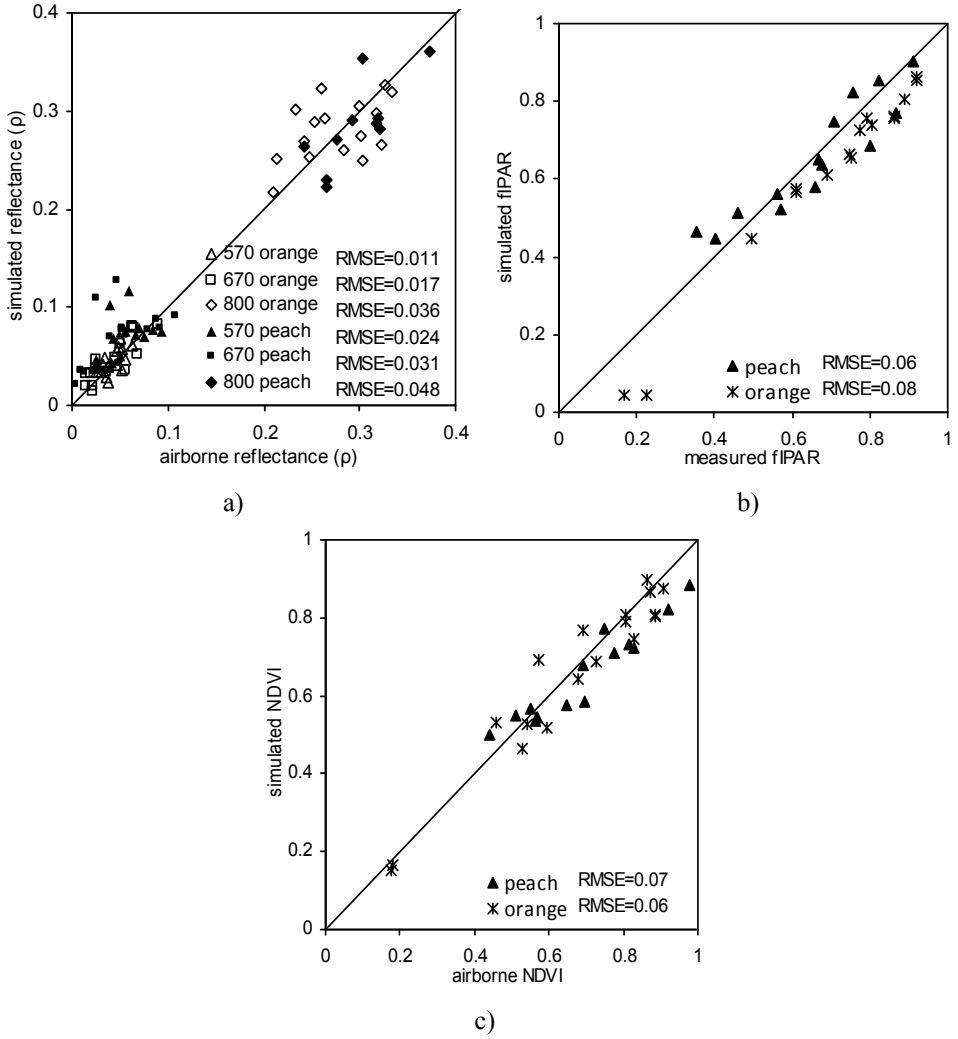

Figure 2.9. Relationships obtained for canopy reflectance at 570, 670 and 800 nm (a), NDVI (b), and fIPAR (c) calculated from multispectral airborne imagery and FLIGHT simulations.

Assessments conducted for NDVI and fIPAR simulated with FLIGHT and obtained from the airborne imagery (NDVI) and ceptometer (fIPAR) are shown in Figure 2.9b and 2.9c, respectively. The analysis of NDVI yielded RMSE=0.06-0.07 in orange and peach orchards, respectively, obtaining RMSE values of 0.06 (peach) and 0.08 (orange) for fIPAR. Plots with low vegetation cover fraction presented higher errors in the simulations

conducted for fIPAR estimation. Considering the complex canopy architecture simulated, the large number of field measurements required for simulations and the atmospheric and image calibration issues, these results seemed acceptable for simulating the 3D row structure architecture conducted with FLIGHT.

2.3.2 Simulation results for fIPAR in row-structured tree canopies

Simulations with FLIGHT were conducted to understand the sensitivity of input parameters, such as vegetation cover fraction, sun angles, row orientation, LAI and the soil reflectance, on the canopy reflectance (ρ), NDVI and fIPAR simulations. The red (670 nm) and NIR (800 nm) bands used for NDVI calculation and fIPAR were simulated as a function of the sun angle for N-S and E-W row orientations for a range of vegetation cover fraction (30-70%) and soil spectra (bright, medium and dark). The effects of the row orientation on NDVI and fIPAR were studied by generating different canopy scenarios on a summer day as shown in Figure 2.10. The figure illustrated three scenarios: NS row oriented tress (Figure 2.10a), EW row oriented trees (Figure 2.10b) and randomly distributed trees (Figure 2.10c) at 8.00, 10.00 and 12.00 GMT. All three cases had the same cover vegetation fraction, but variable percentage shadow due to the tree spatial distribution. The vegetation cover fraction was 48% and LAI=4 in all cases, the height of the trees was set to 2.7 m, and a spherical leaf angle distribution function was assumed. This figure highlights the importance of considering row orientation in the simulations. As such, the analysis focused on row-orientated orchards, while excluding the random distribution simulations.

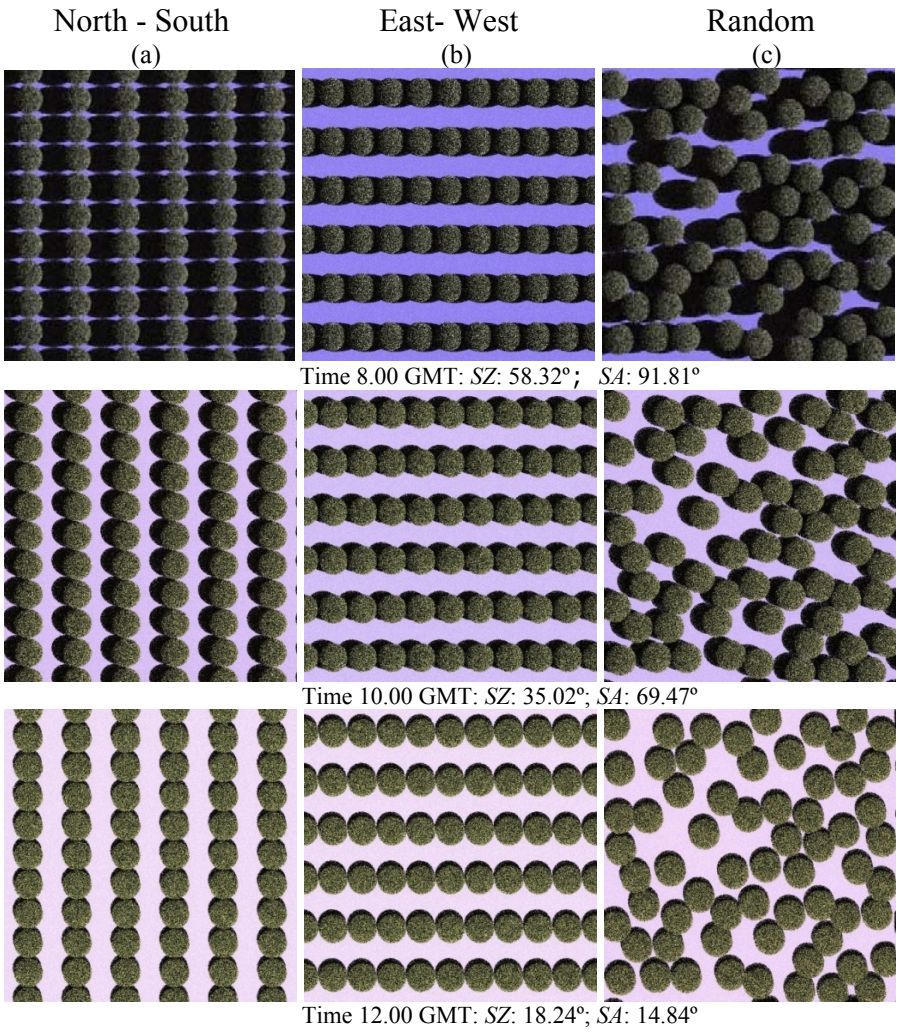

SZ: Solar zenith (degrees from North)
SA: Solar azimuth (degrees from South, clockwise negative)

Figure 2.10. FLIGHT model simulations conducted generating orchard scene at different times of day (8.00, 10.00 and 12.00 GMT) for two different row orientations, NS and EW (a and b, respectively) and a random distribution (c). LAI=4, fractional cover=0.48, leaf size=0.025, fraction of green leaves=0.85, fraction of bark=0, ladf=spherical, crown shape=ellipsoidal, crown radius=1.5 m, tree height=2.7 m, soil roughness=0, aerosol optical thickness=0.1.

The effects of the background were assessed because it is well accepted that variations in soil spectral reflectance have significant effects on NDVI (Huete et al., 1985), especially in open canopies. For North-South row orientations (Figure 2.11a, d and g), larger differences on ρ, NDVI and fIPAR were found as a function of sun angles. NIR and red bands increased up to 0.20 for bright soils from morning until midday, while the diurnal variation of ρ on scenes with dark soils was around 0.10. These differences found between ρ at morning and noon appeared slightly smaller for greater ground cover (70%) (Figure 2.11a). For NDVI, a decrease of up to 0.4 was shown for a dark soil background from 8.00-12.00 GMT. Soil spectra had significant influence on NDVI, mainly at midday (Figure 2.11d). The trend for fIPAR was similar to NDVI, decreasing between 0.3-0.4 for both canopy cover values, but with little effect caused by the background (Figure 2.11g). On the contrary, simulations conducted demonstrated the small sun angle effect on ρ, NDVI and fIPAR for E-W orientations (Figure 2.11b, e and h, respectively). As expected, row-tree lines oriented in the solar plane made the shaded soil component variation a very small contribution to the canopy reflectance (Figure 2.11b and e), and on fIPAR (Figure 2.11h). However, large differences on canopy reflectance, NDVI and fIPAR were found when the vegetation cover fraction was varied, as expected. Changes in soil reflectance affected the canopy reflectance simulations and NDVI (Figure 2.11b and e), while fIPAR simulation was less affected by the background (Figure 2.11h). Variations in the LADF had small effects (Figure 2.11c, f, i). These results demonstrate the importance of canopy modeling methods to understand the behaviour of reflectance, NDVI and fIPAR for different canopy scenarios on row-structured canopies.

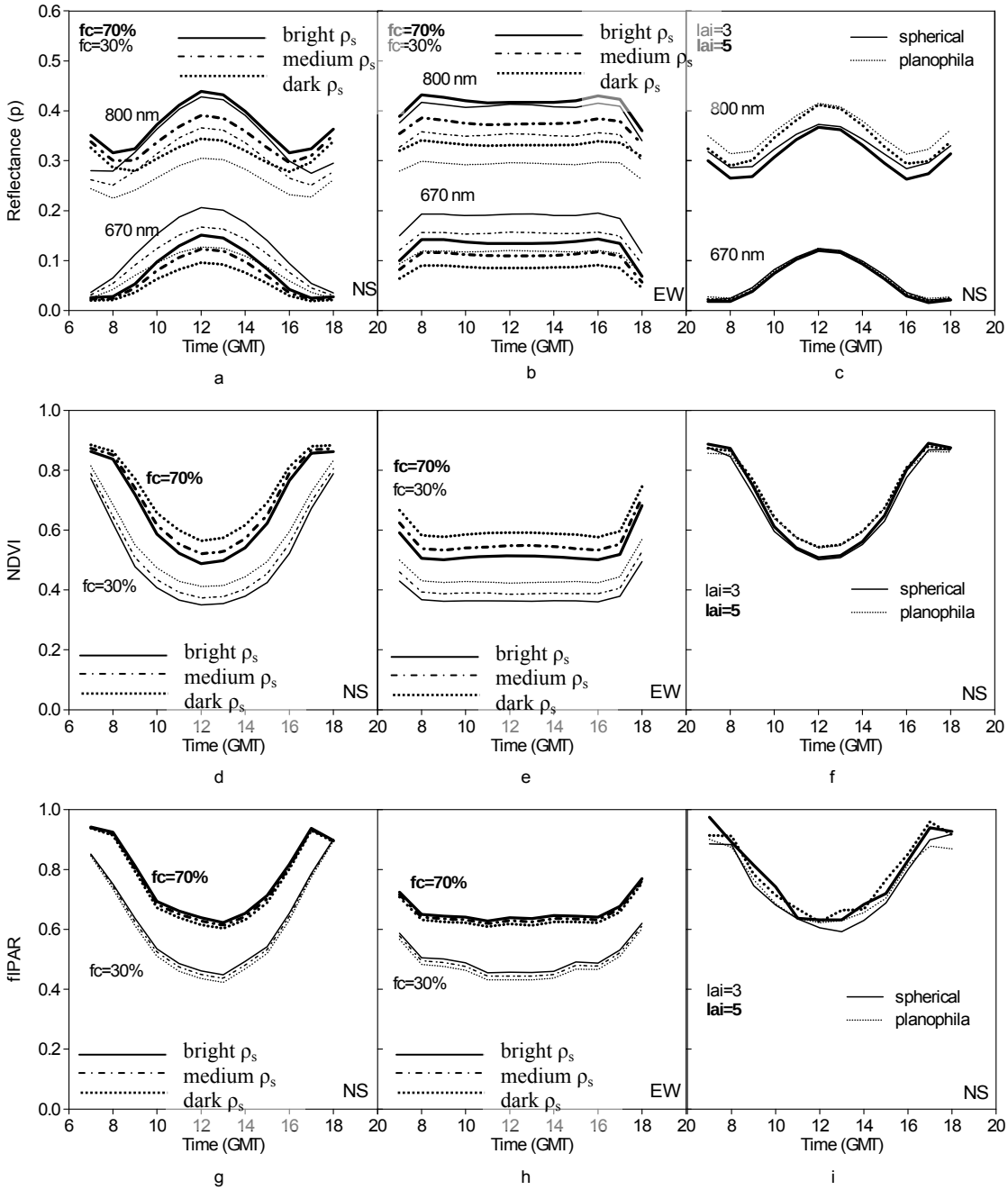

Figure 2.11. Simulations obtained with FLIGHT: variance analysis due to effect of the sun geometry on reflectance (670 and 800 nm), NDVI and fIPAR, considering row orientation N-S (a,d,g) and E-W (b,e,h) as a function of different soil background and vegetation cover fraction (30% and 70%) for the LAI=4 and ladf=spherical. Effects of sun geometry on reflectance (670 and 800 nm), NDVI and fIPAR, considering row orientation N-S as function of different ladf (spherical and planophile) and LAI (3 and 5), medium brightness soil reflectance and 70% vegetation cover fraction (c,f,i).

The instantaneous NDVI-fIPAR relationships as a function of fixed and variable inputs were calculated to build *scaling-up* relationships. The sun geometry was fixed to 10.00 GMT for a summer day (zenith=35.02º from North; azimuth=69.47º from South, clockwise negative) and variation was driven by the vegetation cover fraction (4-70%). The architectural canopy parameters such as tree height (z) were varied for three different levels (z=1.7; 2.9; 4 m) showing a marginal effect on the NDVI-fIPAR relationship (Figure 2.12a). Similar results were found for the LAI variation (data not shown), which confirms previous studies, such as Goward & Huemmrich (1992). The instantaneous NDVI-fIPAR relationships for N-S and E-W row orientations, in combination with changes in the soil optical properties, were also studied for two different sun angles: morning (8.00 GMT) (Figure 2.12b) and midday (12.00 GMT) (Figure 2.12c). At 8.00 GMT, soil reflectance had a significant effect on the NDVI-fIPAR relationship for the E-W row orientation (Figure 2.12b), being less important for North-South row orientation because the soil is completely shaded at such a sun angle (8.00 GMT). On the other hand, shadows almost disappeared at 12.00 GMT. Soil optical properties caused large effects on both East-West and North-South orientations (Figure 2.12c). For example, for NDVI=0.4, differences of 0.17 in fIPAR were found as a function of bright and dark soils (Figure 2.12c) for both orientations. The canopy model results showed high sensitivity of the NDVI-fIPAR relationships to the soil optical properties and row orientation, dependant on the sun geometry.

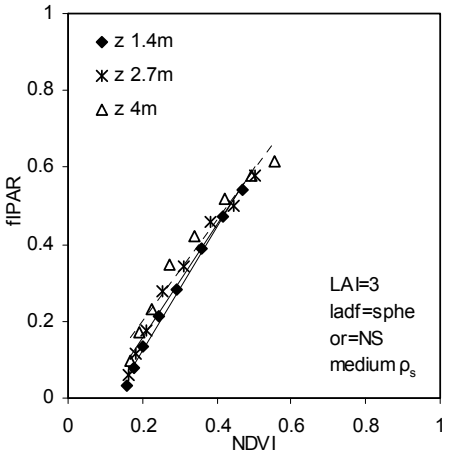

a)

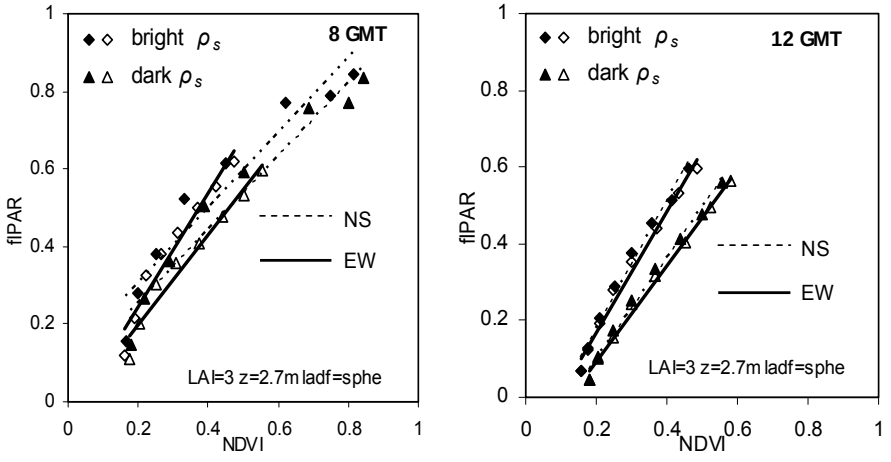

b) c)

Figure 2.12. Variance in the NDVI-fIPAR relationship as a function of the tree height (a), soil type and row orientation for 8.00 GMT (b) and 12 GMT (c).

2.3.3. Estimating intercepted radiation by scaling up and model inversion methods

An analysis of fIPAR estimation with remote sensing imagery was first conducted by obtaining relationships between vegetation indices calculated

from the airborne imagery and fIPAR measured with a ceptometer (Figure 2.13). The aggregated image reflectance from the four central trees of the orchard, including exposed soil and shadows, was used to compute spectral vegetation indices, such as NDVI. The diurnal variation of NDVI for the same plot over the course of the day as related to fIPAR (Figure 2.13a) was mainly driven by soil and shadow variation as a function of the sun geometry. The spatial variation of NDVI vs fIPAR (Figure 2.13b) was obtained through measurements conducted at selected plots with different architectural canopy characteristics at 10.00 GMT (+/- half hour). The results showed high coefficients of determination for NDVI vs fIPAR with $r^2 > 0.9$ for the diurnal trial, and $r^2 > 0.8$ for the spatial variation study. Methodologies to estimate instantaneous fIPAR through *scaling-up* and model inversion methods were then investigated.

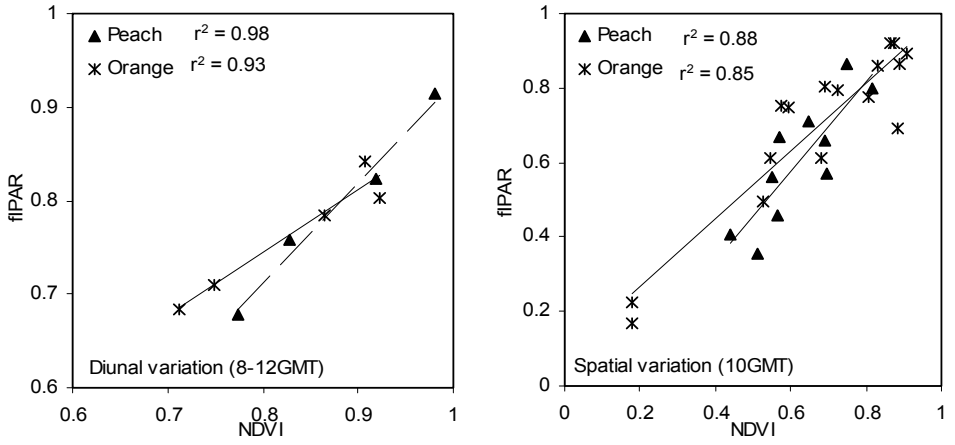

a) b)

Figure 2.13. Relationships obtained between NDVI, calculated from high resolution airborne imagery, and field-measured fIPAR at different sun angles (diurnal variation) for an individual site (a) and multiple sites imaged at solar zenith angle = 35º (spatial variation) (b).

Modeled relationships NDVI vs fIPAR were obtained by the *scaling-up* methodology (Figure 2.14a). Parameters used to obtain these relationships can be found in Table 2.3. After previous understanding of the influence of different parameters on the relationship NDVI-fIPAR, parameters known for each study area were used, such as row orientation, soil reflectance obtained from the airborne imagery and sun geometry function of the time of each flight. Other canopy architecture parameters were varied within a range (Table 2.3). Estimation of fIPAR by scaling-up was compared against ground-measured fIPAR for each plot. Relationships obtained for the citrus orchard yielded estimates with relative RMSE of 0.10 and r^2=0.88. For the peach orchard, a relative RMSE of 0.08 and r^2=0.87 were obtained (Figure 2.14b).

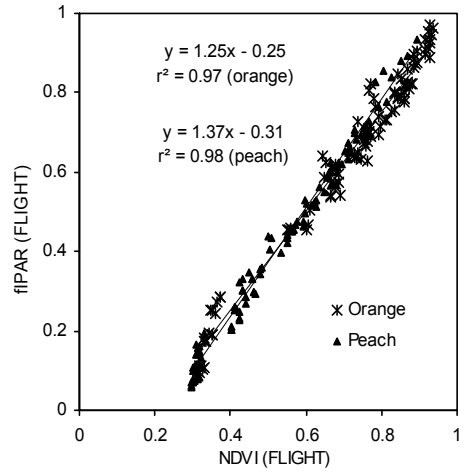

a)

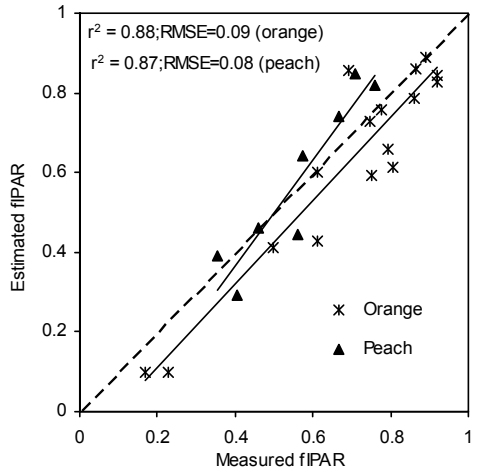

b)

Figure 2.14. Relationships between fIPAR and NDVI obtained for FLIGHT for citrus and peach orchards (a). Estimated intercepted radiation using *scaling-up* equations developed in a), versus measured fIPAR (b).

The simulation study to investigate the retrieval of fIPAR through FLIGHT radiative transfer model inversion was conducted by iteration from the synthetic spectra for peach (Figure 2.15a) and orange orchards (Figure 2.15b). The fIPAR estimates shown in Figure 2.15 were obtained using two approaches. In the first case, only 4 of the 9 bands, 570, 670, 700 and 800

nm, were used for the inversion, and the second case using NDVI. In addition, during the model inversion, some parameters were fixed and others were varied (see Table 2.3) to simulate the typical set of parameters potentially known and unknown. That is the reason for the scatter in the plots between estimated fIPAR and fIPAR calculated from the synthetic spectra. Relative RMSE below 0.09, and coefficients of determination around 0.8 were obtained by using the four bands and NDVI for the model inversion method for both orchards. The modeling exercise conducted with synthetic spectra demonstrated the feasibility of the proposed model inversion method to retrieve fIPAR with the FLIGHT model.

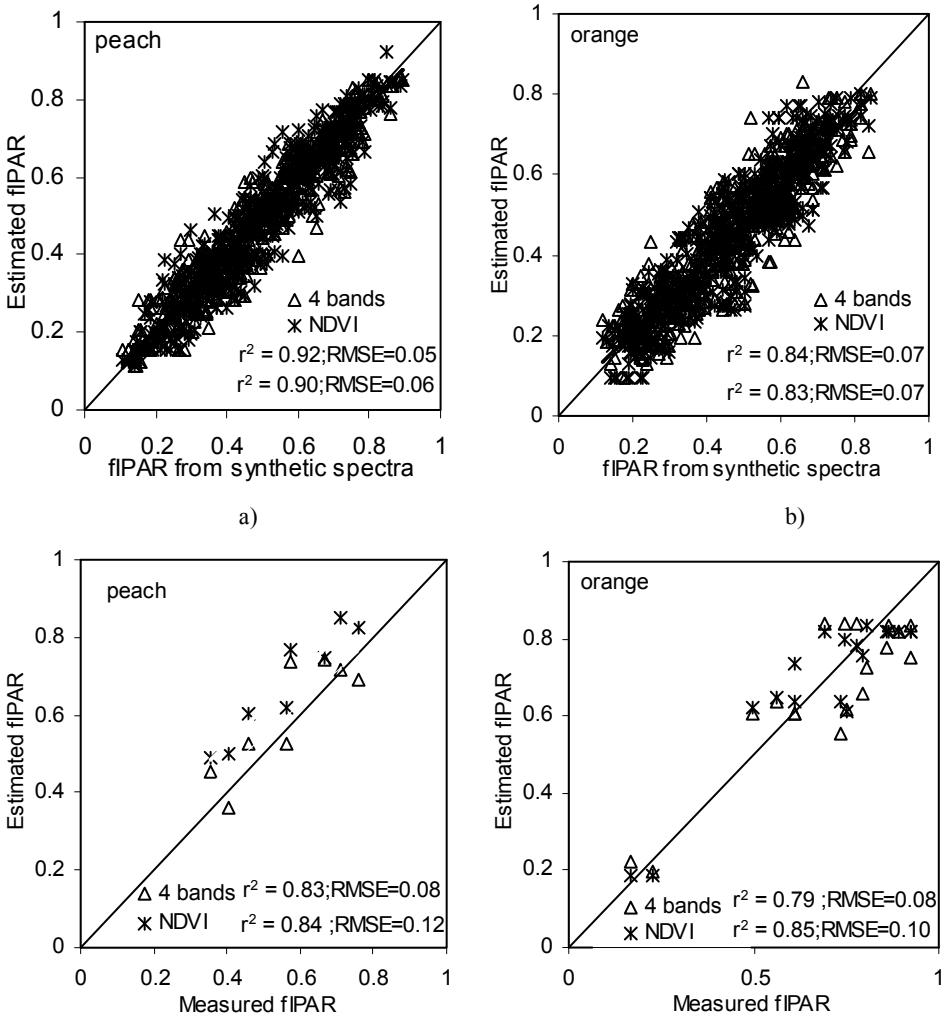

Figure 2.15. Coefficients of determination and RMSE obtained between fIPAR obtained from synthetic spectra for peach (a) and citrus orchards (b). Coefficient of determination and RMSE obtained between field-measured fIPAR and estimated fIPAR by inversion for peach (c) and citrus orchards (d).

Subsequently, the estimation of fIPAR by inversion using airborne imagery was compared with ground measured fIPAR for each plot. LUTs were generated as indicated in Table 2.3. Results obtained from comparing the estimated fIPAR by radiative transfer model inversion against the field-measured fIPAR (Figure 2.15c and d) yielded a relative RMSE of 0.08 and

0.10 for orange and peach orchards, respectively. Building the merit function with (i) four bands, and (ii) NDVI, did not show significant differences. Results obtained by comparing the estimated fIPAR against field measurements demonstrated the feasibility of the model inversion approach for fIPAR estimation using the FLIGHT model.

A direct application of these methodologies enabled obtaining a map of the instantaneous intercepted radiation at orchard scale using airborne imagery. Three orange plots showing a varying percentage cover, together with the downscaled NDVI map, and the estimated fIPAR are shown in Figure 2.16. Large differences can be observed between the three plots, with values of intercepted radiation ranging from 0.18 to 0.88. The intercepted radiation varied within each plot, even for apparent constant ground cover. As shown in Figure 2.16, fIPAR values ranged between 0.7 and 0.9 (first plot), 0.45 to 0.63 (second plot) and from 0.15 to 0.25 (third plot). Figure 2.17 and Figure 2.18 show the complete citrus and peach orchard respectively, the mosaic of canopy reflectance is shown in Figure 2.17a and Figure 2.18a and the fIPAR obtained from apply this methodology are shown in Figure 2.17b and Figure 2.18b.

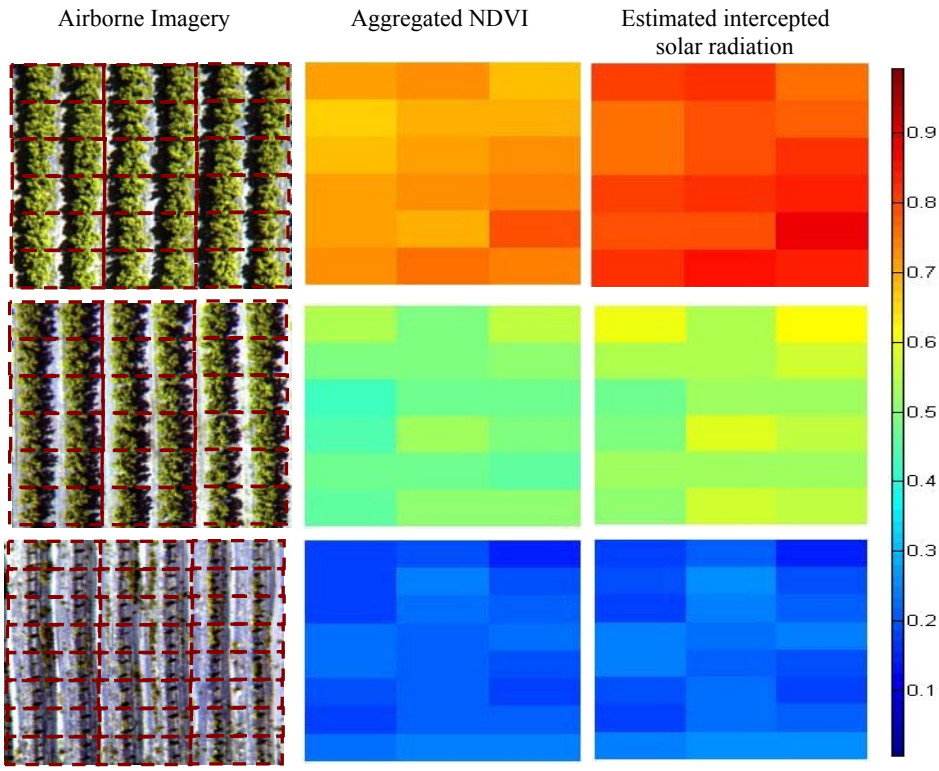

Figure 2.16. Example of three maps of the intercepted radiation at the orchard scale for plots with different plant densities.

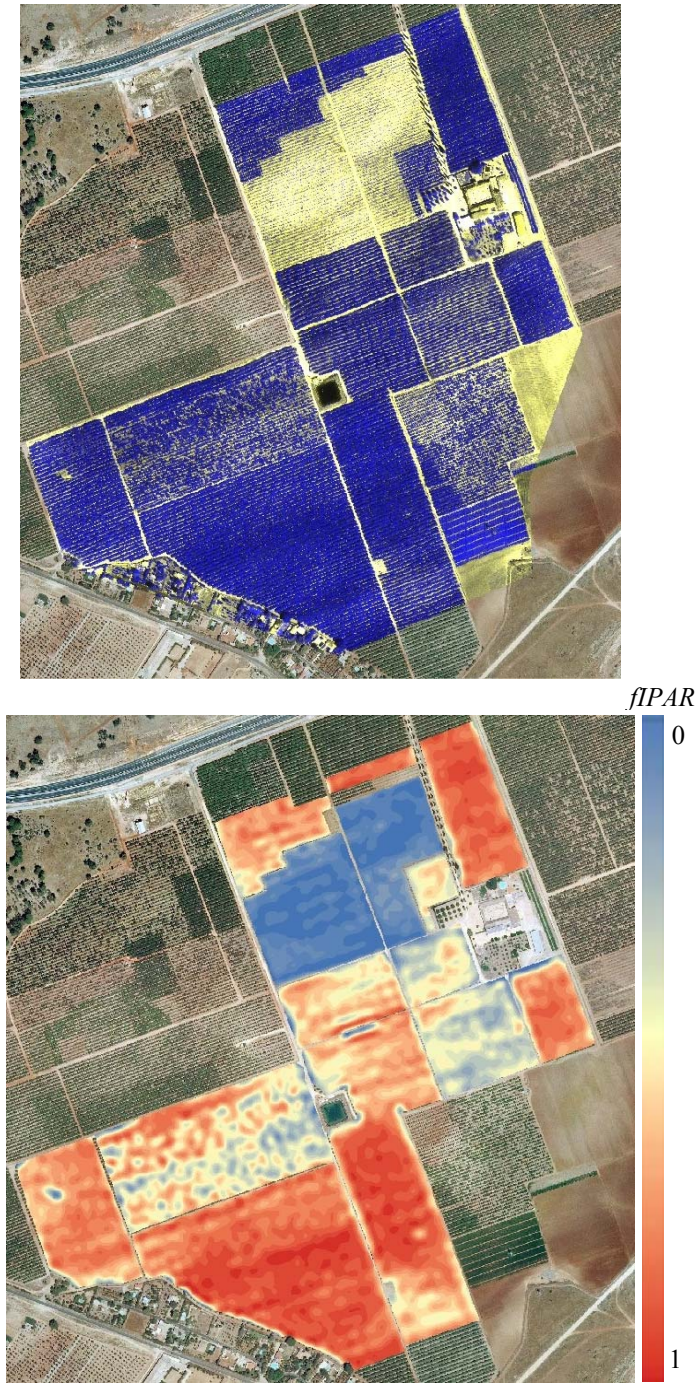

Figure 2.17. Multi-spectral mosaic of the citrus orchard acquired from the UAV platform (a) used to generate a map of fIPAR calculated from the FLIGHT model (b)

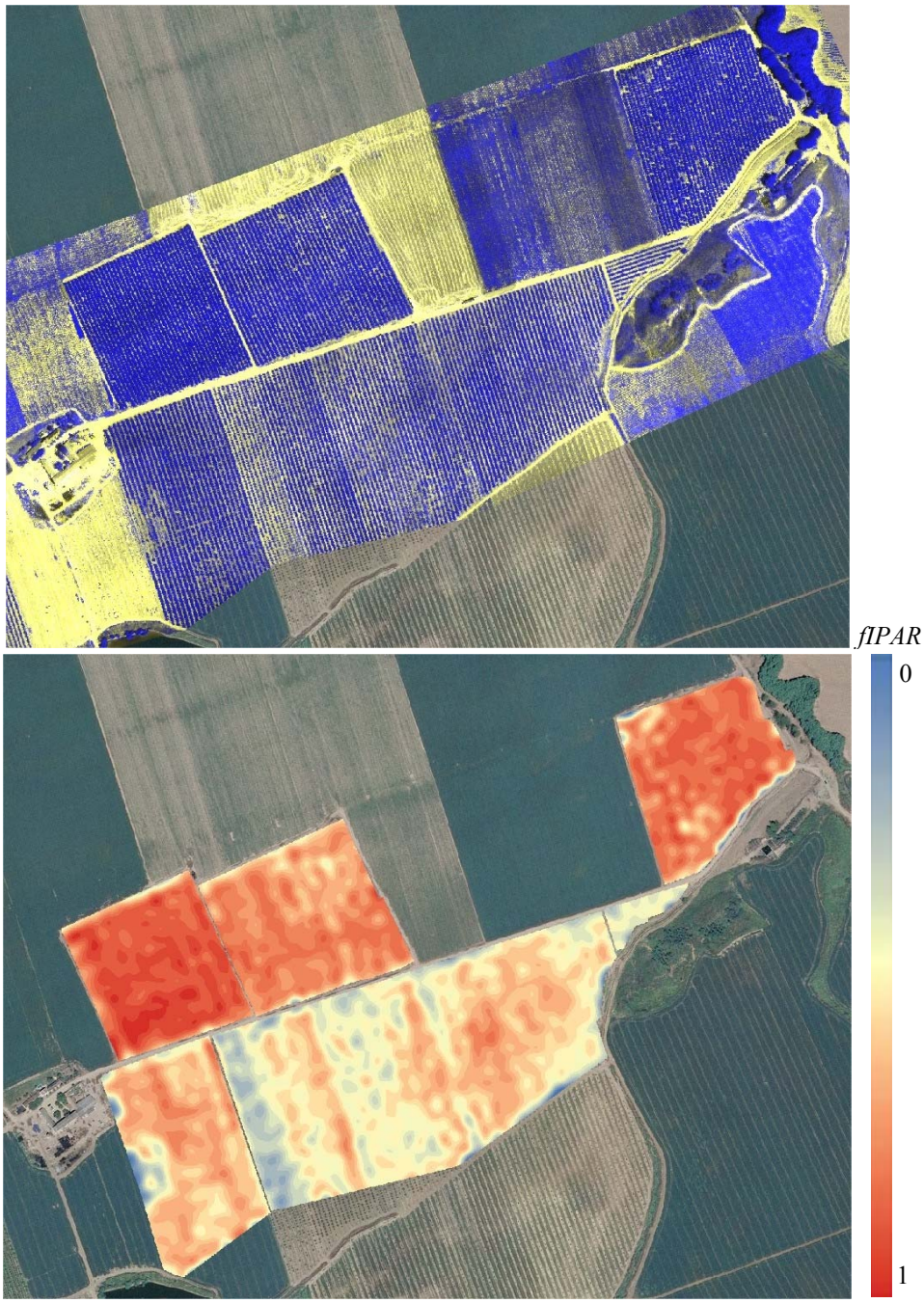

Figure 2.18. Multi-spectral mosaic of the peach orchard acquired from the UAV platform (a) used to generate a map of fIPAR calculated from the FLIGHT model (b).

2.4. Conclusions

This work examines the relationship between canopy reflectance and instantaneous fIPAR in peach and citrus orchards using the 3-D radiative transfer FLIGHT model and measurements conducted with ground and remote instruments on board an unmanned aerial vehicle. Visible and NIR canopy reflectance and fIPAR simulations conducted with FLIGHT were assessed for these row-structured canopies, obtaining a RMSE below 0.03 for the visible bands, and below 0.05 for the NIR band. The main drivers of the relationship NDVI-fIPAR in these heterogeneous canopies were the background optical properties and the row orientation, both as a function of the sun geometry. The background reflectance had significant effects on the aggregated NDVI at midday, when the proportion of shaded soil is minimal. As a consequence, the NDVI-fIPAR relationships were independent of the row orientation at noon. It was demonstrated that the NDVI-fIPAR relationship changes as a function of the soil optical properties and row orientation, due to their large effects on NDVI in non-homogeneous orchard canopies.

This study demonstrated that a robust NDVI-fIPAR relationship can be obtained for row-structured peach and citrus orchards using 3D simulations when accounting for the soil optical properties, sun angles and row orientation. The proposed methods, based on *scaling-up* and model inversion techniques, may be applied to NDVI pixels acquired over heterogeneous orchards to obtain maps of instantaneous intercepted radiation. The methodology demonstrates the feasibility for estimating the spatial distribution of fIPAR in citrus and peach row-structured orchards, yielding RMSE below 0.10. The generation of high-resolution maps of the

intercepted radiation using multi-spectral cameras mounted on operational UAV platforms may be of critical interest for precision agriculture tasks such as the agronomic management of homogeneous zones and the discrimination of potential fruit quality areas for harvest.

Acknowledgements

Financial support from the Spanish Ministry of Science and Innovation (MCI) for the projects AGL2009-13105, CONSOLIDER CSD2006-67, and AGL2003-01468 is gratefully acknowledged, as well as the Junta de Andalucía-Excelencia AGR-595 and FEDER. M.L. Guillén-Climet was supported by a grant JAE of CSIC, co-funded by the *European Social Fund*. Technical support from the UAV Navigation and the Tetracam Inc. for the accommodation of airborne requirements are also acknowledged. M. Medina, A. Vera, D. Notario, L. Suárez, I. Calatrava, I. Moorthy, O. Pérez-Priego, V. González-Dugo, P. Cid, G. Sepulcre-Cantó and A. Soriano are acknowledged for scientific and technical support in field and airborne campaigns.

References

Alton, P.B., North, P.R., & Los, S.O. (2007). The impact of diffuse sunlight on canopy light-use efficiency, gross photosynthetic product and net ecosystem exchange in three forest biomes. Global Change Biology, 13, 1-12.

Asrar, G., Myneni, R.B. & Choudbhury, B.J. (1992). Spatial Heterogeneity in Vegetation Canopies and Remote Sensing of Absorbed Photosynthetically Active Radiation: A Modelling Study. Remote Sensing of Environment, 41, 85-103.

Barton, C.V.M. & North, P.R.J. (2001). Remote sensing of canopy light use efficiency using the photochemical reflectance index. Model and sensitivity analysis. Remote Sensing of Environment, 78, 264-273.

Berni, J.A.J., Zarco-Tejada, P.J., Suarez, L. & Fereres, E. (2009). Thermal and Narrow-band Multispectral Remote Sensing for Vegetation Monitoring from an Unmanned Aerial Vehicle. IEEE Transactions on Geoscience and Remote Sensing, 47, (3), 722-738.

Bouguet, J. (2001). Camera Calibration Toolbox for Matlab. (http://www.vision.caltech.edu/bouguetj/calib_doc). Last accessed January, 2012.

Choudhury, B.J. (1987). Relationships between vegetation indices, radiation absorption, and net photosynthesis evaluated by a sensitivity analysis, Remote Sensing of Environment, 22, 209-233.

Daughtry, C.S.T., Gallo, K.P., & Bauer, M.E. (1983). Spectral estimates of solar radiation by corn canopies, Agronomy Journal, 75, 527-531.

Daughtry, C.S.T., Gallo, K.P., Goward, S.N., Price, S.D. & Kustas, W.P. (1992). Spectral estimates of Absorbed Radiation and Phytomas Production in corn and soybean canopies, Remote Sensing of Environment, 39, 141-152.

De Wit, C.T. (1959). Potential photosynthesis of crop surfaces. Netherlands. The Journal of Agricultural Science, 7, 141-149.

Disney, M. I., Lewis, P. & North, P. R. J. (2000). Monte Carlo ray tracing in optical canopy reflectance modelling. Remote Sensing Reviews, 18 (2– 4), 163– 196.

Gallagher, J.N. & Biscoe, P.V. (1978). Radiation absorption, growth and yield of cereals. The Journal of Agricultural Science 91, 47–60.

Goward, S.N. & Huemmrich, K.F. (1992). Vegetation Canopy PAR Absorptance and the Normalized Difference Vegetation Index: An Assessment Using the SAIL Model. Remote Sensing of Environment, 39, 119-140.

Gueymard, C.A., 2005. SMARTS Code, Version 2.9.5 User's Manual Solar Consulting Services. Online PDF document from http://www.nrel.gov/rredc/smarts/ Last accessed January, 2012.

Hall, F.G., Huemmrich, K.F., Goetz, S.J., Sellers, P.J., & Nickerson, J.E. (1992). Satellite remote sensing of surface energy balance: success, failures, and unresolved issues in FIFE, Journal of Geophysical Results 97, 19,061-19,089

Huemmrich, K.F. & Goward, S.N., (1997). Vegetation canopy PAR Absorptance and NDVI: An Assessment for Ten Species with SAIL model. Remote Sensing of Environment, 61, 254-269.

Huemmrich, K.F. (2001). The GeoSail model: a simple addition to the SAIL model to describe discontinuous canopy reflectance. Remote Sensing of Environment, 75, 423-431.

Huete, A.R. (1989). Soil influences in remotely sensed vegetation canopy-spectra. Theory-Applications of Optical Remote Sensing (G.Asrar, Ed.), New York, Willey, 107-141.

Huete, A.R., Jackson, R.D. & Post, D.F. (1985). Spectral Response of a Plant Canopy with Different Soil Backgrounds. Remote Sensing of Environment, 17, 37-53.

Hunt, R.E., (1994). Relationship between woody biomass & PAR conversion efficiency for estimating net primary production from NDVI. International Journal Remote Sensing. 15, 1725–1730.

Jackson, J.E. (1980). Light Interception and Utilization by Orchard Systems. Horticultural Reviews, 2, 208-267.

Kempeneers, P., Zarco-Tejada, P. J., North, P. R. J., De Backer, S., Delalieux, S., Sepulcre-Cantó, G., Morales, F., Van Aardt, J. A. N., Sagardoy, R., Coppin, P. & Scheunders, P. (2008). Model inversion for chlorophyll estimation in open canopies from hyperspectral imagery. International Journal of Remote Sensing, 29(17-18), 5093-5111.

Koetz, B., Baret, F.,Poilvé, H., & Hill, J. (2005). Use of coupled canopy structure dynamic and radiative transfer models to estimate biophysical canopy characteristics. Remote Sensing of Environment, 95 (1) 115-124.

Lang, A.R.G., Xiang, Y. & Norman, J.M., (1985). Crop structure and the penetration of direct sunlight. Agricultural and Forest Meteorology. 35: 8-101.

Lang, A.R.G., (1987). Simplified estimate of leaf area index from transmittance of the sun's beam. Agricultural and Forest Meteorology. 41: 186-179.

Lemeur, R., (1973). A method for simulating the direct solar radiation regime in sunflower, Jerusalen artichoke, corn and soybean canopies using actual stand structure data. Agricultural and Forest Meteorology. 12, 229-247.

Li-Cor Inc. (1984). Li-Cor model 1800-12 integrating sphere instruction manual (Revision 1984). Li-Cor Incorporated, 4421 Superior Street, PO Box 4425 Lincoln Nebraska, USA, Publication No. 8305-0034.

Loomis, R.S. & Williams, W.A. (1963). Maximum crop productivity: An estimate. Crop Science 3, 67-72.

Mariscal, M.J., Orgaz, F. & Villalobos, F.J. (2000). Modelling and measurement of radiation interception by olive canopies. Agricultural and Forest Meteorology, 100 (183-197).

Monteith, J.L., (1972). Solar radiation and productivity in tropical ecosystems. Journal of Applied Ecology. 9, 747-766.

Moriondo, M., Maselli, F.& Bindi, M. (2007). A simple model of regional wheat yield based on NDVI data. European Journal of Agronomy, 26, 266–274.

Myneni, R.B. & Williams, D.L. (1994). On the Relationships between FAPAR and NDVI. Remote Sensing of Environment, 49, 200-211.

Moran, M.S., Inoue, Y. & Barmes, E.M. (1997). Opportunities and limitations for image-based remote sensing in precision crop management. Remote Sensing of Environment, 61 (3), 319-346.

North. P.R.J. (1996). Three-Dimensional Forest Light Interaction Model Using a Monte Carlo Method. IEEE Transaction on Geoscience and Remote Sensing, 34, (4), 946-956.

North. P.R.J. (2002). Estimation of f_{APAR}, LAI, and vegetation fractional cover from ATSR-2 imagery. Remote Sensing of Environment, 80, 114-121.

Pinty, B., Widlowski, J.L., Gobron, N. & Verstraete, M.M, (2002). Uniqueness of multi-angular information—Part 1: A surface heterogeneity indicator from MISR. IEEE Transactions on Geosciences and Remote Sensing, 40**,** 1560–1573.

Prieto-Blanco, A., North, P.R.J., Barnsley, M.J. & Fox, N. (2009). Satellite-driven modelling of Net Primary Productivity (NPP): Theoretical analysis. Remote Sensing of Environment, 113, 137-147.

Robinson, T. & Lakso, A., (1991). Bases of Yield and Production Efficiency in Apple Orchard System. Journal American. Society Horticulture. Science, 116(2) 188-194.

Ross, J., (1981). The Radiation Regime and Architecture of Plant Stands. W. Junk, The Hague, The Netherlands.

Suárez, L., Zarco-Tejada, P.J., Berni, J.A.J., González-Dugo, V. & Fereres, E. (2009). Modelling PRI for Water Stress Detection using Radiative Transfer Models. Remote Sensing of Environment, 113, 730-744.

Suárez, L., Zarco-Tejada, P.J., González-Dugo, V., Berni, J.A.J.,Sagardoy, R., Morales, F. & Fereres, E. (2010). Detecting water stress effects on fruit quality in orchards with time-serie PRI airborne imagery. Remote Sensing of Environment, 114, 286-298.

Villalobos, F.J., Orgaz, F. & Mateos, L. (1995). Non-destructive measurement of leaf area in olive (Olea europaea L.) trees using a gap inversion method. Agricultural and Forest Meteorology, 73, 29-42.

Weiss, M., Baret, F., Myneni, R.B., Pragnère, A. & Knyazikhin, Y. (2000). Investigation of a model inversion technique to estimate canopy biophysical variables from spectral and directional reflectance data. Agronomie, 20 (1) 3-22.

Widlowski, J-L., Taberner, M., Pinty, B., Bruniquel-Pinel, V., Disney, M., Fernandez, R., Gastellu-Etchegorry, J-P., Gobron, N., Kuusk, A., Lavergne, T., Leblanc, S., Lewis, P.E., Martin, E., Mottus, M., North, P.R.J., Quin, W., Robustelli, M., Rochdi, N., Ruiloba, R., Soler, C., Thompson, R., Verhoef, W., Verstraete, M.M. & Xie, D. (2007). Third Radiation transfer Model Intercomparison (RAMI) exercise: Documenting progress in canopy reflectance models. Journal of Geophysical Research, 112, D09111.

Widlowski, J-L., Pinty, B., Disney, M., Gastellu-Etchegorry, J-P., Lavergne, T., Lewis, P.E., North, P. R. J., Robustelli, M., Thompson, R. & Verstraete, M.M., (2008). The RAMI on-line model checker (ROMC): a web-based benchmarking facility for canopy reflectance models. Remote Sensing of Environment 112(3), pp.1144-1150.

Widlowski, J-L. (2010) On the bias of instantaneous FAPAR estimates in open-canopy forests. Agricultural and Forest Meteorology 150, 1501-1522.

Zarco-Tejada, P.J., Berjón, A., López-Lozano, R., Miller, J.R., Martín, P., Cachorro, V., González, M.R. & Frutos, A. (2005), Assessing Vineyard Condition with Hyperspectral Indices: Leaf & Canopy Reflectance Simulation in a Row-Structured Discontinuous Canopy. Remote Sensing of Environment, 99, 271-287.

Zarco-Tejada, P.J., Berni, J.A.J., Suárez, L. & Fereres, E. (2008). A new era in remote sensing of crops with unmanned robots. SPIE Newsroom, doi:10.1117/2.1200812.1438.

Zarco-Tejada, P.J., González Dugo, V. & Berni, J.A.J. (2012). Fluorescence, temperatura and narrow-band indices acquired from a UAV platform for water stress detection using a micro-hyperspectral imager and a thermal camera, *Remote Sensing of Environment*, 117, 322-337.

Zhang, Q., Middleton, E.M., Margolis, H.A., Drolet, G.G., Barr, A.A. & Black, T.A. (2009). Can a satellite-derived estimate of the fraction of PAR absorbed by chlorophyll ($FAPAR_{chl}$) improve predictions of light-use efficiency and ecosystem photosynthesis for a boreal aspen forest? Remote Sensing of Environment, 113, 880-888.

3. Mapping radiation interception in an olive orchard using a physical models and airborne imagery

"...
¡Viejos olivos sedientos
bajo el claro sol del día,
olivares polvorientos
del campo de Andalucía!
¡El campo andaluz, peinado
por el sol canicular,
de loma en loma rayado
de olivar y de olivar!
..."

Machado, A. (Los olivos)

Chapter 3

Mapping radiation interception in an olive orchard using a physical model and airborne imagery.

Abstract

This study was conducted to estimate the fraction of Intercepted Photosinthetically Active Radiation (fIPAR) in an olive orchard. The method proposed to estimate fIPAR in olive canopies consisted on a coupled radiative transfer model which linked the 3-D *Forest Light Interaction Model* (FLIGHT) and the *Orchard Radiation Interception Model* (ORIM). Methods to assess the estimation of instantaneous fIPAR as a function of planting grids, percentage cover and soil effects were conducted. The linked model was tested against field measurements of fIPAR acquired on a commercial olive orchard, where study plots showing a gradient in the canopy structure and percentage cover were selected. High-resolution airborne multispectral imagery was acquired at 10 nm bandwidth and 15-cm spatial resolution, and the reflectance used to calculate vegetation indices from each study site. In addition, simulations of the land surface bidirectional reflectance were conducted to understand the relationships between canopy architecture and fIPAR on typical olive orchard planting patterns. Input parameters used for the canopy model, such as the leaf and soil optical properties, the architecture of the canopy, and sun geometry were studied in order to assess the effect of these inputs on the vegetation index NDVI and fIPAR relationships. FLIGHT and ORIM models were independently assessed for fIPAR estimation using structural and ceptometer field data collected from each study site, yielding RMSE values of 0.1 for the FLIGHT model, while the specific olive simulation model by ORIM yielded lower errors (RMSE=0.05). The reflectance simulations conducted as a function of the orchard architecture suggested the usefulness of the modeling methods for this heterogeneous olive crop, and the high sensitivity of the *Normalized Difference Vegetation Index* (NDVI) and fIPAR to background, percentage cover and sun geometry on these heterogeneous orchard canopies. The fIPAR estimations obtained from the airborne imagery through scaling-up yielded RMSE error values of 0.11 when using FLIGHT to simulate both the canopy reflectance and the fIPAR of the study sites. The coupled FLIGHT+ORIM model yielded better results, obtaining RMSE=0.05 when using airborne remote sensing imagery to estimate fIPAR.

Keywords: Olive orchards, remote sensing, fIPAR estimation, radiative transfer modeling

3.1 Introduction

The olive industry have experimented several major technological changes during the last two decades (Villalobos et al., 2006). Traditional olive cultivation, grown in rain-fed condition with low density (80-90 olive trees/ha), have been very well adapted and able to survive periods of intense drought with acceptable production (Fernandes-Silva et al., 2010; Pastor et al., 2007). Nevertheless, such traditional olive orchards are being substituted by new intensive, drip irrigated and fertilized plantation for high early yields (Beede and Goldhammer, 1994; Villalobos et al., 2006; Pastor et al., 2007). This transition requires a better understanding of the olive orchard, including longer term effects of these structural changes to better adapt the required management for these canopies. Therefore, the interest in the research community for the olive tree cultivation and management practices is growing considering the historical importance of this crop throughout the Mediterranean countries (Ben-Gal et al., 2011; Vossen, 2007). A comprehensive review of scientific research in olive crops can be found in Connor and Fereres (2005). In such study, the authors emphasized that future research should prioritize studies of olive trees as a whole, rather than just leaf-level analyses. Subsequent studies conducted in olive orchards have focused on optimizing water use at tree level (Testi et al., 2006; Orgaz et al., 2007; Iniesta et al., 2009; Fernandes-Silva et al., 2010), optimizing the tree density (Pastor et al., 2007), or determining biophysical parameters (Gómez et al., 2011). Some of these studies used the *Orchard Radiation Interception Model* (ORIM) to estimate the fIPAR in olive orchards (Mariscal *et al*., 2000). The rationale is that a first step in productivity assessment is the estimation of radiation interception (Connor and Fereres, 2005), therefore

requiring simulation models to quantify the relationships with the orchard architecture. In fact, biomass production is directly related to the intercepted radiation (Monteith, 1977), and this has been shown to be true for olive canopies (Mariscal et al., 2000). Therefore, the use of crop simulation models is required as a consequence of the wide variability and complexity of these canopies (Villalobos et al., 2006). The field measurements of IPAR and/or the related fraction of intercepted PAR (fIPAR) would be inefficient and time consuming in these orchards. The large variation that olive orchards show in tree dimensions, canopy architecture and ground cover are consequence of the transformation from rain-fed to irrigation schemes, with high density in areas of chronic water shortages (Testi et al., 2006). Moreover, olive tree orchards are grown as horizontally non-homogeneous canopies, and the amount of PAR intercepted is defined by the combination of tree spacing (row and inter-row), tree height, row orientation, vertical projection of the canopy cover and canopy volume (Connor and Fereres, 2005). In this context, along with radiative transfer modelling efforts, remote sensing methods are useful for the assessment of large areas and to map the within-field and between orchard spatial variability of biophysical parameters.

This study is focused on the estimation of the intercepted photosynthetically active radiation (IPAR) in olive orchards using remote sensing imagery and radiative transfer modelling methods. It was emphasized in the previous chapter that in other studies, empirical and modelled relationships between vegetation indices and fIPAR have been developed for homogeneous canopies, such as wheat, maize or soybean crops (e.g., Daughtry et al., 1983; Asrar et al., 1984; Wiegand et al., 1991; Hall et al., 1992 and Moriondo et al., 2007) and forest canopies (e.g.,

Myneni and Williams, 1994; Roujean and Breon, 1995; Huemmrich and Goward, 1997; Huemmrich, 2001; De Castro and Fetcher, 1998; and Zhang et al., 2009). With the development of 3-D canopy reflectance models, the sensitivity of these relationships between vegetation indices and the fraction of PAR, absorbed or intercepted, can be investigated considering architectural characteristics of the canopy. However, these studies focused on herbaceous crops and closed-canopy forestry areas are not applicable to non-homogeneous, open-canopy olive orchards. A first step to model the implications of the structure on the instantaneous fIPAR requires appropriate simulation methods to account for the canopy optical properties and background. In fact, previous works indicated that the use of radiative transfer models capable of handling row orientations is a requisite for remote sensing in horticulture (Stuckens et al., 2009; Kempeneers et al., 2008). Along these efforts, radiative transfer models that aim at deriving the amount and distribution of fIPAR in non-homogeneous crop canopies have been reviewed by Mariscal et al. (2000) who developed a model to simulate fIPAR in olive orchard canopies. The 3-D Forest Light Interaction Model (FLIGHT) (North, 1996) was proposed to estimate fAPAR in forest canopies (North, 2002 and Prieto-Blanco et al., 2009), and more recently in orange and peach canopies (chapter 2). While methods for modeling and estimating fIPAR in homogenous vegetation are relatively mature (Mariscal et al., 2000), further research is needed for robust estimate of fIPAR in open canopies. The objectives of this study were: (i) to evaluate modelling strategies to asses the estimation of instantaneous fIPAR in olive orchards; and, (ii) to use remote sensing imagery and modeling methods to estimate instantaneous fIPAR in olive canopies using visible (VIS) and near-infrared

(NIR) bands, as well as to generate a maps of the spatial variability of fIPAR.

3.2. Materials and Methods

3.2.1. Study area

The experimental field was located at "La Conchuela" farm, Córdoba, Spain (37º 48'N, 4º 48'W) at 147 m above sea level. The olive orchard was planted in 1993 with trees at 6 m x 7 m spacing (238 tree ha^{-1}) with rows oriented 64º from North. Figure 3.1 shows six of the eight plots selected for the ground measurements. They were selected to ensure a gradient in fraction of vegetation cover, ranging between 30% and 60%. The study sites comprised a range of crown leaf area densities (LAD) ranging from 0.45 to 1.02, tree heights between 3.5 and 5.2 m, and horizontal crown diameters between 1.8 and 2.9 m (Figure 3.1 and Table 3.1). The field campaign was conducted in summer 2008. The ground measurements were conducted on the selected plots coincident with the airborne flight campaigns.

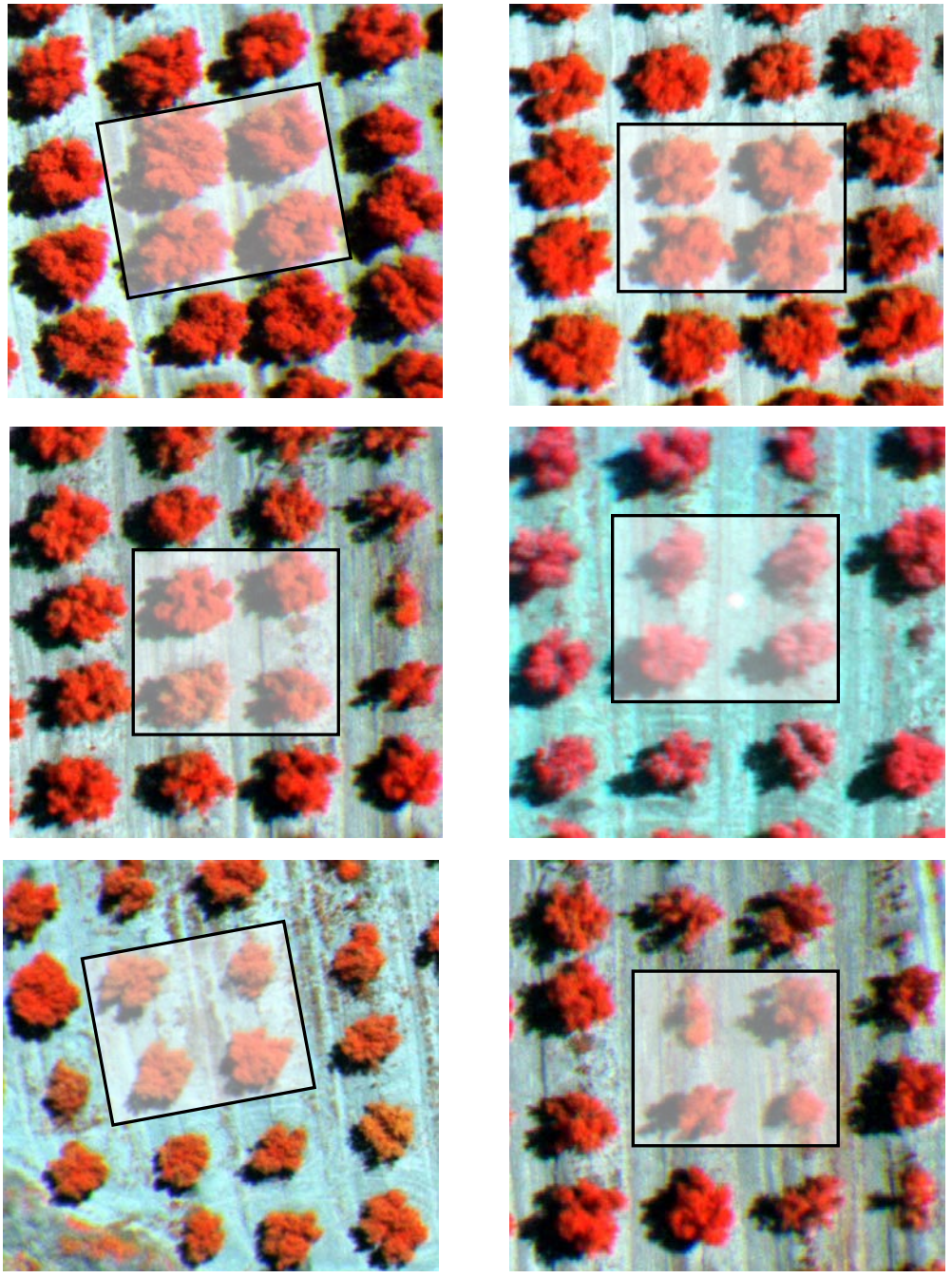

Figure 3.1. Multispectral reflectance images acquired at 10 nm FWHM and 15 cm spatial resolution, showing six study plots used in the study. The central block area of 4 trees selected on each study site for field data collection is shown.

Table 3.1. Structural data collected from each study area.

Stand	*Crown radio (m)*	*Tree height (m)*	*LAD (m^2m^{-3})*	*LAI (m^2m^{-2})*	*Fraction of vegetation fraction (%)*
1	2.3	4.4	0.54	0.57	39.5
2	1.8	3.5	1.02	0.6	24.2
3	2.9	5.2	0.43	0.9	63
4	2.0	4.1	0.62	0.5	30
5	2.8	4.9	0.45	0.8	58.6
6	2.1	3.8	0.97	0.9	33
7	2.5	4.0	0.56	0.7	46.7
8	2.3	4.0	0.54	0.6	39.5
Planting grid: 7 m x 6 m					

3.2.2 Ground and remote sensing airborne campaigns

Field campaigns were conducted for both airborne imagery acquisition and intercepted PAR field measurements collected to asses the effects of the variability of the intercepted solar radiation and reflectance bands as a function of orchard architecture. The interception of solar radiation by the orchard canopy on each study site was measured with a ceptometer (SunScan Canopy Analysis System, Delta-T Devices Ltd, Cambridge, UK). The instrument comprises two units, as it was detailed in previous chapter: (i) a probe, portable instrument of 1-m long, for measuring the transmitted photosynthetically active radiation (PAR) flux beneath the canopy; and (ii) a beam fraction sensor (BFS) that measures PAR incident over the canopy at the same time. Therefore, the area comprising the 4 central trees of each study area was selected to conduct the field measurements of fIPAR. The measurements of transmitted PAR made in the area beneath the four central trees of each plot were in a 1 m x 0.5 m grid. A schematic view is shown in Figure 3.2a, and the actual measurements for two study areas are depicted in Figure 3.2b. For the assessment of the spatial variation of fIPAR among the different selected plots with a gradient in structural parameters, measurements were conducted at 10.00 GMT (+/- half-hour).

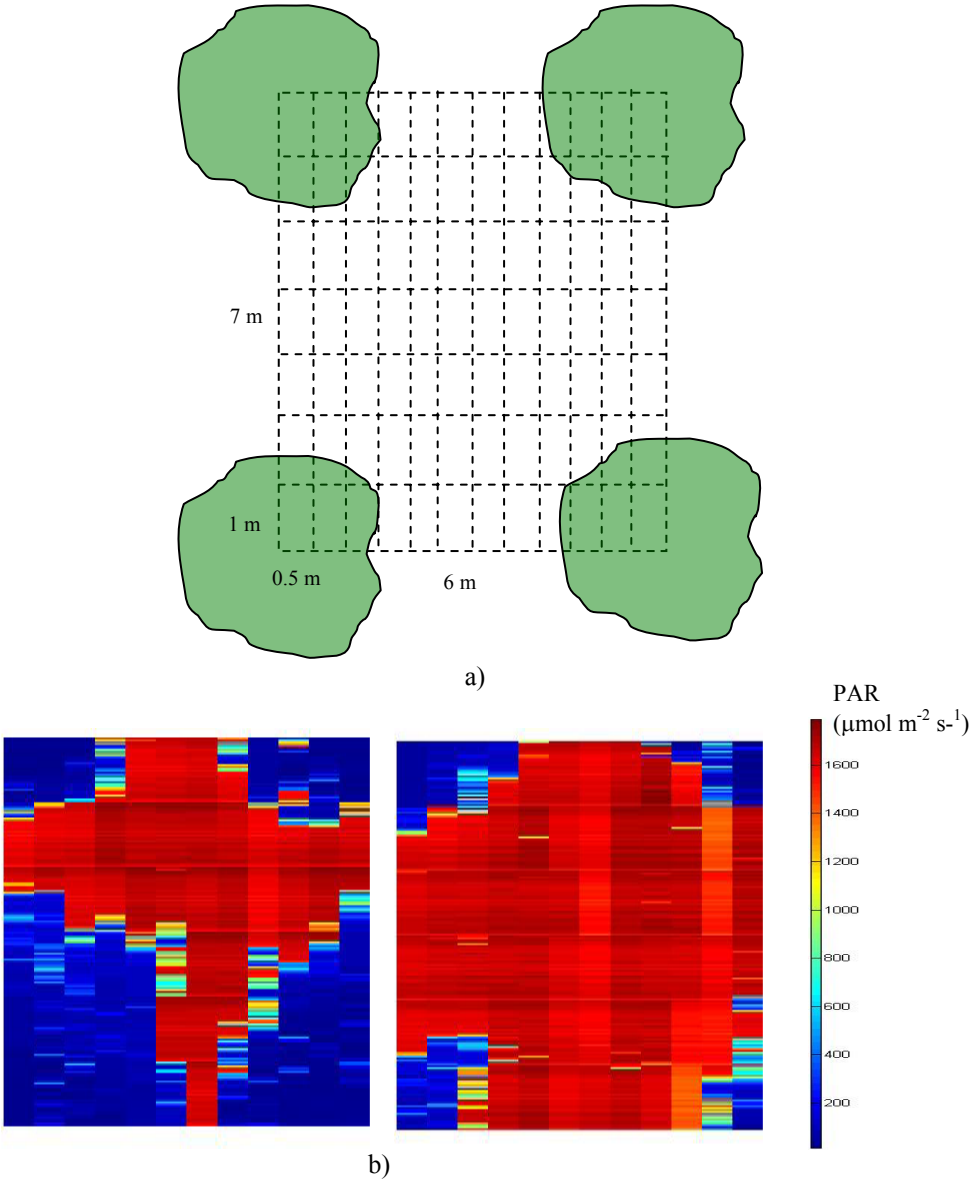

Figure 3.2. Schematic view of the 1 m x 0.5 m grid used for field measurements conducted with the ceptometer (a); PAR data measured by ceptometer at the ground level (b).

Additional ground-level efforts were made to collect in situ measurements of crown structure, leaf and soil optical properties to characterize the different study plot and used as input for the models. Dimensional properties, namely crown height and crown width, were

measured at multiple points within a given olive tree. The crown was divided into eight sections, in each one the tree silhouette was estimated by measuring the upper and lower limits of the canopy with a vertical scaled pole which was systematically moved away from the tree centre outwards in 0.2 m increments (Villalobos et al., 1995). In addition to in situ measurements of crown dimensions, the LAI-2000 Plant Canopy Analyzer (PCA) was used to estimate leaf area index at the individual crown level used before in olive canopies by Villalobos et al (1995) and more recently Moorthy et al. (2011) and Gómez et al. (2011). This device measured the fraction of diffuse incident radiation transmitted through a plant canopy by calculating the ratio of the below and above-canopy radiation measurements. It has a set of optical sensors that simultaneously measure diffuse radiation in five range of zenith angles (this methodology is described in detail in Gómez et al., 2011).The leaf angle distribution function used was the ones measured by Mariscal et al. (2000) in adult trees (Figure 3.2).

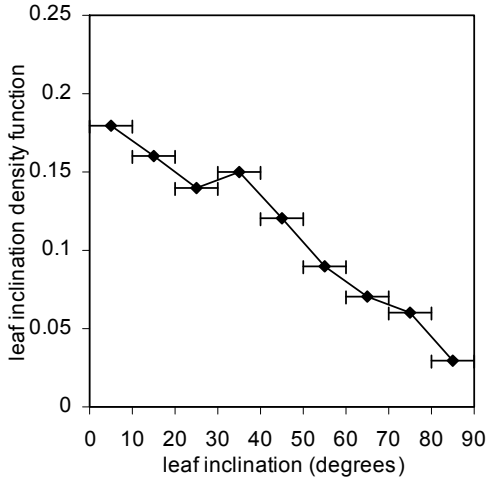

Figure 3.3 Leaf angle distribution function in 10º intervals measured for olive adults trees (Mariscal et al., 2000).

The multispectral sensor used in this study was a 6-band multispectral camera (MCA-6, Tetracam Inc., California, USA). The sensor was on board an unmanned aerial vehicle (UAV) as it was specified in previous chapter. Also details about the camera are described in chapter 2. High resolution multispectral images acquired over the olive orchards enabled the identification of each study site used for field measurements of crop structure and fIPAR. The plots were marked in the field using bright ground control points easily detectable on the imagery. The bandsets selected for this study comprised centre wavelengths at 670 and 800 nm with 10 nm full width at half maximum (FWHM) used for computing the *Normalized Difference Vegetation Index* (NDVI) and bands centered at 490, 530, 570 and 700 nm to compute other spectral indices such as the *Photochemical Reflectance Index* (PRI) for stress detection studies, and the red edge for chlorophyll estimation. Figure 3.1 shows the imagery acquired by the multispectral airborne sensor at 15 cm spatial resolution, representing six fields used in this study with a range in fraction of vegetation cover, and the block of 4-trees selected on each study site for field data collection of radiation interception. The high spatial resolution acquired enabled targeting pure scene components, such as pure soil and vegetation, separately as well as on aggregated pixels. Atmospheric correction and radiometric calibration methods were applied to the imagery to calculate the spectral reflectance. These methods are explained previously in chapter 2.

Leaf optical properties, reflectance and transmittance measurements, were acquired on leaf samples using an Integrating Sphere (Li-Cor 1800-12, Inc., Lincoln, NE, USA), coupled with a 200-μm diameter single mode fibre to a spectrometer (Ocean Optics Inc. model USB2000, Dunedin, FL, USA), with a 1024 element detector array, 0.5 nm sampling interval, and 7.5 nm

spectral resolution in the 340-940 nm range. The single leaf values for reflectance (ρ) and transmittance (τ) were acquired as described in the manual of the Li-Cor 1800-12 system (Li-Cor, 1983) and in Zarco-Tejada et al. (2005), using a custom-made port of 0.5 cm diameter suited to typical olive leaf dimensions and thereby obtaining the leaf optical properties. A total of 300 leaves were sampled**.** Figure 3.4a shows the mean leaf reflectance and transmittance measured on olive leaves. The spectral range for the leaf optical properties used as input for the models was selected according to the bandset used in the airborne imagery (Figure 3.4b). Sunlit soil reflectance was extracted from the airborne imagery (Figure 3.5).

Table 3.1 and Figure 3.3, Figure 3.4 and Figure 3.5 show the field measurements collected on each study site. They will be later used as inputs for the 3D canopy modelling work conducted with FLIGHT on the aggregated reflectance and fIPAR estimation, as well as for the ORIM model. Table 3.2 shows the input parameters required by these models.

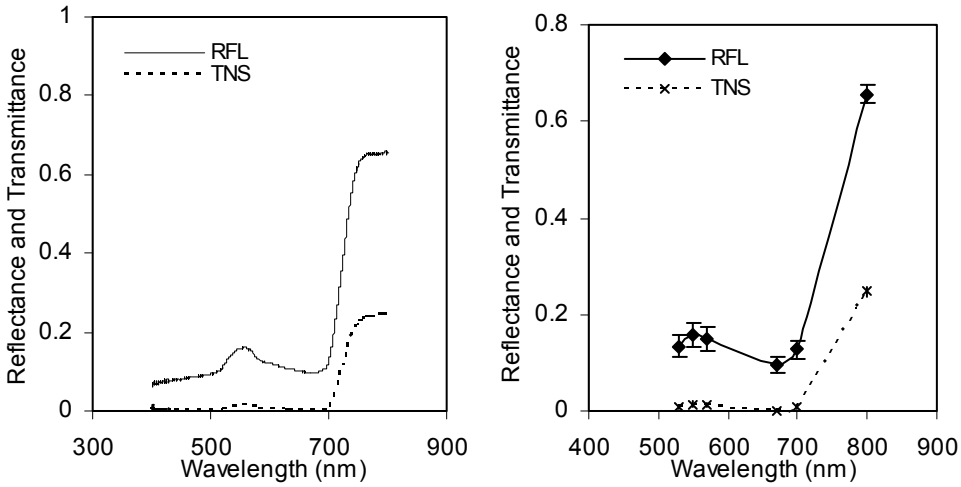

Figure 3.4. Reflectance and transmittance spectra measured by integrating sphere for olive leaves (a); reflectance and transmittance spectra for the olive leaves with the bandset used in this study (b).

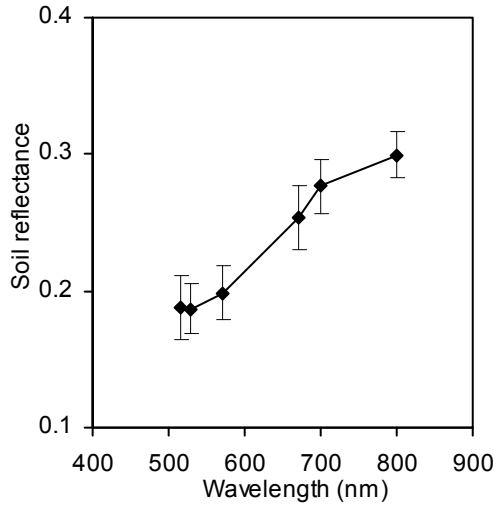

Figure 3.5. Soil optical properties of the study area.

Table 3.2. Nominal values and range of parameters used for canopy modelling with FLIGHT and ORIM models.

FLIGHT model. Input parameters	**Values /Unit used**
Leaf optical and structural parameters	
Hemispherical reflectance and transmittance of green leaves	Integrating Sphere
Hemispherical reflectance and transmittance of senescent leaves	Not used
Leaf equivalent radius	m
Canopy layer and structural parameters	
Leaf area index of vegetation	See table 3.1
Fractional cover	30 – 60 %
Leaf angle distribution function	Empirical
Fraction green leaves	1
Fraction senescent leaves	0
Fraction of bark	0
Hemispherical reflectance and transmittance of bark	Not used
Number of stands and position coordinates	Coord. (m)
Crown shape	Elliptical
Crown height and radius	m (see table 3.1)
Trunk height and radius	m (see table 3.1)
Background and viewing imagery geometry	
Solar zenith and azimuth angles	Degrees
Sensor zenith and azimuth angles	Degrees
Soil reflectance	From image
Soil roughness	0
Aerosol optical depth (AOD)	0.15
ORIM model. Input parameters	**Values /Unit used**
Crown height and radius	m
Planting pattern	m x m
LAD (leaf area density)	$m^2 m^{-3}$
Row and column angles	Degrees
Soil PAR reflectance	From image
Latitude	37.8° N
Internal parameters	
G-function	measured *(Mariscal et al., 2000)*
Leaf reflectance and transmittance	measured *(Mariscal et al., 2000)*

3.2.3. fIPAR estimation in olive orchards from remote sensing data

3.2.3.1. FLIGHT and ORIM models for simulating fIPAR in olive orchards

Two models are proposed in this manuscript to estimate fIPAR in olive orchards: a 3-D model of light interaction with vegetation canopies FLIGHT (North, 1996) and ORIM (Mariscal et al., 2000) a model of PAR interception by olives canopies. The FLIGHT model is based on the Monte Carlo ray tracing method as a tool to simulate the radiative transfer in a canopy structure (North, 1996). In the FLIGHT model, an accurate treatment of the light interception and multiple scattering between foliage elements and soil boundary is obtained by iteration (North, 2002). In this study, FLIGHT was selected because it allowed the simulation of row orientations, tree dimensions, soil background effects, making easily to generate several 3D scenes for the assessment of the effects of the architecture, crown structure and biochemical inputs. This model has been previously used in other work simulating row-orientated orchards, such as orange and peach, with successful results (Suárez et al., 2009, 2010; and chapter 2). The FLIGHT model inputs consist of: (i) geometric characteristics (ii) optical properties; (iii) sun and view azimuth and zenith angles; and (iv) other parameters such as soil roughness, aerosol optical thickness and the number of photons simulated. Table 3.2 shows the input parameters required to run the model. The output of FLIGHT is a 3D hyperspectral image and the estimated intercepted PAR (*IPAR*) for the scene.

The ORIM model is reliable for estimating radiation intercepted by any olive orchard at instantaneous and daily levels (Mariscal et al., 2000). The model works at an hourly time step, integrating the radiation reaching a convenient number of spatial cells. It was later modified to obtain a

simplified PAR interception model for practical purposes with daily time steps (Orgaz et al., 2007). This model allows simulating row orientation, tree dimensions and slope of the field. It has been used by Iniesta et al. (2009) and Fernandes-Silva et al. (2010), among others, to estimate the amount of annual IPAR. The inputs required by ORIM are the planting pattern, row and column angles, soil PAR reflectance, latitude, height, tree perpendicular radii of the crown, and leaf area density (LAD) (Table 3.2). Leaf reflectance and transmittance, and *G-function* are internal parameters calculated for olive trees. ORIM model outputs are estimations of all the components of the radiation balance for hourly, daily and seasonal periods.

A detailed simulation of fIPAR was undertaken to assess the performance of both FLIGHT and ORIM models for this type of row-tree structure olive canopies. The study areas were simulated using the structural and optical measurements collected at each plot (see Figure 3.3, Figure 3.4 and Figure 3.5 for leaf angle distribution function and the leaf and soil optical properties, and Table 3.1 for the structural measurements used). Model assessment for the fIPAR simulations was conducted by comparing the modelled fIPAR obtained from each model against the ceptometer measurements acquired on each plot, calculating the RMSE obtained. Once the two models were assessed for fIPAR estimation from field datasets, a second step consisted on testing each model for fIPAR estimation on all plots from the airborne remote sensing imagery acquired. This second assessment was carried out with predictive relationships developed between NDVI and fIPAR obtained through modelling; two methods were used (i) obtaining the canopy reflectance and fIPAR from FLIGHT; (ii) using simulated canopy reflectance from FLIGHT coupled with ORIM model (FLIGHT + ORIM). Therefore, FLIGHT and ORIM models were assessed

for their capability to estimate fIPAR both from field data and airborne imagery (Figure 3.6). The aggregated image reflectance from the four central trees of the orchard, including exposed soil and shadows, was used to compute spectral vegetation indices, such as NDVI.

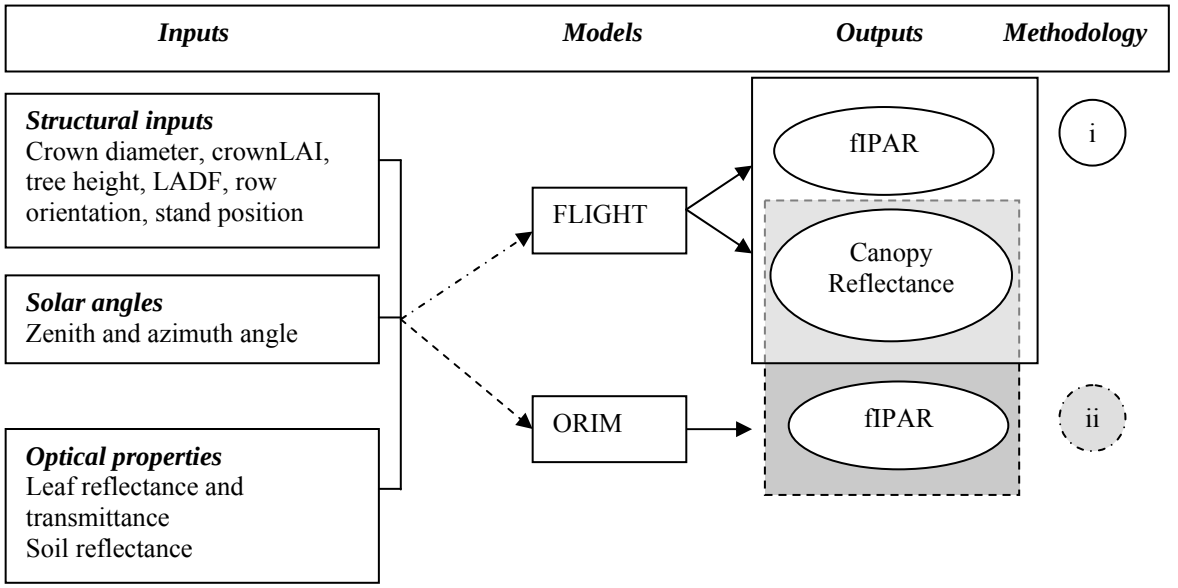

Figure 3.6. Schematic view of the coupling method between FLIGHT and ORIM models to develop predictive relationships between NDVI and fIPAR.

Previous to the estimation of fIPAR using airborne remote sensing imagery, a study was carried out with modelling methods to understand the influence of the architecture of the canopy on aggregated NDVI and fIPAR. The fraction of vegetation cover was varied from 20 to 60 % for three different solar angles (*solar zeniths 70.9º; 43.1º and 29.6º*) and two types of soil reflectance spectra were used to study their effects on NDVI and fIPAR.

3.2.3.2 fIPAR estimation from remote sensing imagery using modelling methods

Relationships between NDVI and fIPAR were developed to estimate the instantaneous fIPAR in the olive orchards using the airborne imagery acquired on each study site using pixels that integrated each study site. In particular, the objective was to develop predictive relationships NDVI-fIPAR calculated under specific canopy assumptions valid for the study sites under study. These relationships were obtained (i) with FLIGHT; (ii) with the canopy reflectance module from FLIGHT linked to the *ORIM* fIPAR estimation model (Figure 3.6).

The fIPAR predictive relationships for the olive canopies were developed with input parameters fixed according to mean field measurements: leaf angle distribution function, leaf optical properties, planting grid and soil reflectance extracted from the airborne image, and the solar geometry depending on the time of flight. The specific input parameters varied within the typical range of variation for these orchards to account for the canopy structure. In the case of crown radii variation was 0.5 to 3 m, tree height ranged from 2 to 6 m, and LAI from 0.1 to 1 (Table 3.3). The modeled relationships NDVI vs fIPAR obtained for each study plot were then applied to the multispectral airborne imagery reflectance to estimate the instantaneous fIPAR for each study site. Relationships were obtained for the olive orchard with both model approaches: i) FLIGHT; and ii) FLIGHT + ORIM (Figure 3.6). This methodology enabled the application of sensor-derived optical indices for NDVI-fIPAR that are a function of canopy structure, optical properties and the viewing geometry. Relationships between vegetation indices and fIPAR have been suggested in previous works, mainly in studies dedicated to herbaceous crop or forest canopy. To

assess the behaviour on heterogeneous open-tree orchards of these relationships originally developed for homogeneous canopies, a relationship by Myneni and Williams (1994) (fAPAR = 1.1638*NDVI – 0.1426) was applied to the study plots selected on this work, and the error obtained was calculated.

Table 3.3: Inputs used to generate predictive fIPAR-NDVI algorithms. Determination coefficients and RMSE values obtained between the ground-measured fIPAR and the estimated fIPAR from FLIGHT and FLIGHT + ORIM.

Inputs parameters for predictive relationships NDVI vs fIPAR		
Fixed parameters	LADF	Measured (figure 3.3)
	Leaf (ρ and τ)	Measured (figure 3.4b)
	Row orientation	63º from North
	Sun geometry	SZ:35.02º; SA:69.5º
	Soil (ρ_s)	Obtained from image (figure 3.5)
Variable parameters	Tree radius (m)	0.5 – 3
	Tree height (m)	2 – 6
	LAI	0.1 – 1

Results	r^2 ;*(RMSE)*
FLIGHT	0.85; 0.11
FLIGHT + ORIM	0.83; 0.05

SZ: solar zenith (degrees from the North)
SA: solar azimuth (degrees from South, clockwise negative)

3.3. Results

3.3.1 Results for fIPAR estimation from FLIGHT and ORIM models

The simulations corresponding with the different study plots in the olive orchard were assessed with both models to evaluate the correspondence of the simulations with fIPAR field measurements. Figure 3.7 illustrates four scenarios corresponding with four different study plots in the olive orchard. Error assessments conducted for fIPAR estimated with FLIGHT and ORIM models using ceptometer field data are shown in Figur 3.8a and Figure 3.8b, respectively. The estimation of fIPAR yielded RMSE=0.10 with coefficient

of determination of r^2=0.5 when using FLIGHT, and RMSE=0.05, r^2=0.81 for ORIM simulations. The ORIM model therefore yielded better results than FLIGHT for simulating fIPAR from field-measured architectural and structural parameters in olive canopies. The simulations conducted with FLIGHT and ORIM models to assess the sensitivity of the input parameters, such as fraction of vegetation cover, sun angles and the soil reflectance on NDVI and fIPAR were investigated generating canopy scenarios (Figure 3.9a for NDVI, and Figure 3.9b for fIPAR). It is observed from Figure 3.9a and Figure 3.9b the larger effect of soil optical properties on the aggregated NDVI than in fIPAR estimates. In scenes with 60% vegetation cover and solar zenith angle 43.1º, NDVI varied from 0.53 for a dark soil to 0.43 for a bright soil, while fIPAR for the same canopy scenario changed only from 0.50 to 0.48. The large soil reflectance variation largely affects the NDVI vs fIPAR relationship as a function of the background. The solar angle showed to have effects on both fIPAR and NDVI, as expected. For a north-south rectangular planting grid orchard, the intercepted PAR was higher at high zenith angles: fIPAR varied from 0.7 in the morning (*sz=70.9º*) to 0.4 at midday (*sz=43.1º*) for a 60% vegetation cover and dark soil (Figure 3.9b). The differences found in NDVI for different solar angles were caused also by the soil reflectance and the amount of shadows; nevertheless the effect was smaller than in fIPAR. NDVI varied from 0.5 to 0.4 for a 60% vegetation cover and dark soil, and from 0.62 to 0.48 in a bright soil (Figure 3.9a). The study showed that NDVI vs fIPAR relationships cannot be readily applied to open canopy orchards due to the large effects caused by parameters such as soil reflectance and sun angle, and appropriate modelling techniques are needed to develop accurate relationships for the fIPAR estimation in these orchards.

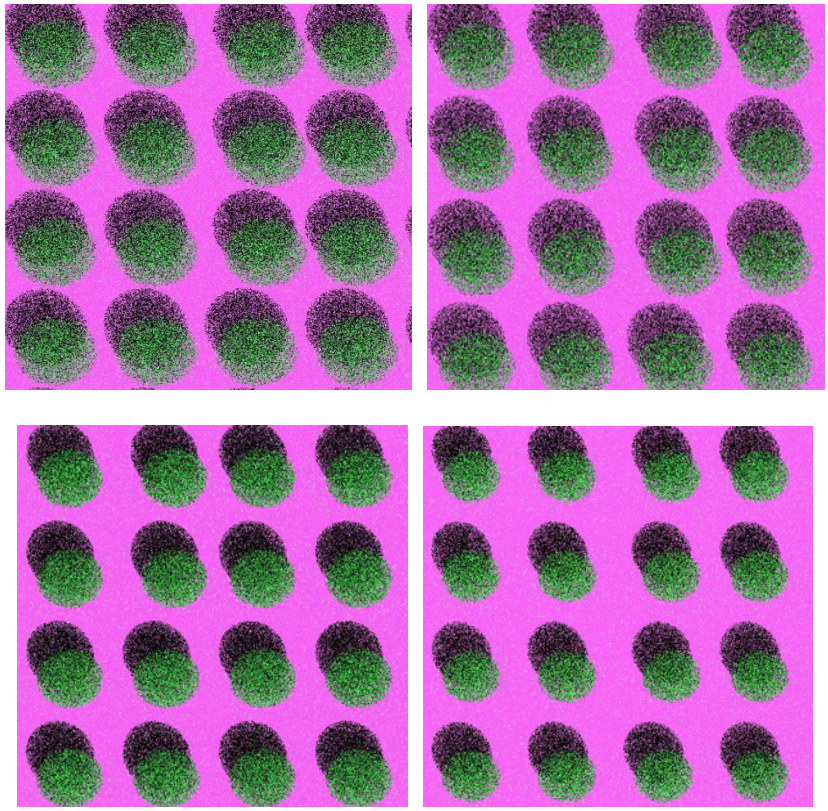

Figure 3.7. Model simulations conducted with FLIGHT to generate orchard scenes for different fractions of vegetation cover.

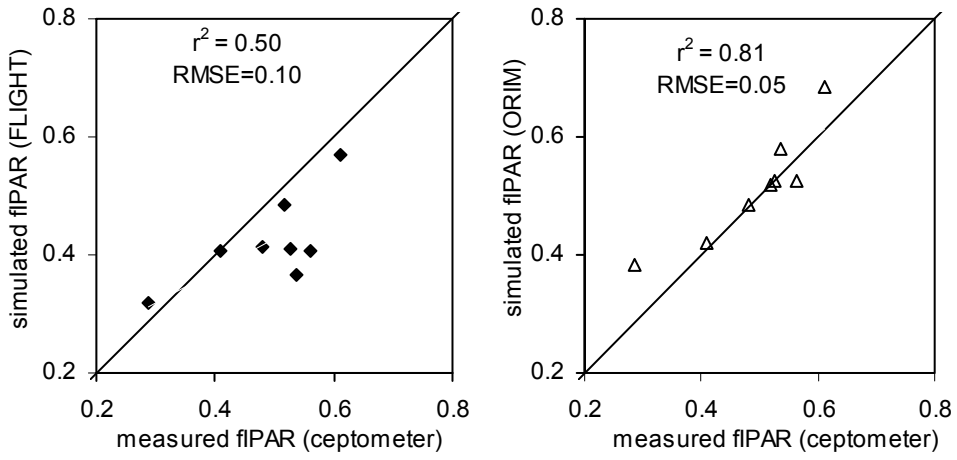

Figure 3.8. Relationships between fIPAR ground measurements and fIPAR estimations using FLIGHT (a) and ORIM (b). The input parameters used for both models were the ground measurements collected at each study site (Table 3.1, Figure 3.3).

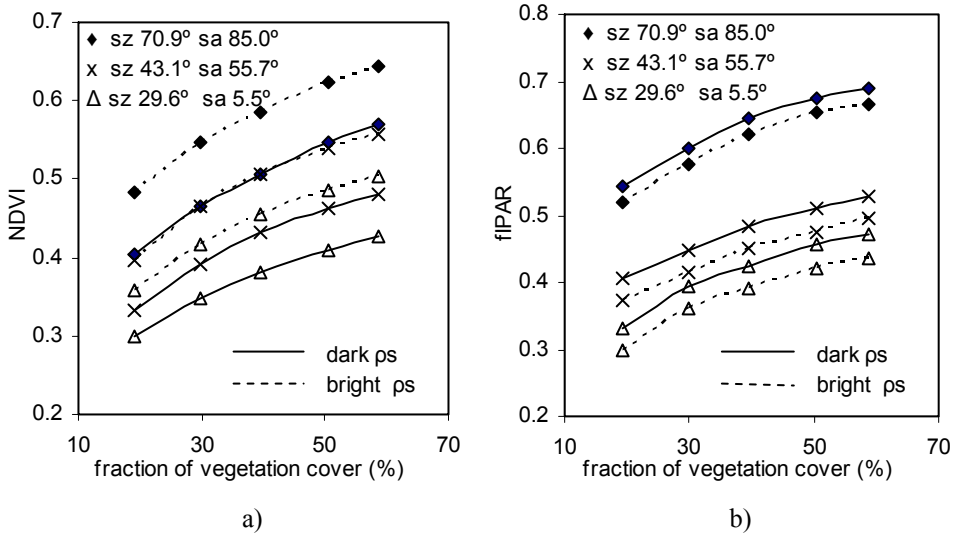

sz: Solar zenith (degrees from North)
sa: Solar azimuth (degrees from South, clockwise negative)

Figure 3.9. Variance analysis to study the effect of the sun geometry, soil optical properties and fraction of vegetation cover on NDVI (a) and fIPAR (b) using the FLIGHT model. It was considered row orientation N-S, LAI=0.8, leaf size=0.0075, fraction of green leaves=1.0, fraction of bark=0, LADF defined by user, ellipsoidal crown shape, soil roughness=0, and aerosol optical thickness=0.1.

3.3.2. Estimating fIPAR using FLIGHT and the coupled FLIGHT+ORIM model

An analysis on fIPAR estimation with remote sensing imagery was conducted by developing relationships between vegetation indices calculated from the airborne imagery and fIPAR measured with a ceptometer (Figure 3.10). The variation of NDVI vs fIPAR (Figure 3.10) was obtained through measurements conducted at selected plots with different architectural canopy characteristics at 10.00 GMT (+/- half hour). The results showed high coefficient of determination for NDVI vs fIPAR with $r^2 > 0.9$ for a polynomial regression.

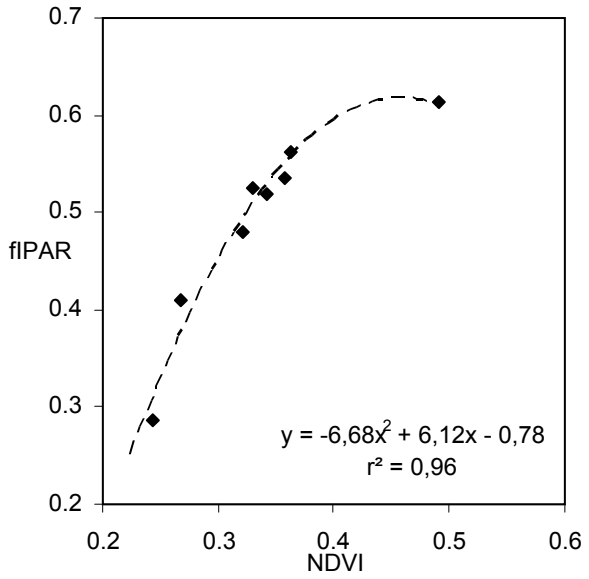

Figure 3.10. Relationships between airborne imagery NDVI and field-measured fIPAR for the eight study sites imaged at solar zenith angle = 43.1º.

The modeled relationships NDVI vs fIPAR were obtained with FLIGHT model (Figure 3.11a) and with FLIGHT and *ORIM* model (Figure 3.11b). Input parameters were field-measured, while the inputs related with canopy

architecture were ranged within the typical range of variation for these orchard crops (see Table 3.3). Relationships obtained for the olive orchard with both models: i) FLIGHT, and ii) FLIGHT + ORIM (Figure 3.6), yielded slightly different results, showing better agreements with FLIGHT + ORIM coupled simulation model (Figure 3.11b). Estimation of fIPAR by predictive relationships was compared against ground measured fIPAR for each plot. The fIPAR output from FLIGHT was slightly underestimated when compared against FLIGHT+ORIM. Relationships obtained for the orchard yielded fIPAR estimates with relative RMSE of 0.11 and r^2=0.85 when FLIGHT was used, and RMSE=0.05 and r^2=0.83 for FLIGHT+ORIM coupled models.

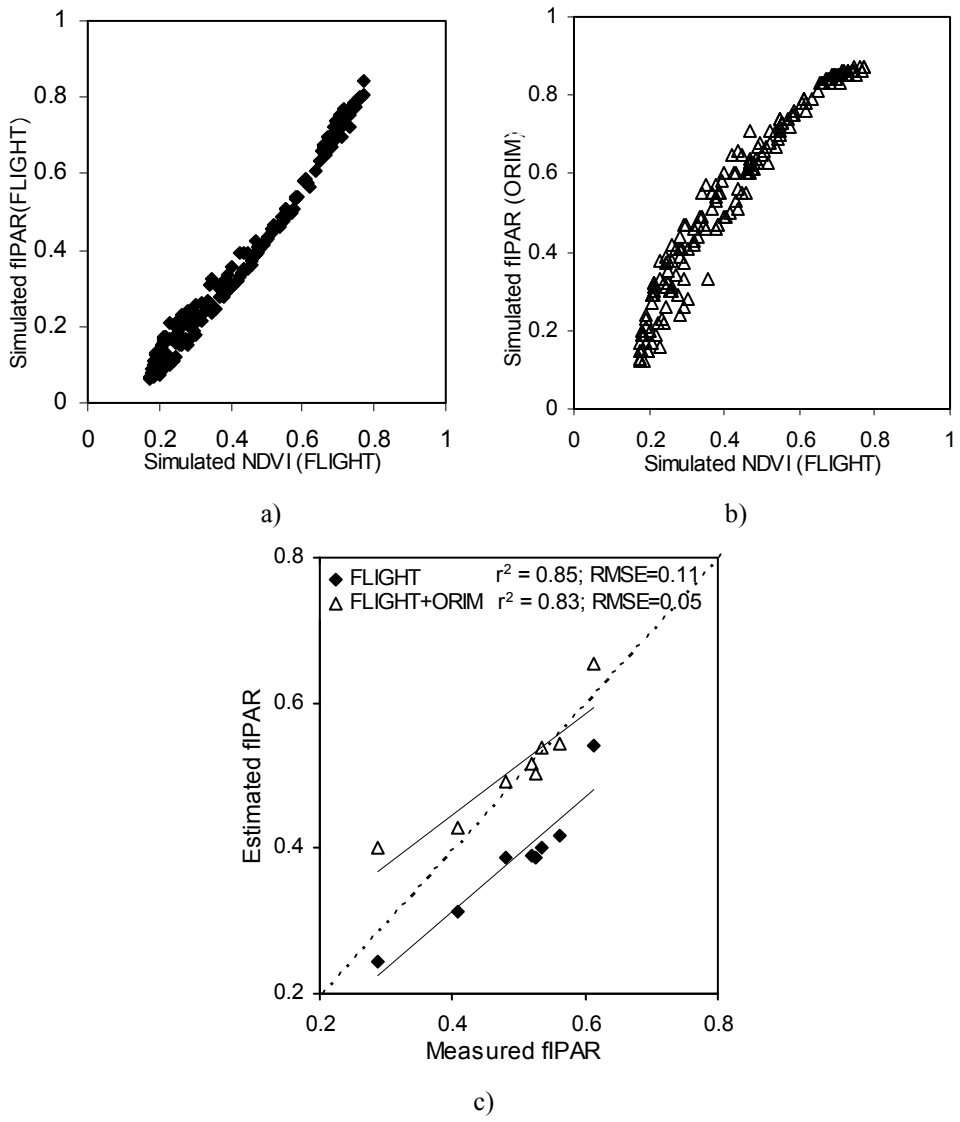

Figure 3.11. Predictive relationships obtained between NDVI and fIPAR from FLIGHT (a) and FLIGHT + ORIM (b) for olive orchards. Estimated fIPAR using predictive relationships developed in a) and b) versus measured fIPAR (c).

The assessment of the Myneni et al. (1994) relationship developed for homogeneous crop (fAPAR = 1.1638*NDVI – 0.1426) when applied to the study plots selected for this work yielded an error of RMSE=0.24. This result demonstrates that higher errors were obtained as compared to FLIGHT

(RMSE=0.11) and FLIGHT + ORIM (RMSE=0.05) simulations (Figure 3.12).

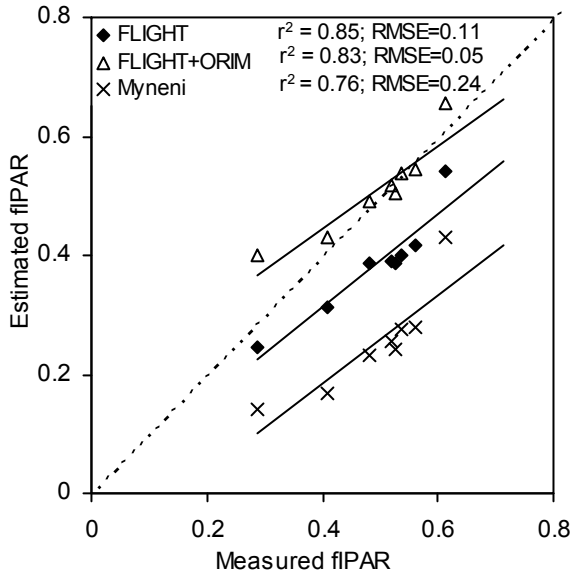

Figure 3.12. Estimated fIPAR using the predictive relationships developed in this manuscript versus the one published for homogeneous crops (Myneni et al., 1994).

Finally, a high-resolution multispectral mosaic acquired over one of the study areas (Figure 3.13a) was used to generate a map of the spatial variability of the radiation interception. The map was generated following the methodology described in this chapter. The aggregated reflectance and NDVI was calculated from a grid, each comprised of four trees, shadows and soil. The FLIGHT+ORIM predictive relationships were then applied to the grid NDVI scene of the olive orchard, generating a map of the spatial variability of the instantaneous fIPAR (Figure 3.13b).

a)

b)

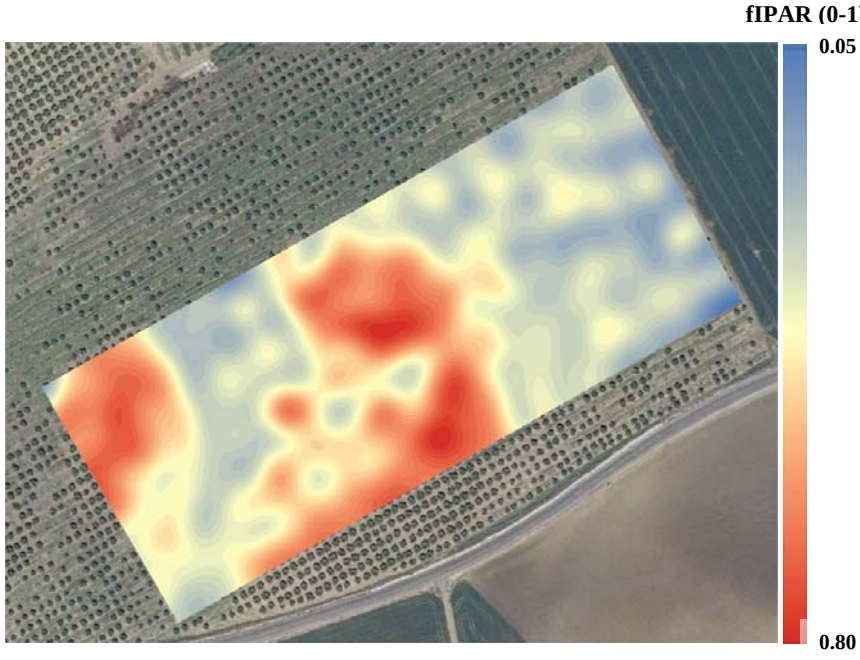

Figure 3.13. Multispectral mosaic of the olive orchard (a) used to generate a map of fIPAR calculated from the coupled FLIGHT+ORIM model (b) using the methodologies described in this study.

3.4. Conclusions

A remote sensing study focused on estimating fIPAR on olive tree canopies was conducted in this chapter. This work investigated the relationship between canopy reflectance and instantaneous fIPAR in olive orchards using radiative transfer modelling methods and field measurements. The PAR intercepted by the orchard canopy was simulated through two approaches: i) using the FLIGHT 3D model; and ii) using a specific simulation approach to estimate fIPAR in olive orchards, ORIM model. Both models were firstly assessed using input parameters measured in the field at different study plots. The FLIGHT model yielded a RMSE of 0.1 for fIPAR, while the ORIM model obtained better results with a RMSE of 0.05 when compared against fIPAR ground-measured data. In conclusion, these results demonstrated better fIPAR estimates when using the ORIM model and ground data collected over the study sites used for the model assessment. In addition, this study examined the effect of varying background optical properties, sun angles and fraction of vegetation cover on fIPAR and NDVI index when aggregating the canopy reflectance from the four central trees of the simulated scenes. The NDVI-fIPAR relationships were showed not to be applicable to all canopy types due to the important effects caused by soil and shadows. In a set of simulations conducted on two scenes with varying soil reflectance results showed important effects on NDVI, with an almost negligible influence on fIPAR. In such set of simulations, NDVI varied from 0.35 to 0.45 for two different soil types, while fIPAR changed from 0.37 to 0.39 for the same fraction of vegetation cover and solar angles due only to the different soils backgrounds. In conclusion, the NDVI vs fIPAR relationship is critically affected by the soil optical properties in such open

tree orchards, requiring the use of radiative transfer models for an accurate estimation of fIPAR in olive canopies.

The results obtained from predictive NDVI-fIPAR relationships showed that the ones from the coupled FLIGHT + ORIM model were more accurate than the results obtained with FLIGHT only. The trend showed a polynomial relationship between NDVI and fIPAR with FLIGHT+ORIM, while FLIGHT showed a linear trend. The application of the predictive algorithms for fIPAR estimation yielded a relative RMSE of 0.11 (r^2=0.85) for FLIGHT model, and a RMSE of 0.05 (r^2=0.83) for the combination of FLIGHT + ORIM models. Although FLIGHT performed well for fIPAR estimation, the ORIM model showed superior performance. The ORIM model was formulated, calibrated and validated specifically for olive orchards.

The methodology presented demonstrates the feasibility for estimating the spatial distribution of the instantaneous fIPAR in complex non-homogeneous orchard canopies. As expected, the use of NDVI-fIPAR relationships obtained in previous works for homogeneous canopies yielded a higher error, with RMSE = 0.24. Thus the particularities of the different type of canopies need to be accounted for when estimating fIPAR and others biophysical parameters. Further work will focus on other plant-grid plantations, such us the current intensive olive plantations, including diurnal studies to investigate the variability and uncertainties associated with these methodologies. In addition, the estimation of daily PAR interception from estimated instantaneous fIPAR on these non-homogeneous complex canopies will be assessed. Obtaining maps of the spatial variability of fIPAR may provide valuable information for decision makers to design new plantations according to water availability and crop potential.

Acknowledgements

Financial support from the Spanish Ministry of Science and Innovation (MICINN) for the projects AGL2009-13105, CONSOLIDER CSD2006-67, and AGL2003-01468 are gratefully acknowledged, as well as the Junta de Andalucía-Excelencia AGR-595 and FEDER. M.L. Guillén-Climent was supported by a grant JAE of CSIC, co-funded by the *European Social Fund*. P.R.J. North is gratefully acknowledged for sharing the FLIGHT code. The members of the QuantaLab-IAS-CSIC are acknowledged for scientific and technical support in field and airborne campaigns.

References

Asrar, G., Fuchs, M., Kanemasu, E.T., & Hatfield, J.H. (1984). Estimating absorbed photosynthetic radiation and leaf area index from spectral reflectance in wheat. Agronomy Journal, 76, 300-306.

Beede, R. H. & Goldhamer, D.A. (1994). Olive irrigation management In Olive Production Manual, L. Ferguson, G. S. Sibbett, and G. C. Martin, eds. University of California Publication 3353. pp. 61-68.

Ben-Gal, A., Yermiyahu, U., Zipori, I., Presnov, E., Hanoch, E. & Dag, A. (2011). The influence of bearing cycles on olive oil production response to irrigation, 29, 253-263.

Connor, D.J. & Fereres, E. (2005). The Physiology of Adaptation and Yield Expression in Olive. Horicultural Reviews, 31.

Daughtry, C.S.T., Gallo, K.P., & Bauer, M.E. (1983). Spectral estimates of solar radiation by corn canopies, Agronomy Journal, 75, 527-531.

De Castro, F. & Fetcher, N. (1998). Three dimensional model of the interception of light by a canopy. Agricultural and Forest Meteorology, 90, 215-233.

Fernades-Silva, A.A., Ferreira, T.C., Correia, C.M., Malheiro, A.C. & Villalobos, F.J. (2010). Influence of different irrigation regimes on crop yield and water use efficiency of olive. Plant Soil 333, 35-47.

Gómez, J.A., Zarco-Tejada, P.J., García-Morillo, J., Gama, J. & Soriano, M.A. (2011) Determining Biophysical Parameters for Olive Trees Using CASI-Airborne and Quickbird-Satellite Imagery. Agronomy Journal, 103, 3

Hall, F.G., Huemmrich, K.F., Goetz, S.J., Sellers, P.J., & Nickerson, J.E. (1992). Satellite remote sensing of surface energy balance: success, failures, and unresolved issues in FIFE, Journal of Geophysical Results 97, 19,061-19,089

Huemmrich, K.F. & Goward, S.N., (1997). Vegetation canopy PAR Absorptance and NDVI: An Assessment for Ten Species with SAIL model. Remote Sensing of Environment, 61, 254-269.

Huemmrich, K.F. (2001). The GeoSail model: a simple addition to the SAIL model to describe discontinuous canopy reflectance. Remote Sensing of Environment, 75, 423-431.

Iniesta, F., Testi L., Orgaz F. & Villalobos F.J. (2009) The effects of regulated and continuous eficit irrigation on the water use, growth and yield of olive trees. Eur J Agron 30:258–265.

Kempeneers, P., Zarco-Tejada, P. J., North, P. R. J., De Backer, S., Delalieux, S., Sepulcre-Cantó, G., Morales, F., Van Aardt, J. A. N., Sagardoy, R., Coppin, P. &

Scheunders, P. (2008). Model inversion for chlorophyll estimation in open canopies from hyperspectral imagery. International Journal of Remote Sensing, 29(17-18), 5093-5111.

Mariscal, M.J., Orgaz, F. & Villalobos, F.J. (2000). Modelling and measurement of radiation interception by olive canopies. Agricultural and Forest Meteorology, 100 (183-197).

Monteith, JL (1977) Climate and the efficiency of crop production in Britain. Philos Trans R Soc London Ser B 281:277–294

Moorthy, I., Miller, J.R., Berni, J.A.J., Zarco-Tejada, P.J., Hu, B., Chen, J.,Field characterization of olive (Olea europaea L.) tree crown architecture using terrestrial laser scanning data (2011). Agricultural and Forest Meteorology, Vol 151, Issue 2, 204-214

Moriondo, M., Maselli, F.& Bindi, M. (2007). A simple model of regional wheat yield based on NDVI data. European Journal of Agronomy, 26, 266–274.

Myneni, R.B. & Williams, D.L. (1994). On the Relationships between FAPAR and NDVI. Remote Sensing of Environment, 49, 200-211.

North, P.R.J. (1996). Three-Dimensional Forest Light Interaction Model Using a Monte Carlo Method. IEEE Transaction on Geoscience and Remote Sensing, 34, (4), 946-956.

North, P.R.J. (2002). Estimation of f_{APAR}, LAI, and vegetation fractional cover from ATSR-2 imagery. Remote Sensing of Environment, 80, 114-121.

Orgaz, F, Villalobos FJ, Testi L & Fereres E (2007) A model of daily mean canopy conductance for calculating transpiration of olive canopies. Func Plant Biol 34: 178–188.

Pastor, M., García-Vila, M., Soriano, M.A., Vega, V. & Fereres, E. (2007). Productivity of olive orchards in response to tree density. Journal of Horticultural Science & Biotechnology, 82 (4), 555-562.

Prieto-Blanco, A., North, P.R.J., Barnsley, M.J. & Fox, N. (2009). Satellite-driven modelling of Net Primary Productivity (NPP): Theoretical analysis. Remote Sensing of Environment, 113, 137-147.

Roujean, J.L. & Breon, F.M. (1995) Estimating PAR Absorbed by Vegetation from Bidirectional Reflectance Measurement. Remote Sensing of Environment, 51, 375-384.

Stuckens, J., Somers, B., Delalieux, S., Verstraeten, W.W.& Coppin, P. (2009). The impact of common assumptions on canopy radiativa transfer simulations: A case study in *Citrus* orchards. Journal of Quantitative Spectroscopy & Radiative Transfer, 110, 1-21.

Suárez, L., Zarco-Tejada, P. J., Berni, J. A. J., González-Dugo, V., & Fereres, E. (2009). Modelling PRI for water stress detection using radiative transfer models. Remote Sensing of Environment, 113, 730−744.

Suárez, L., Zarco-Tejada, P.J., González-Dugo, V., Berni, J.A.J.,Sagardoy, R., Morales, F. & Fereres, E. (2010). Detecting water stress effects on fruit quality in orchards with time-serie PRI airborne imagery. Remote Sensing of Environment, 114, 286-298.

Testi, L., Villalobos, F.J., Orgaz, F. & Fereres, E., (2006). Water requirements of olive orchards. I. Simulation of daily evapotranspiration for scenario analysis. Irrig. Sci. 24 (2), 69–76.

Villalobos, F.J., Orgaz, F. & Mateos, L. (1995). Non-destructive measurement of leaf area in olive (Olea europaea L.) trees using a gap inversion method. Agricultural and Forest Meteorology, 73, 29-42.

Villalobos FJ, Testi L, Hidalgo J, Pastor M & Orgaz F (2006). Modelling potential growth and yield of olive (Olea europaea L.) canopies. Eur J Agron 24:296–303

Vossen P (2007) Olive oil: history, production and characteristics of the world's classic oils. HortScience 42:1093–1110

Wiegand, C.L., Richardson, A.J., Escobar, D.E., & Gerbermann, A.H. (1991). Vegetation indices in crop assessments, Remote Sensing of Environment, 35, 105-119.

Zhang, Q., Middleton, E.M., Margolis, H.A., Drolet, G.G., Barr, A.A. & Black, T.A. (2009). Can a satellite-derived estimate of the fraction of PAR absorbed by chlorophyll ($FAPAR_{chl}$) improve predictions of light-use efficiency and ecosystem photosynthesis for a boreal aspen forest? Remote Sensing of Environment, 113, 880-888.

4. Evaluating hybrid and 3D ray tracing canopy models for vineyard canopy reflectance and vegetation index simulation using high-resolution diurnal airborne imagery

Chapter 4

Evaluating hybrid and 3D ray tracing canopy models for vineyard canopy reflectance and vegetation index simulation using high-resolution diurnal airborne imagery.

Abstract

Current research efforts in precision viticulture and the temporal and spatial monitoring of *Vitis vinifera* L. require the development of remote sensing modeling methods for the accurate estimation of vine biophysical variables such as vine density, shape, size, and vigour. These are key parameters required for early assessment of crop conditions and successful monitoring of the vineyard physiological condition. However, these row-structured crops are complex because bare soil and shadows between the vine rows contribute substantially to the canopy reflectance (CR). The use of radiative transfer models is needed for an understanding of the influence of vineyard architecture and viewing geometry on canopy reflectance. In this study, vineyard canopy reflectance is simulated using hybrid models, such as the *Markov-Chain Canopy Reflectance Model* (MCRM) and the *Scattering by Arbitrary Inclined Leaves* (SAIL) model, both modified to simulate the row crop structure (rowMCRM and rowSAIL, respectively). In addition, a more complex approach was applied, based on a *Forest Light Interaction Vegetation Model* (FLIGHT), which in turn was based on the Monte Carlo ray tracing method that enabled the generation of 3D scenes as a function of vineyard architecture and viewing geometry. Model simulations with both approaches were compared against 15-cm resolution imagery acquired with a multispectral sensor and 10-nm full-width at half-maximum (FWHM) bandset. For the green band, a relative root mean square error (rRMSE) below 0.28 was obtained from the rowMCRM and rowSAIL models, and was approximately 0.11 for FLIGHT. For the near-infrared (NIR) band (800 nm), rowMCRM and FLIGHT yielded a rRMSE between 0.08 and 0.12, with higher errors for rowSAIL (rRMSE = 0.26). The *Normalized Difference Vegetation Index* (NDVI), *Transformed Chlorophyll Absorption in Reflectance Index*/*Optimized Soil-Adjusted Vegetation Index* (TCARI/OSAVI) and *Photochemical Reflectance Index* (PRI) were also simulated with the three models and compared against the airborne images. A rRMSE between 0.15 and 0.26 were obtained with FLIGHT for the three indices assessed. FLIGHT and rowMCRM were the models yielding lower rRMSE values, with rowSAIL yielding larger errors for the NIR region.

Keywords: radiative transfer modeling, vineyards, high spatial and temporal resolution, LAI estimation

4.1 Introduction

Grape production is an important economic activity where an early assessment of crop conditions is critical to maximize grape, and consequently, wine quality (Pieri, 2010). Grapevine (*Vitis vinifera* L.) health and productivity are influenced by vine biophysical variables such as crop density, shape or size, while leaf biochemicals such as chlorophyll a+b (*Cab*) and carotenoid (Car), anthocyanins (Anth) and xanthophyll content, are related to nutrient and water stress (Hall et al., 2002; Zarco-Tejada et al., 2005; Martín et al., 2007). The spatial variation in these factors causes variability in grape quality and yields within vineyards, and can result in suboptimal wine quality and volume (Hall et al., 2002). For this reason, the use of remote sensing for precision viticulture to obtain the correct assessment of grapevine leaf and canopy status has had a growing interest. Recently, numerous studies have been published focused on the estimation of biophysical and structural parameters (e.g., Hall et al., 2002; 2003; 2008; 2010; Delenne et al., 2008; 2010; Johnson et al., 2001; López-Lozano et al., 2009) and leaf biochemistry, such as *Cab* content (Zarco-Tejada et al., 2005; Meggio et al., 2008, 2010) using remote sensing methods. These studies highlighted the importance of employing high spatial resolution imagery linked to canopy reflectance (CR) models for the successful retrieval of leaf and canopy parameters. The models are needed to interpret the optical remote sensing data which aggregate different scene components, such as sunlit and shadows soil and vegetation areas, as a function of canopy architecture and viewing geometry. The complexity in vineyards arises because they are planted in rows, and the bare soil and shadows between rows contribute substantially to the canopy reflectance observed by satellite sensors used for vegetation monitoring. To overcome the difficulties of these

canopies, the mathematical and physical complexity of canopy reflectance models used to estimate these parameters have increased considerably. They have mainly evolved from simple empirical approaches to more physically based approaches that are greatly rooted in our understanding of the radiation regime of the vegetation canopies (Liang, S., 2004). Early models that have impacted this field significantly are Suits (1972), in which the canopy is assumed to consist of only vertical and horizontal leaves, and the model is parameterized with canopy structure and solar/viewing geometry. Verhoef (1984) developed SAIL, which allowed the variation of leaf angles. A year later, Kuusk (1985) introduced the hotspot effects in the canopy reflectance according to the assumption that scatterers are randomly distributed in space and therefore gap probabilities obeys the Poisson distribution. These approaches work well in dense homogeneous canopies. In an effort to include new formulations for row-structured and heterogeneous canopies, new models were developed based on these. Suits (1972) was modified by Verhoef and Bunnik (1976) and later by Suits (1983) including the row effect by adding the concept of density modulation. Kuusk developed the so-called Markov canopy reflectance model, MCRM (1995a, 1995b, 1996, 2001) including Markov stand geometry, which considers that the correlation of leaf positions in adjacent layers influences the gap probability in a stand, and consequently, the canopy reflectance and its angular distribution. Plant row effects in this model were added by J. Praks in 2001. Input parameters defining the geometrical structure, such as vine width and length, and distance between rows, as well as row orientation described the canopy structure. Proportions of sunlit soil, shaded soil and vegetation from the nadir field of view are computed by the model. This model was developed within the framework of *Crop Reflectance operational*

Models for Agriculture (CROMA) project, and it was called rowMCRM. The rowMCRM model has been previously validated in other studies, like that of Meggio et al. (2008) who used the rowMCRM model to improve the estimation of *Cab* proposed by Zarco-Tejada et al. (2005), considering the effects of row orientation and sun geometry on the TCARI/OSAVI index (Haboudane et al., 2002) suggested for chlorophyll content estimation. The SAIL code was modified by V. Lefèvre in 2002 where the inputs to describe rows as a rectangular cross-section with bare soil in between were also included. The model was called rowSAIL, which has not been validated yet. A new row model based on a novel mathematical treatment of the four-stream SAIL model has been recently developed by Zhao et al. (2010). This type of row models are a hybrid integration of turbid medium modeling techniques with geometrical models, and are therefore suitable for handling sparse vegetation canopies with regularly shaped crowns (Liang, S., 2004). A more accurate computation of the radiation distribution over complex canopy configuration is given by Monte Carlo ray tracing models, based on a sampling of photon trajectories within the vegetation canopies. A review of the Monte Carlo methods for optical canopy reflectance modeling may be found in Disney et al. (2000).

In this study, vineyard canopy reflectance was simulated with two modeling techniques: a 3D model based on the Monte Carlo ray tracing method (FLIGHT), and two hybrid canopy models. The FLIGHT model is flexible and can simulate 3D canopy scenes with different crown shapes, including vineyard trellises. Monte Carlo simulation allows highly accurate estimation of light interception and bidirectional reflectance (Barton and North, 2001). The hybrid canopy models were the rowMCRM and rowSAIL, previously described. Validation of such crop models required the collection

of a large imagery database comprising study areas with structurally diverse canopies with extreme row orientations, as well as architectural properties. The simulations conducted with the three row-structured simulation approaches were compared against high-resolution reflectance imagery acquired with a multispectral airborne sensor. The objective was to show if simulations obtained from simple models, such as rowMCRM and rowSAIL provide accurate results in comparison with more computationally intensive models, such as FLIGHT.

4.2. Materials and Methods

4.2.1. Study area and description

The ground truth data and airborne imagery required for this study were acquired in commercial row-structured vineyard orchards located in western Ribera del Duero Apellation d'Origin, northern Spain (41º 22' N; 4º 4' W), at an altitude of 800 m above sea level during the summers of 2008 and 2009. The distance between rows was 3 m with 1.5 m between vines. The study sites used for ground and airborne data collection were selected to ensure a large variation in the vegetation cover fraction (12%-57%) and row orientations (1º-103º from the north). A total of 8 fields were selected for architectural parameter measurements, comprising a total of 21 plots flown with the airborne sensor (Table 4.1). Field sampling was conducted in these areas concurrent with airborne overflights for testing and validating row-structured models to retrieve canopy reflectance and vegetation indices. Figure 4.1 shows six false-colour images acquired with the multispectral airborne sensor at 15-cm spatial resolution, displaying a wide variability in percent vegetation cover, row orientations and soil brightness levels.

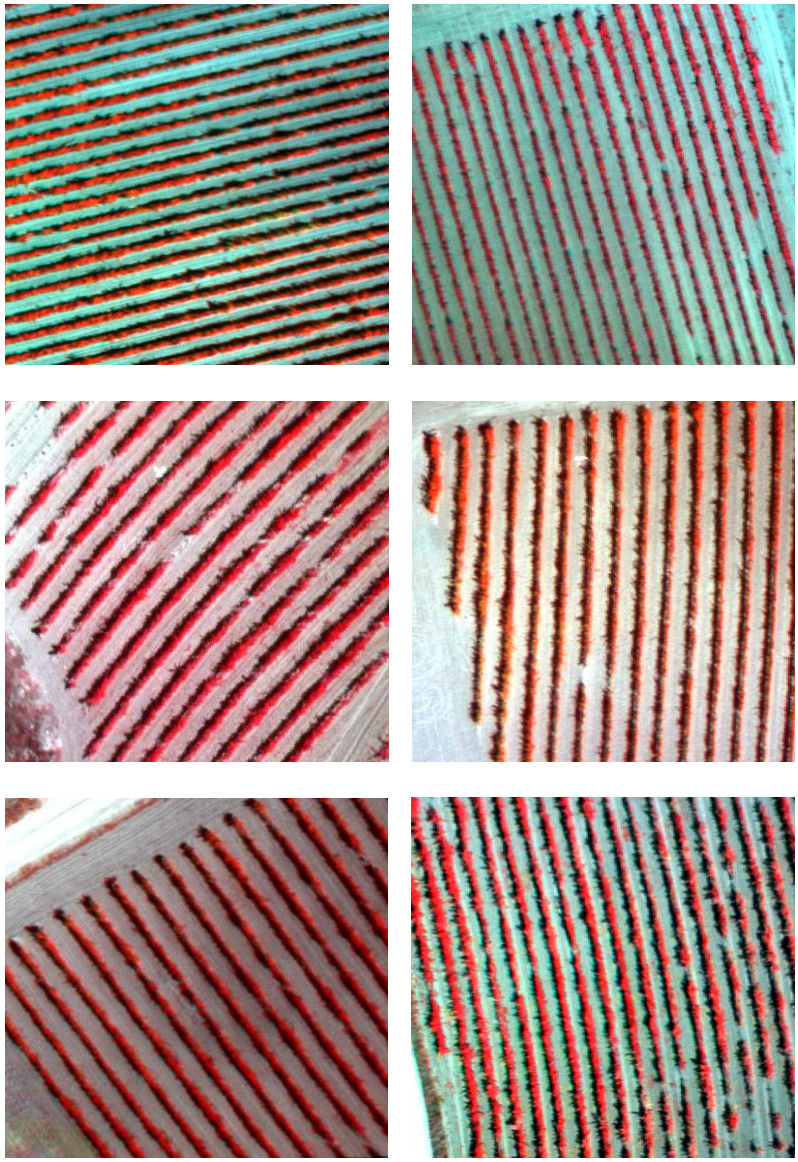

Figure 4.1 Multispectral reflectance imagery acquired at 10 nm FWHM and 15 cm spatial resolution showing variability of row orientation and cover vegetation fraction in six of the selected regions of interest.

4.2.2. Airborne and field campaigns

The multispectral sensor used in this study was a 6-band multispectral camera (515, 530, 570, 670, 700 and 800 nm) consisting of 6 independent image sensors and optics with user-configurable 10-nm full-width at half-maximum (FWHM) spectral filters (Berni et al., 2009). The image resolution is 2592 x 1944 pixels with 10 bit radiometric resolution, optics focal length of 8.4 mm, and angular field of view (FOV) of 38.04º x 28.53º, yielding 15 cm spatial resolution at 150 m flight altitude. Multispectral images acquired over each vineyard plot enabled the identification of the study area for field validation purposes. The bandsets selected for this study comprised centre wavelengths at 670 and 800 nm used for computing the *Normalized Difference Vegetation Index* (NDVI) (Rouse et al., 1974), with bands 570, 670, 700 and 800 nm used to calculate the *Transformed Chlorophyll Absorption in Reflectance Index*/*Optimized Soil-Adjusted Vegetation Index* (TCARI/OSAVI) index for chlorophyll content estimation (Haboudane et al., 2002), and bands at 530 nm and 570 nm used to calculate the *Photochemical Reflectance Index* (PRI) (Gamon et al., 1992). The three indices are described in equations [4.1-4.3].

$$NDVI = \frac{R_{800} - R_{670}}{R_{800} + R_{670}} \quad [4.1]$$

$$TCARI/OSAVI = \frac{3\left[\left(R_{700} - R_{670}\right) - 0.2\left(R_{700} - R_{550}\right)\left(R_{700} / R_{670}\right)\right]}{\left(1 + 0.6\right)\left(R_{800} - R_{670}\right)/\left(R_{800} + R_{670} + 0.16\right)} \quad [4.2]$$

$$PRI = \frac{R_{570} - R_{530}}{R_{570} + R_{530}} \quad [4.3]$$

Where R stands for reflectance at the specific band.

Atmospheric correction and calibration methods were applied to all images to calculate the spectral reflectance. Radiometric calibration was conducted using coefficients derived from measurements made in the laboratory with an uniform calibration body (integrating sphere, CSTM-USS-2000C Uniform Source System, LabSphere, NH, USA) at 4 levels of irradiance and 11 different integration times. Radiance values were converted to reflectance using the total incoming irradiance. The irradiance at the time of the flights was simulated with SMARTS (Gueymard, C.A., 2005) using Microtops II sunphotometer data (Solar Light Co., Philadelphia, PA, USA) collected in the study area at the time of data acquisition to derive aerosol optical depth at 550 nm. The airborne flight campaigns and the sunphotometer data were collected under clear sky conditions.

The diurnal field campaigns and the airborne imagery acquisition were conducted every two hours from 07.00 GMT until 13.00 GMT in summer 2009 (Table 4.1). The objective was to acquire a large number of images to account for the variation of canopy reflectance and vegetation indices over the diurnal cycle as a function of soil shaded area due to sun geometry and row orientation. Figure 4.2 shows the diurnal variation of the shadow proportions in a vineyard with a North-South (N-S) oriented rows. The image reflectance extracted from 6 m x 3 m study plots including soil and shadows (Figure 4.1a) and pure vegetation pixels (Figure 4.3b) were later used to compute spectral vegetation indices. The diurnal variation of the aggregated CR (Figure 4.3c) deviates from the diurnal sun-angle effects found on pure vine reflectance (Figure 4.3d) due to the large effects caused by shadows on aggregated pixels. These images were later used to validate the modeling methods employed by the hybrid and ray tracing approaches,

07.00 GMT

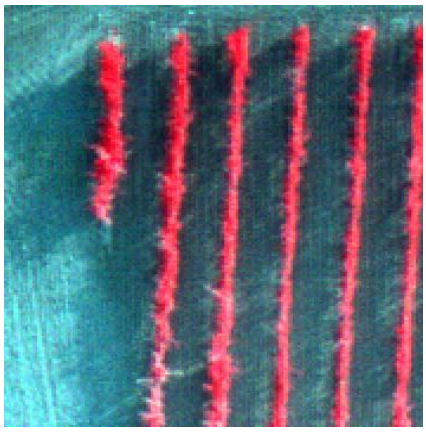

(a)

09.00 GMT

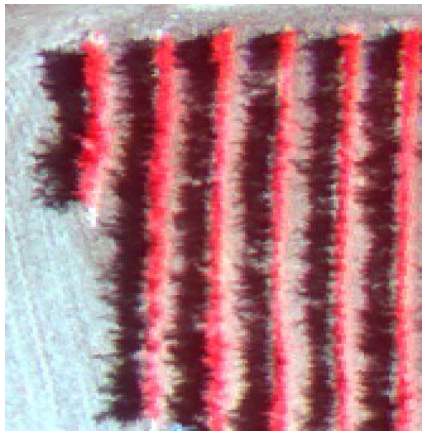

(b)

11.00 GMT

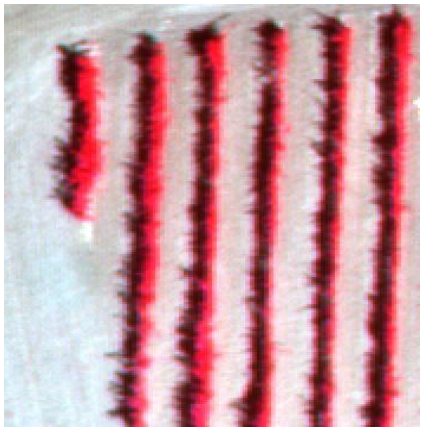

(c)

13.00 GMT

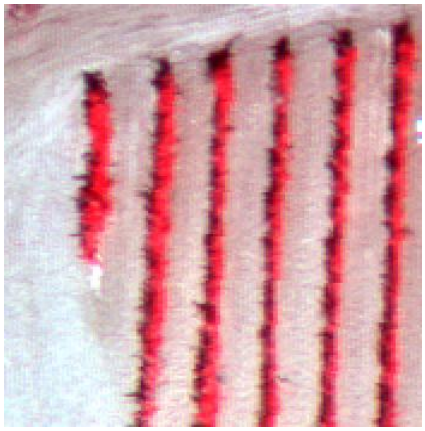

(d)

Figure 4.2. Time course of shadow are in a vineyard with N-S oriented rows at the four times of the airborne flights (*3rd September 2009*)

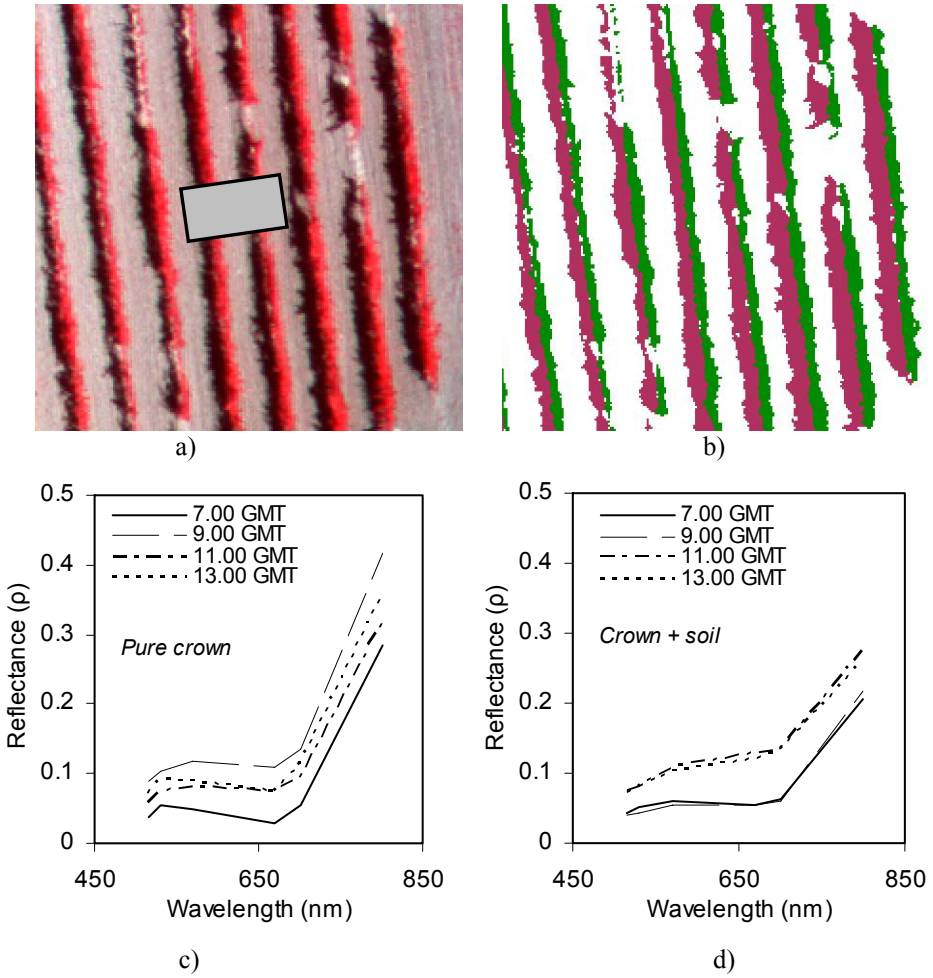

Figure 4.3. Multispectral image (15-cm spatial resolution) with the selected study area to study the aggregate spectra (a). Detail of the components of the scene: pure vegetation (green), shadows (pink), and sunlit soil (white) (b). Pure crown (c) and aggregated spectra (d) at the four times of the airborne flights. (*3rd September 2009*)

conducting the simulations with input parameters collected on each vineyard field concurrent with airborne overflights. Architectural vegetation parameters, such as width and canopy height, leaf area index (LAI) were measured. Crown height (without considering the trunk) and width of the rows were measured at three different places of the stand within the 6 m x 3 m plot, obtaining the mean values for each site (Table 4.2). The LAI was

calculated using the methodology from Perez et al., 2002, and Carbonneau et al., 1976. Specific leaves were selected from 20 tendrils within the vineyard. The central nerve length (L) is measured for every third leaf along each tendril and the calculation of foliar area (A) is calculated as:

$$A = 0.01055412 \cdot (L \cdot 10)^2 + 0.23713115 \cdot (L \cdot 10) \quad [4.4]$$

As such the foliar area for the plant (A_v) is calculated using the following Equation [4.5]

$$A_v = A \cdot 3 \cdot \text{nºtrendrils/plant} \quad [4.5]$$

where:

nºtrendrils/plant ~ 16, (is the average value found in this area).

The leaf area index (LAI) of the vineyard is then calculated by dividing the A_v by the ground area, per plant (4.5 m^2).

Table 4.1. Solar geometry of multispectral data acquisition

Imagery details
Imagery acquired on 3rd September 2009 at four different times: **1.** **SZ**:80.02º **SA**:88.40º **2.** **SZ**:57.23º **SA**:110.08º **3.** **SZ**:37.40º **SA**:147.6º ***4.*** **SZ**:34.00º **SA**:190º *SZ : solar zenith; SA: solar azimuth (degrees from North)*
Airborne multispectral imagery *Wavelength selection: 515, 530, 570, 670, 700 and 800 nm* *15 cm pixel size*

Table 4.2. Measured parameters for the vine study sites used for the simulation work.

Vineyards (Ribera del Duero, Lat 41º 22' N; Long 4º 4' W)					
Plantting grid (*m x m*) *3 x 1.5*					
Plot	Row orientation (º) *(degrees from North)*	Width (m)	Height (m)	LAI	LAD
1	96.05	0.6	1.3	1.1	4.23
2	93.06	0.55	1.4	0.8	3.12
3	20.07	0.2	0.8	0.3	5.63
4	20.07	0.4	0.8	0.5	4.69
5	103.1	0.5	1.15	0.96	5.01
6	103.1	0.6	1.05	1.15	5.48
7	93.06	0.7	1.32	1.26	4.09
8	75.2	0.9	1.5	1.4	3.11
9	1.02	0.8	1.4	1.4	3.75
10	1.02	0.6	1.2	0.8	3.33
11	93.06	0.41	0.7	0.4	4.18
12	93.06	0.7	1.5	1.2	3.43
13	47.5	0.6	1.2	0.75	3.13
14	47.5	0.55	0.9	0.6	3.64
15	47.5	0.8	1.1	0.8	2.73
16	28.5	0.9	1.3	1.48	3.79
17	28.5	1.1	1.7	1.3	2.09
18	49.5	0.8	1.45	1.07	2.77
19	49.5	0.6	1.45	1.25	4.31
20	61.42	0.75	1.4	1.56	4.46
21	61.42	0.85	1.35	1.37	3.58

4.2.3. Vineyard canopy reflectance simulations with rowMCRM, rowSAIL and FLIGHT models.

4.2.3.1 Canopy model testing for simulating vineyard architecture

The rowMCRM and rowSAIL hybrid models were tested to simulate bidirectional reflectance in vineyards. These models were linked to PROSPECT leaf radiative transfer model (Jacquemoud & Baret, 1990; Jacquemoud et al., 1996) to simulate the leaf optical properties. The inputs required for the linked PROSPECT-row models used in this study are shown in Table 4.3. Leaf optical properties, as well as the leaf angle distribution function (LADF), relative leaf size, Markov parameter, factor for refraction index (used for the calculation of specular reflection of the leaf surface) and leaf hair index were the nominal range parameters proposed in Zarco-Tejada et al. (2005). The rest of the canopy structural parameters such as the visible soil strip, background and viewing geometry were measured for each plot (Table 4.2). The visible soil strip width is the space between the edges of two vineyards in parallel rows, and corresponds to visible soil as seen from nadir. The soil reflectance was measured from the airborne image at the beginning of the row for each single study site. It was measured for all flight times (Table 4.1) at each location. Sun azimuth and row orientation angles are linked in the model by the alpha-row parameter (ψ), calculated as the angular difference between sun azimuth and row orientation, both of which were measured in a clockwise direction from north.

In a previous study, a comparison between the rowMCRM canopy reflectance simulation and the *Compact Airborne Spectrographic Imager* (CASI) airborne imagery for two viewing geometries (Zarco-Tejada et al., 2005; Meggio et al., 2008) enabled the validation of TCARI/OSAVI *scaling*

up relationships for Cab estimation. In this study, the rowSAIL and FLIGHT models were also used. To simulate vineyard architecture with FLIGHT, overlapped ellipsoids were generated (Figure 4.4), with the smaller radius corresponding to the canopy width (Table 4.3). Figure 4.4 shows the scene for two plots with North-South (N-S) orientation at 09.00 GMT (Figure 4.4a) and 13.00 GMT (Figure 4.4b), and East-West (E-W) orientation for the same sun angles (Figure 4.4c and Figure 4.4d, respectively).

Table 4.3 Nominal values and range of parameters used for leaf and canopy simulation with PROSPECT, rowMCRM, rowSAIL and FLIGHT for vine study sites.

	Nominal values and range
PROSPECT	
Leaf parameters	
Chlorophyll a+b C_{ab} *(ug cm^{-2})*	40
Leaf water content, C_w *(cm)*	0.025
Leaf dry matter content, C_m *(g cm^{-2})*	0.0035
Leaf internal structure parameter, *N*	1.62
rowMCRM and rowSAIL	
Canopy layer and structure parameters	
Leaf area index (LAI)	See Table 4.2
Leaf angle distribution function (LADF)	ϵ = 0.95; θ_n=45º (plagiophile)
Relative size (h_s)	0.083
Markov parameter (λ_z)	1.1
Refraction index (0.7-1.2)	0.9
Leaf hair index (I_h)	0.1
Canopy height, (C_H)	See Table 4.2
Crown width, (C_W)	See Table 4.2
Visible soil strip length, (V_s)	See Table 4.2
Row orientation	1-103º
Background and viewing geometry	
Soil reflectance, ρ_s	Specific for each site
Armstrong turbidity factor (β)	0.18
Sun azimuth angle	See Table 4.1
Sun zenith angle (θ)	See Table 4.1
FLIGHT	
Leaf optical and structural parameters	
Hemispherical reflectance and transmittance of green leaves	PROSPECT simulations
Hemispherical reflectance and transmittance of senescent leaves	Not used
Leaf equivalent radius	0.083 m
Canopy layer and structural parameters	
Leaf area index (LAI)	See Table 4.2
Fractional cover	12-60%
Leaf Angle Distribution Function (LADF)	plagiophile
Fraction of green leaves	1
Fraction of senescent leaves	0
Fraction of bark	0
Number of stands and position coordinates	Not used
Crown shape	Elliptical
Crown height and radius	See Table 4.2
Trunk height and radius	Not used
Background and viewing imagery geometry	
Solar zenith and azimuth angles	See Table 4.1
Sensor zenith and azimuth angles	Degrees
Soil reflectance	Specific for each site
Soil roughness	0
Aerosol Optical Depth (AOD)	0.15

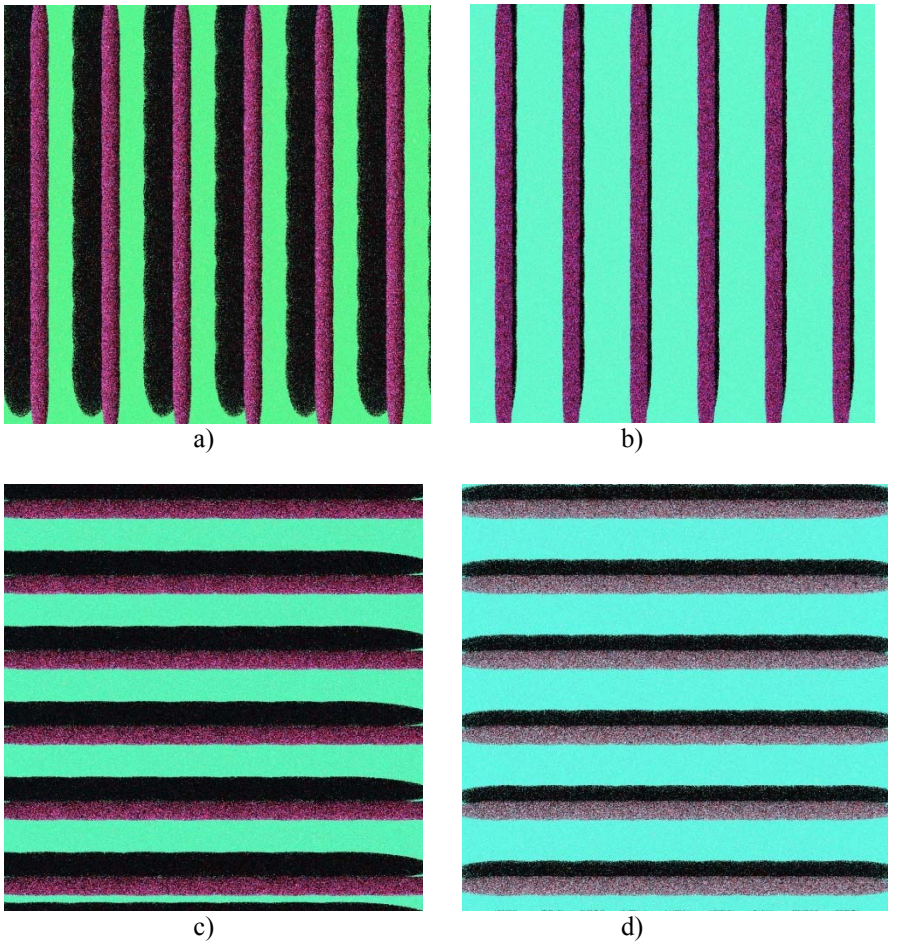

Figure 4.4. Sceneries obtained with FLIGHT using ellipsoids to simulate the geometry of vineyards. North-South rows at 09.00 GMT (a) and 13.00 GMT (b), and East-West orientation at 09.00 GMT (c) and 13.00 GMT (d).

Simulations conducted with the three models were then compared against the high spatial resolution imagery. Band-to-band and vegetation index comparisons between model-simulated reflectance and the airborne reflectance were then used to calculate the relative RMSE (rRMSE) for all the study sites. The TCARI/OSAVI index, used as an indicator of Cab concentration, NDVI index used to track structural changes on the canopy,

and PRI, used as an indicator of xanthophyll pigments and recently proposed for water stress detection in crops, were all modeled for each plot and compared with the measured values, indices calculated from the airborne imagery, focusing on configuration parameters, such as the sun azimuth, sun zenith and the row orientation angles, soil reflectance and structural parameters.

4.2.3.2 Sensitivity analysis.

Simulations were conducted to understand the sensitivity of CR to the input parameters (row orientation, solar view geometry, LAI and background) by varying the inputs independently, keeping the remaining parameters fixed. In the same way, the sensitivity of the Spectral Vegetation Indices (SVI) to canopy geometry, soil optical properties and sun angle were evaluated to assess the influence of the architecture and observational geometry on the aggregated NDVI, TCARI/OSAVI and PRI indices, the input parameters were varied and the simulated reflectance per plot was aggregated, including the soil between vineyards rows and shadows (see Figure 4.3a and Figure 4.3b). Simulations were carried out by the three models. While ray tracings methods are based on a sampling of photon trajectories within the vegetation, geometrical optical models assume that the reflectance of the canopy is the area-weighted sum of different sunlit/shadow components. The fractions of different components are calculated based on the geometric optical principles. Thus, differences in canopy reflectance and SVI obtained between models are influenced by the physical theory assumptions of each model. As such, differences in inherent model assumptions were tested in terms of the description of the component

fractions and the corresponding reflectance values for both hybrids and ray tracing models.

4.3. Results and Discussion

4.3.1. Comparisons between rowSAIL, rowMCRM and FLIGHT vineyard simulations and diurnal airborne imagery

Reflectance spectra comparisons for 21 vineyard plots were obtained with the three models by studying canopy reflectance simulations from visible to near-infrared wavelengths for four different sun view geometries and a wide range of row orientations. The reflectance spectra increased along the entire spectrum when zenith angles decreased. This effect is more evident in N-S orientated row plots since the shaded soil contribution changes more in this orientation. Figure 4.5**Figure 4.5** shows two study areas with similar percent vegetation cover and two different row orientations, N-S (Figure 4.5a, c and e) and E-W (Figure 4.5b, d and f). The trend observed in the airborne imagery between 07.00 and 13.00 GMT, showing vineyard reflectance increasing with time due to reduced shaded area, was captured by the three models.

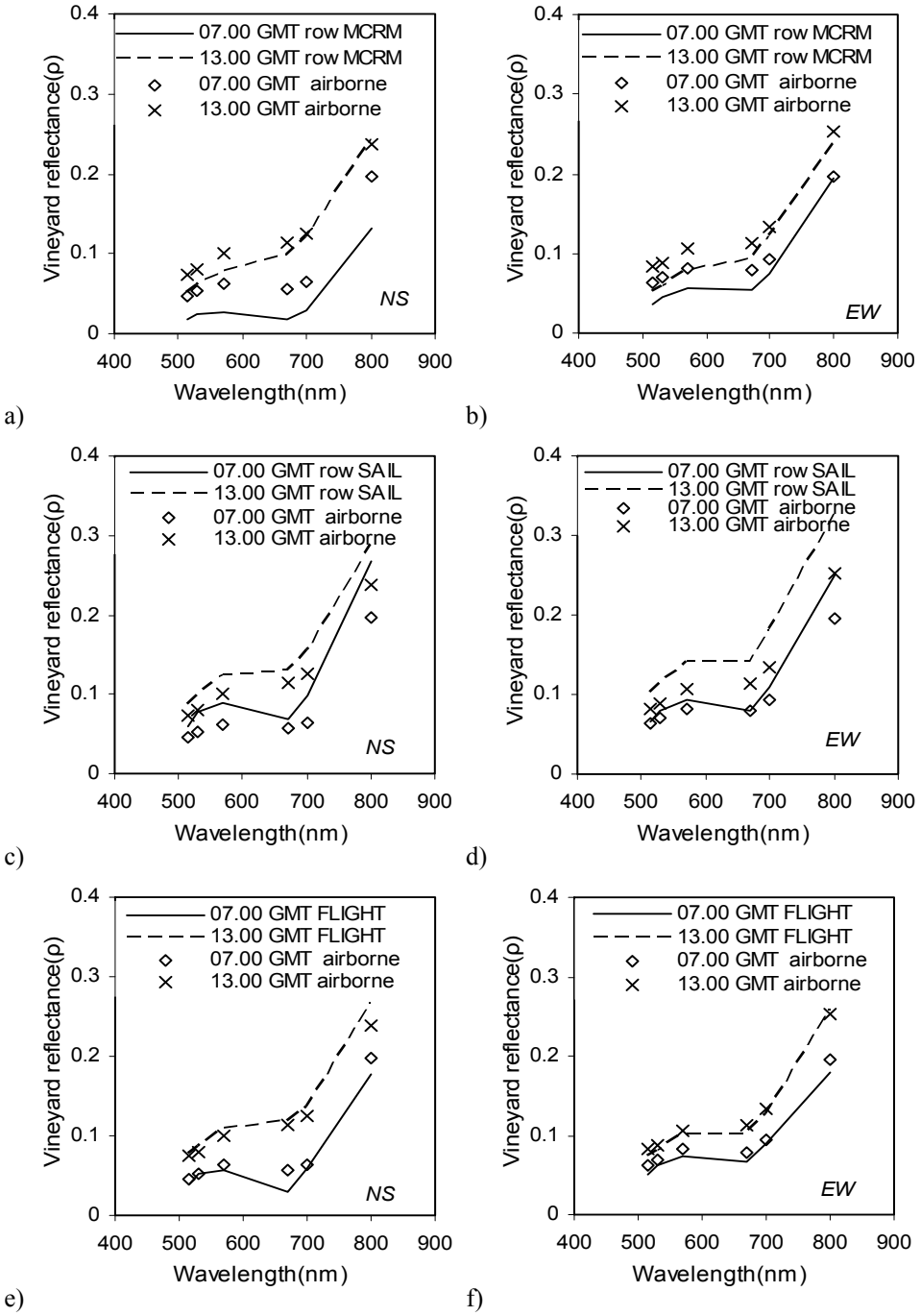

Figure 4.5. Spectra obtained for aggregated vegetation-soil pixels: Multispectral image spectra collected at 07.00 and 13.00 GMT (*3rd September 2009*) and canopy spectra simulation conducted with rowMCRM (a,b), rowSAIL (c,d) and FLIGHT (e,f). Left column corresponds to North-South and right column to East-West row orientated plots.

Results of the relationships between the simulated and measured reflectance are shown in Table 4.4. A rRMSE value between 0.20 and 0.30 was found for all spectral bands at the different flight times for the rowMCRM model. Similar results were obtained with the rowSAIL model, excepting the first time that present lower accuracy. The 3D FLIGHT model simulations yielded a rRMSE between 0.10 and 0.20. When all the times are considered together excepting the lower zenith angle, the simulations for the red region (670 nm) yielded rRMSE values below 0.16 for the rowMCRM and rowSAIL models (Figure 4.6a and c, respectively). FLIGHT yielded better results, with rRMSE = 0.09 (Figure 4.6e). For NIR, 800 nm, rRMSE are 0.08 and 0.10 for FLIGHT and rowMCRM respectively (Figure 4.6a and e), being underestimated with rRMSE of 0.20 for rowSAIL (Figure 4.6b). Although rowSAIL presented higher errors in the NIR region, smaller errors compared with the other two models were found for SVI. Thus rRMSE of 0.12 is obtained for NDVI with rowSAIL (Figure 4.6d), and rRMSE 0.17 and 0.14 with rowMCRM and FLIGHT (Figure 4.6b and f, respectively). The validation and evaluation of canopy reflectance together with SVI is needed to study the weakness of the different models. The SVI minimize the variability to external factors and they are developed to establish functional relations between crop characteristic and remote spectral. The use of radiative transfer models helps to understand these relations as well as understand the influence of different optical and geometrical parameters on SVI.

Table 4.4 Relative RMSE obtained from multispectral airborne imagery and simulations canopy reflectance for the study sites at four solar geometries.

		07.00 GMT			09.00 GMT			11.00 GMT			13.00 GMT		
		rowMCRM	**rowSAIL**	**FLIGHT**	**rowMCRM**	**rowSAIL**	**FLIGHT**	**rowMCRM**	**rowSAIL**	**FLIGHT**	**rowMCRM**	**rowSAIL**	**FLIGHT**
NS	**530**	0.530	0.323	0.174	0.362	0.201	0.065	0.252	0.118	0.108	0.258	0.227	0.104
	570	0.503	0.345	0.173	0.293	0.211	0.054	0.195	0.145	0.112	0.290	0.239	0.098
	670	0.558	0.198	0.288	0.207	0.298	0.101	0.196	0.158	0.086	0.180	0.225	0.112
	700	0.461	0.223	0.151	0.151	0.338	0.060	0.149	0.184	0.123	0.128	0.252	0.091
	800	0.203	0.248	0.117	0.112	0.287	0.079	0.083	0.283	0.095	0.049	0.244	0.108
SVI	**PRI**	0.165	0.144	0.229	0.297	0.173	0.140	0.245	0.107	0.081	0.288	0.114	0.126
	TCARI/OSAVI	0.384	0.451	0.451	0.275	0.557	0.243	0.312	0.216	0.228	0.274	0.457	0.223
	NDVI	0.421	0.272	0.276	0.199	0.133	0.183	0.241	0.289	0.211	0.237	0.173	0.206

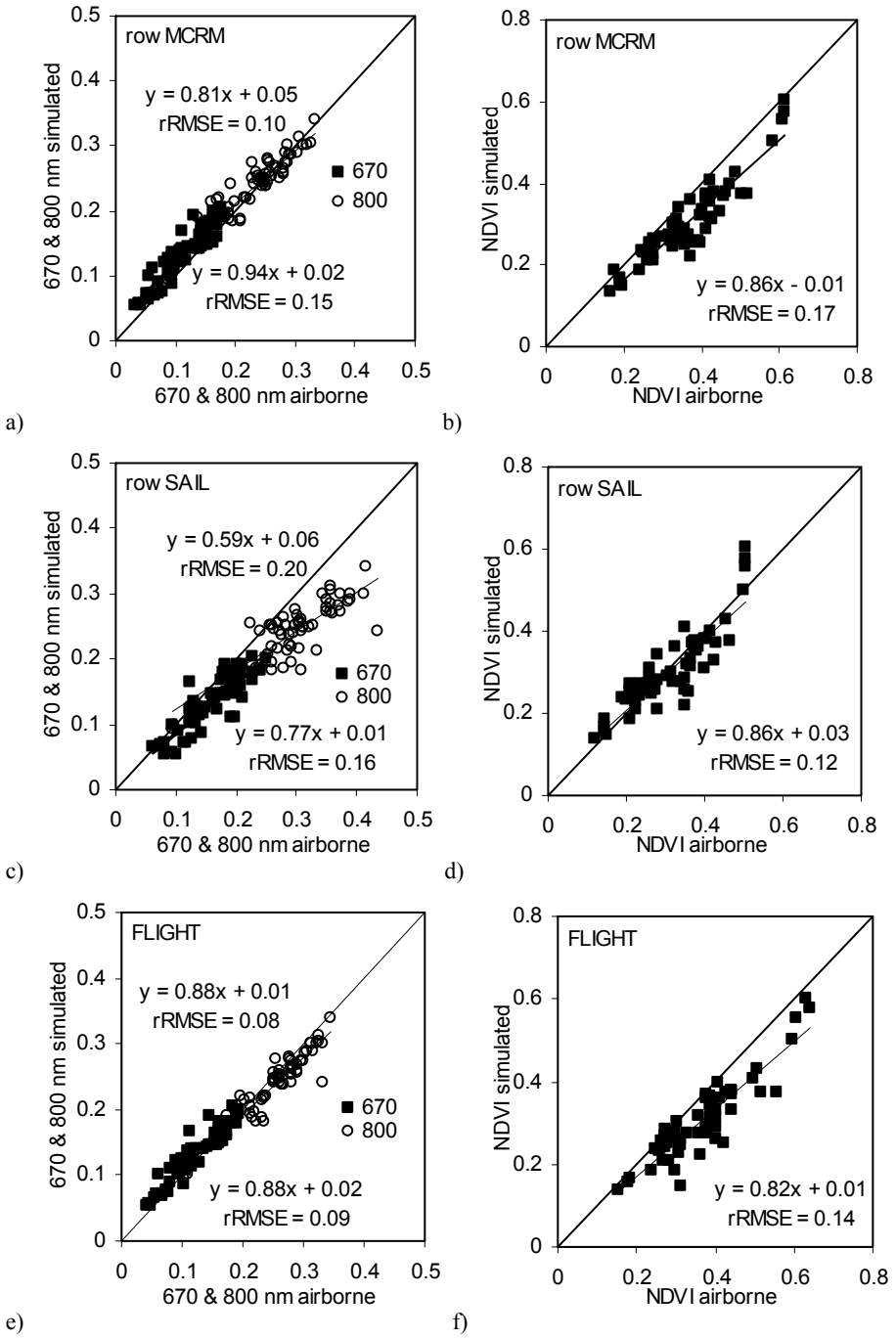

Figure 4.6. Relationships between actual and simulated reflectance at 670 nm and 800 nm (a, c, e) and NDVI (b, d, f) with rowMCRM, rowSAIL and FLIGHT respectively

4.3.2. Simulated CR and vegetation indices as a function of viewing geometry and canopy structure.

Simulations with the three models were conducted for row orientations of 0º, 30º, 60º and 90º under fixed sun angles. Differences in CR ranging between 0.04 at the green region and 0.1 at the NIR were observed between E-W and N-S orientations (Figure 4.7a). The effect of solar view geometry was studied by varying the angles from sunrise until noon, with the remaining parameters fixed (Figure 4.7b). In addition, different LAI values with fixed dimensions of the canopy were used as input for the models, observing important differences when leaf area index increased from 0.5 to 2, with smaller effects as LAI increased beyond 2 (Figure 4.7c). The background effect was also studied, using dark, medium and bright soil reflectance spectra as input. Results demonstrated differences in CR ranging between 0.02 at the green region and 0.1 at the NIR as a function of the soil reflectance levels (Figure 4.7d).

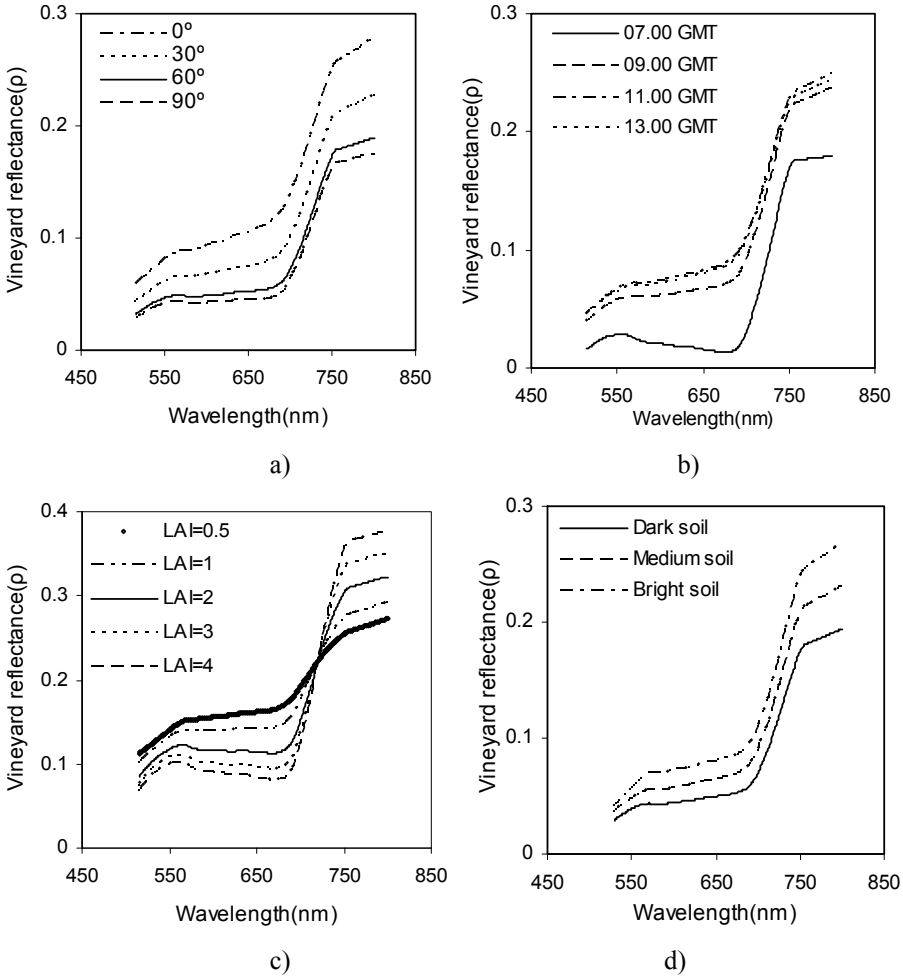

Figure 4.7. Effect of row orientation (a), sun angle variation (b), LAI (c), and soil reflectance (d) on row-canopy reflectance. Simulations obtained with rowMCRM

The NDVI, TCARI/OSAVI and PRI indices as a function of sun angle (Figure 4.8) were simulated with FLIGHT for N-S and E-W vine row orientations (named as αrow). N-S orientation (αrow = 0º) (Figure 4.8a, c and e) and E-W orientation (αrow = 90º) (Figure 4.8b, d and f) for a range of soil spectra (bright, medium, dark) and visible soil strip widths of 1.7 m. Simulations demonstrated the small sun angle effect on the three indices for E-W row orientations (Figure 4.8b, d and f). As expected, row lines oriented

in the solar plane made the shaded soil component variation very small on the three indices studied.

For N-S row orientations (Figure 4.8a, c and e), large differences in the three indices were found as a function of the sun position: NDVI decreased from 0.8 down to 0.42 from early morning to midday (Figure 4.8a); TCARI/OSAVI varied from 0.11 to 0.2 for the same time frame for bright soil backgrounds, showing smaller variation for darker soils (Figure 4.8c); PRI varied from 0.15 up to 0.27 from sunrise to midday for a visible soil strip of 2.3 m and bright soil (Figure 4.8e).

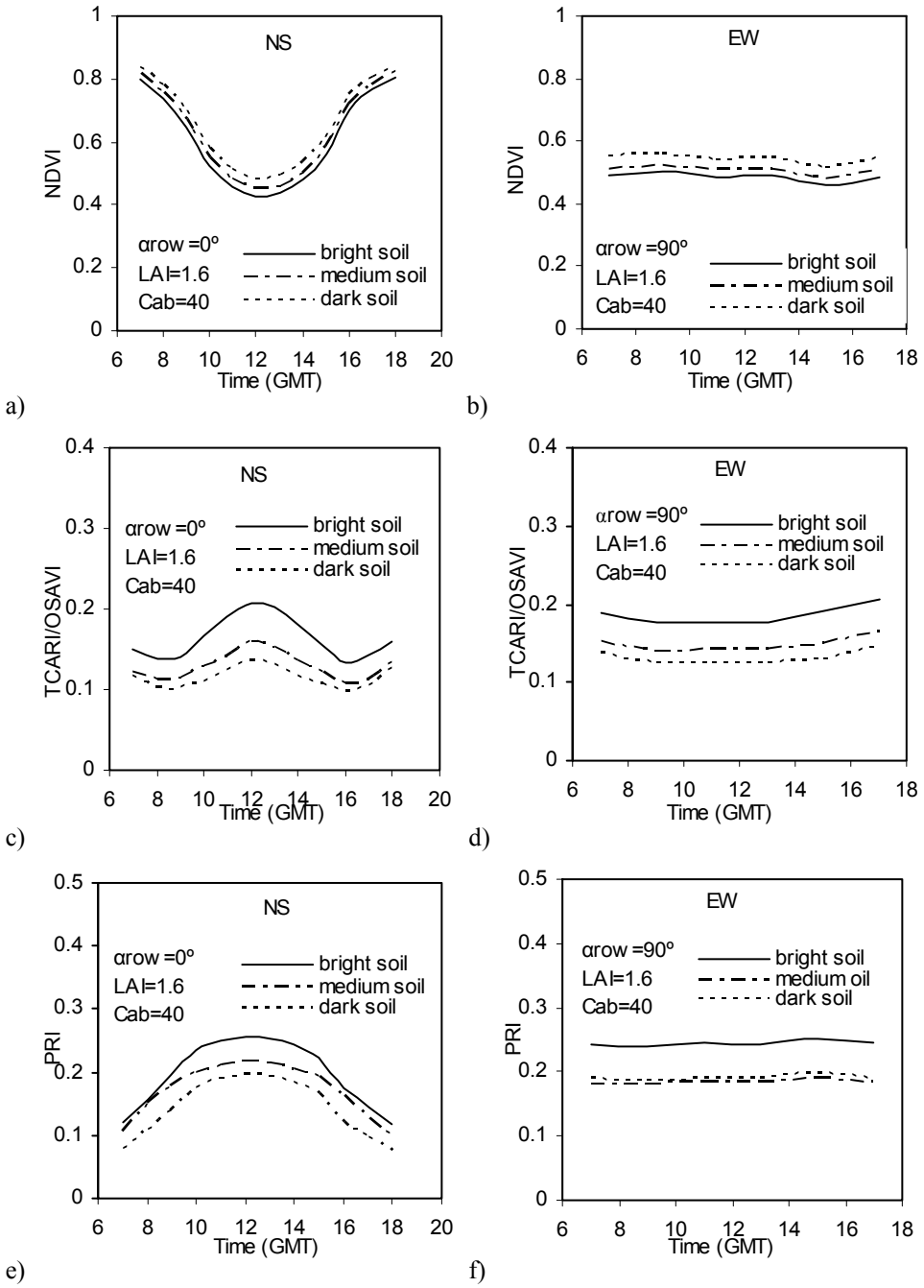

Figure 4.8. Simulations obtained with FLIGHT: effect of the sun geometry on NDVI, TCARI/OSAVI and PRI, considering row orientation variation N-S (a, c and e) and E-W (b, d and f) as a function of different soil backgrounds, setting the LAI = 1.6, visible soil strip = 1.7 m and the Cab content to 40µg·cm^{-2}.

Simulations conducted for the NDVI, TCARI/OSAVI and PRI indices as a function of sun angle, visible soil strip and background (Figure 4.9) demonstrated the effects due to the variation of canopy leaf area: LAI = 0.5 (Figure 4.9a, c and e) and LAI = 1.6 (Figure 4.9b, d and f) for N-S row orientation were simulated with rowMCRM. The three indices varied as a function of sun angles from early morning to midday for both LAI values, showing larger effects for higher LAI due to the effects on the shadow proportions, as expected. These results demonstrate the importance of canopy modeling to understand the diurnal behaviour of the indices used for vegetation monitoring in row-structured canopies. As expected, a low diurnal variation in the indices was found for low LAI canopies (Figure 4.9a, c and e) due to the smaller shadow component casted by the vegetation.

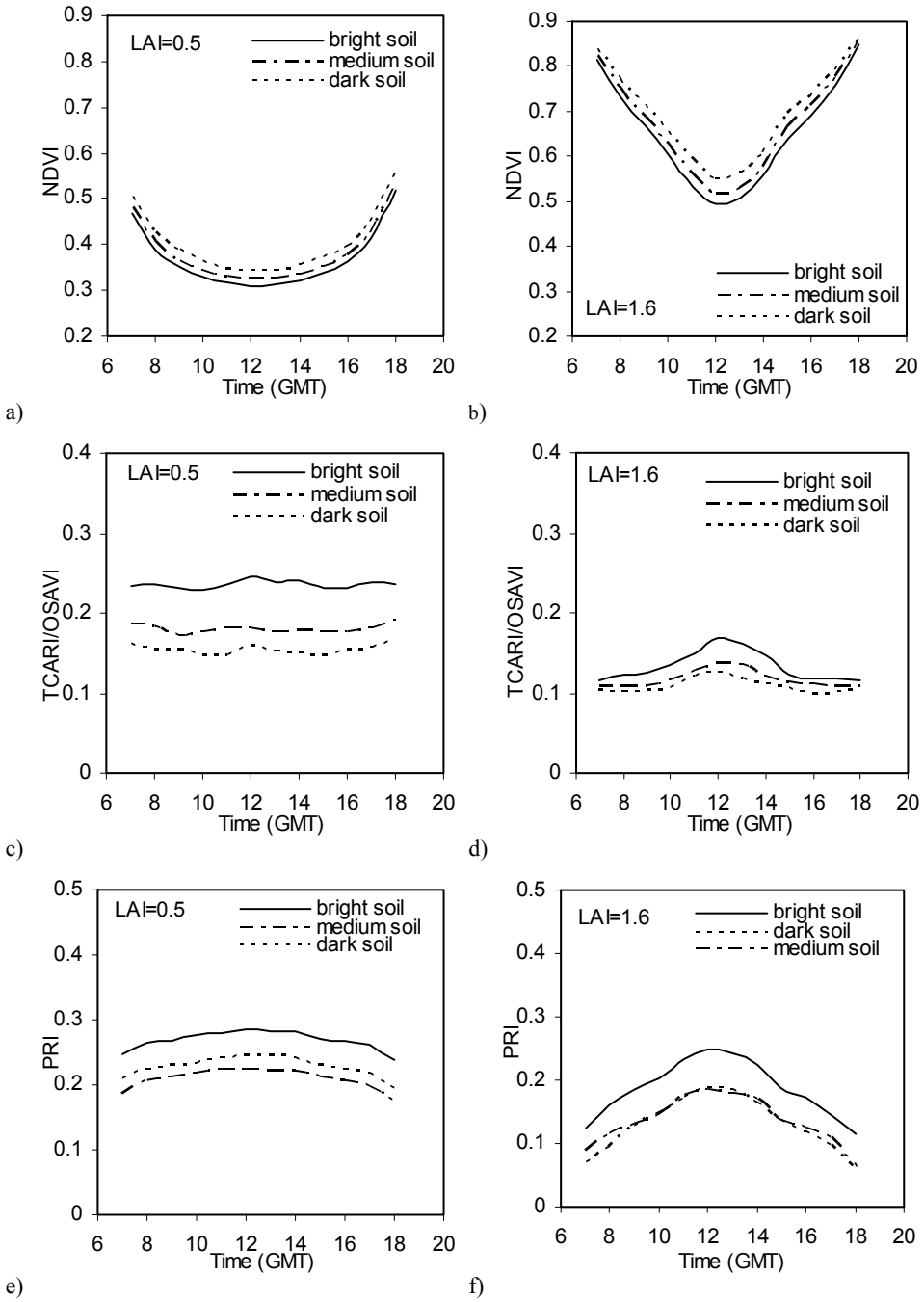

Figure 4.9. Simulations obtained with rowMCRM: effect of the sun geometry on NDVI, TCARI/OSAVI and PRI, considering LAI variation, LAI = 0.5 (a, c and e) and LAI = 1.6 (b, d and f) as a function of different soil backgrounds, fixing the row orientation to N-S, Vs=1.7m and the Cab content to 40μg·cm^{-2}.

The study focused on the simulation of each fraction of the scene components (sunlit and shaded soil and vegetation) was conducted for a scene with vegetation cover fraction of 30%, LAI = 1.6, height = 1.7 m, modeled for different sun geometries for NS and EW row orientation (Figure 4.10 and Figure 4.11). Figure 4.10 shows the sunlit and shaded soil fractions computed by rowMCRM and FLIGHT models. Differences among models for the simulated fraction of sunlit (Figure 4.10a) and shaded soil (Figure 4.10c) reached 26% in the morning for North-South orientation, being negligible at midday. For East-West row orientation, differences between scene components were minimal early in the morning and late in the afternoon, reaching differences of up to 16 % at midday (Figure 4.10b and Figure 4.10d). An important difference between both modeling methods is that the fractions of sunlit and shaded leaves are not computed for the rowMCRM model, while FLIGHT separates both fractions. Figure 4.11 shows the percentage of shaded and sunlit vegetation simulated by FLIGHT for row orientations NS and EW (Figure 4.11a and Figure 4.11b, respectively). The percentage of shaded vegetation varied from 25% in the early morning down to 11% at midday for EW orientation. For NS orientation, the percentage of shaded vegetation varied from 19% in the early morning down to 12% at midday. These results are consistent given that the shadows are casted into the vegetation at large zenith angles for the EW orientation, while shadows are casted into the soil for the NS orientation.

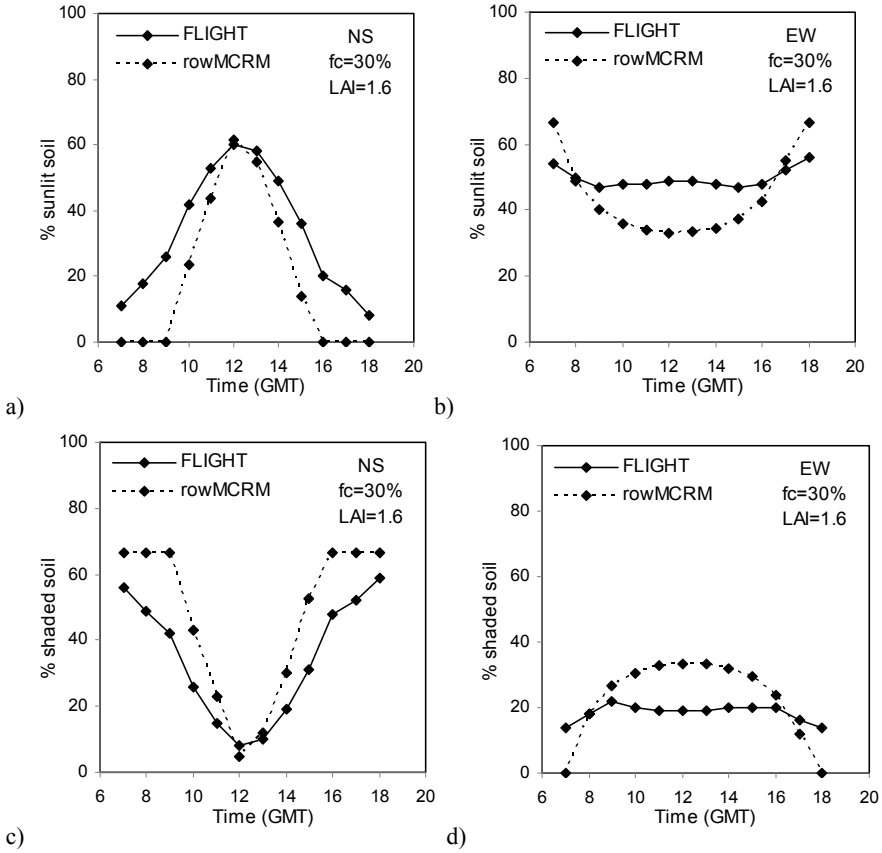

Figure 4.10. Percentage of sunlit soil component over total scenery simulated by FLIGHT and rowMCRM model for NS (a) and EW orientation (b). Percentage of shaded soil simulated by FLIGHT and rowMCRM model for NS (c) and EW orientation (d).

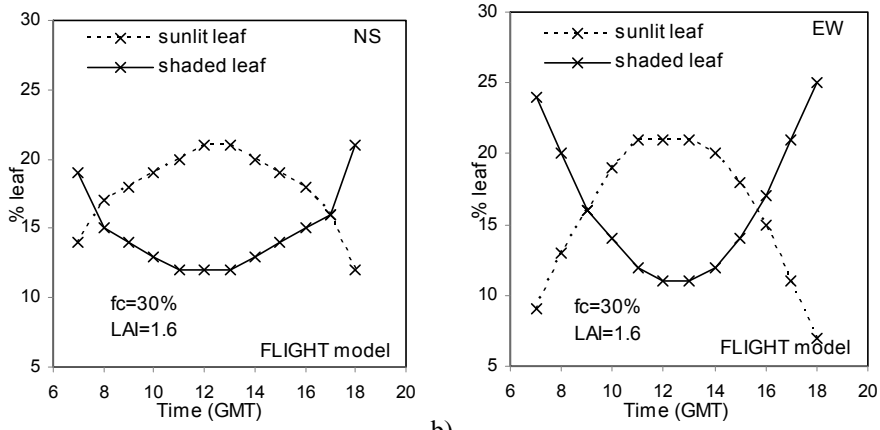

Figure 4.11. Percentage of sunlit and shaded vegetation components simulated by FLIGHT model for NS (a) and EW orientation (b).

4.4. Conclusions

Row crops are a complex target for radiative transfer models since canopy reflectance is affected by background. This study investigated the use of hybrid models, rowMCRM and rowSAIL, to simulate canopy reflectance in vineyards as a function of row orientations and sun viewing geometry, as well as canopy architectural parameters. The capability of the models to adequately describe diurnal changes as a function of input parameters was validated against canopy reflectance obtained by an airborne multispectral sensor acquiring high-resolution imagery in the visible and near-infrared regions. A large airborne and field dataset acquired at different sun angles was required in order to validate the modeling approaches and hypotheses. These results were also compared against simulations obtained with a model based on the Monte Carlo ray tracing method (FLIGHT). This was conducted to assess the differences found with both types of radiative transfer models with varying complexities and assumptions.

The agreement between measured and simulated canopy reflectances were explored. The FLIGHT model yielded rRMSE values below 0.12, when all visible and NIR bands were considered, whereas row-structured models showed an error greater than 0.20. Higher errors (rRMSE = 0.26) in the NIR region were obtained with rowSAIL, likely due to the poor modeling of the multiple-scattering contributions to canopy reflectance, as suggested in Zhao et al. (2010). Regarding optical vegetation indices (NDVI, TCARI/OSAVI and PRI), FLIGHT yielded better results with rRMSE values between 0.1 and 0.25 for all indices, while row models yielded higher errors (rRMSE = 0.3). This study shows that more work should be done to improve the accuracy of row models. Nevertheless this investigation also revealed that the models correctly simulate the trends of canopy reflectance under different optical and geometric conditions. Furthermore, these models can adequately explain the influence of different parameters on overall canopy reflectance, as well as on specific spectral vegetation indices.

In this chapter, we demonstrated the validity of discrete row models (rowMCRM, rowSAIL) as well as 3D model (FLIGHT) to simulate vineyard canopy reflectance. Simulations using rowMCRM and rowSAIL are computationally simpler and faster. The row models are found to be practical when *look-up* table methodologies are used for biophysical and biochemical parameter extraction, where a high number of simulations is needed. However, if more detailed input parameters are available, FLIGHT was shown to be more accurate. In addition, FLIGHT yielded detailed radiation interception values, which will be the focus of the research in Chapter 5.

Acknowledgements

Financial support from the Spanish Ministry of Science and Innovation (MCINN) for the AGL2009-13105, CONSOLIDER CSD2006-67, and AGL2003-01468 projects is gratefully acknowledged, as well as the Junta de Andalucía-Excelencia AGR-595 project co-funded by FEDER (Fondo Europeo de Desarrollo Regional). M.L. Guillén-Climet was supported by a I3P grant from CSIC, co-funded by the European Social Fund. Gratefully acknowledged are A. Kuusk and J. Praks for sharing the rowMCRM code, P.R.J. North for the FLIGHT code, and V. Lefèvre and F. Baret for the rowSAIL model. P. Martin, M.R. Gonzalez, J.A.J. Berni, L. Suárez, M. Medina, A. Vera, A. Hornero and D. Notario are also acknowledged for their scientific and technical support in field and airborne campaigns.

References

Barton, C.V.M. & North, P.R.J. (2001). Remote sensing of canopy light use efficiency using the photochemical reflectance index. Model and sensitivity analysis. Remote Sensing of Environment, 78, 264-273.

Berni, J.A.J., Zarco-Tejada, P.J., Suarez, L. & Fereres, E. (2009). Thermal and Narrow-band Multispectral Remote Sensing for Vegetation Monitoring from an Unmanned Aerial Vehicle. IEEE Transactions on Geoscience and Remote Sensing, 47, (3), 722-738.

Carbonneau, A. (1976). Principes et methods de mesure de la surface foliaire. Essai de caractérisation des types de feuilles dans le genre vitis. Ann. Amélior. Plantes 26, 327-343.

Delenne, C., Durrieu, S., Rabatel, G., Deshayes, M., Bailly, J.S., Lelong, C. & Couteron, P. (2008). Textural approaches for vineyard detection and characterization using very high spatial resolution remote sensing data. International Journal of Remote Sensing, Vol. 29, Issue 4, 1153-1167.

Delenne, C., Durrieu, S., Rabatel, G. & Deshayes, M. (2010). From pixel to vine parcel: A complete methodology for vineyard delineation and characterization using remote-sensing data. Computers and Electronics in Agriculture, Vol. 70, Issue 1, 78-83.

Disney, M.I., Lewis, P., & North, P.R.J. (2000). Monte Carlo ray tracing in optical canopy reflectance modeling. Remote Sensing Reviews, 18 (2– 4), 163-196.

Gamon, J.A., Peñuelas, J., & Field, C.B. (1992). A narrow-wave band spectral index that tracks diurnal changes in photosynthetic efficiency. Remote Sensing of Environment, 41, 35-44.

Gueymard, C.A., (2005). SMARTS Code, Version 2.9.5 User's Manual Solar Consulting Services. Online PDF document from http://www.nrel.gov/rredc/smarts/

Haboudane, D., Miller, J.R., Tremblay, N., Zarco-Tejada, P.J., & Dextraze, L. (2002). Integration of hyperspectral vegetation indices for prediction of crop chlorophyll content for application to precision agriculture. Remote Sensing of Environment, Vol. 81, (2-3), 416-426.

Hall, A., Lamb, D.W., Holzapfel, B., & Louis, J. (2002). Optical remote sensing applications in viticulture - a review, Australian Journal of Grape and Wine Research, Vol. 8, No. 1, 36-47.

Hall, A., Louis, J., & Lamb, D.W. (2003). Characterising and mapping vineyard canopy using high-spatial-resolution aerial multispectral images. Computers and Geosciences, Vol. 29, 813-822.

Hall, A., Louis, J., & Lamb, D.W. (2008). Low-resolution remotely sensed images of winegrape vineyards map spatial variability in planimetric canopy area instead of leaf area index. Australian Journal of Grape and Wine Research, 14, 9-17.

Hall, A., Lamb, D.W., Holzapfel, B.P. & Louis, J.P. (2010). Within-season temporal variation in correlations between vineyard canopy and winegrape composition and yield. Precision Agriculture, 1-15.

Jacquemoud, S. & Baret, F. (1990). Prospect: A model of leaf optical properties spectra. Remote Sensing of Environment, 34, 75-91.

Jacquemoud, S., S.L. Ustin, J. Verdebout, G. Schmuck, G. Andreoli & B. Hosgood. (1996). Estimating leaf biochemistry using the PROSPECT leaf optical properties model. Remote Sens. Environ. 56:194-202.

Johnson, L.F., Bosch, D.F., Williams, D.C., & Lobitz, B.M. (2001). Remote sensing of vineyard management zones: Implications for wine quality. Applied Engineering in Agriculture, 17(4), 557-560.

Kuusk, A. (1985). The hotspot effect of a uniform vegetation cover. Sov. Journal of Remote Sensing, 3, 646-658.

Kuusk, A. (1995a). A fast, invertible canopy reflectance model. Remote Sensing of Environment, Vol. 51, pp. 342-350.

Kuusk, A. (1995b). A Markov chain model of canopy reflectance. Agricultural and Forest Meteorology, Vol. 76, pp. 221-236.

Kuusk, A. (1996).A computer-efficient plant canopy reflectance model. Computers & Geosciences. Vol. 22, 2, pp. 149-163.

Kuusk, A. (2001). A two-layer canopy reflectance model. Journal of Quantitative Spectroscopy and Radiative Transfer**,**Vol. 71,1, pp 1-9.

Liang, S. (2004). Quantitative Remote Sensing of Land Surfaces. ISBN: 978-0-471-28166-5, pp. 560

López-Lozano, R., Baret, F., García de Cortázar-Atauri, I., Bertrand, N. & Casterad, M.A. (2009). Optical geometric configuration and algorithms for LAI indirect estimates under row canopies: The case of vineyards. Agricultural and Forest Meteorology, 149, pp. 1307-1316.

Martín, P., Zarco-Tejada, P.J., González, M.R. & Berjón, A. (2007). Using hyperspectral remote sensing to map grape quality in "Tempranillo" vineyards affected by iron deficiency chlorosis. Vitis, Vol. 46, No. 1, pp. 7-14.

Meggio, F., Zarco-Tejada, P.J., Miller, J.R., Martín, P., González, M.R. & Berjón, A. (2008). Row orientation and viewing geometry effects on row-structured vine crops for chlorophyll content estimation. Canadian Journal of Remote Sensing, Vol. 34, No. 3, pp. 220-234.

Meggio, F., Zarco-Tejada, P.J., Núñez, L.C., Sepulcre-Cantó, G., Gonzalez, M.R. & Martín, P. (2010). Grape quality assessment in vineyards affected by iron deficiency chlorosis using narrow-band physiological remote sensing indices. Remote Sensing of Environment, 114, 1968-1986.

North, P.R.J. (1996). Three-Dimensional Forest Light Interaction Model Using a Monte Carlo Method. IEEE Transaction on Geoscience and Remote Sensing, 34, (4), 946-956.

Pérez, M.A. (2002). Densidad de plantación y riego: Aspectos ecofisiológicos, agronómicos y calidad de la uva en cv. Tempranillo (Vitis vinifera L.). Tesis Doctoral, Dpto. producción vegetal: Fitotecnia. Universidad Politécnica de Madrid. 287 p.

Pieri, P. (2010). Modeling radiative balance in a row-crop canopy: Cross-row distribution of net radiation at the soil surface and energy available to clusters in a vineyard. Ecological Modeling, Vol. 221, pp. 802-811.

Rouse J.W., Haas R.H., Schell J.A., Deering D.W. & Harlan J.C. (1974). Monitoring the vernal advancements and retrogradation of natural vegetation in Nasa/Gsfc final report (ed. MD, U.G.) p. 371.

Suits, G.H. (1972). The calculation of the directional reflectance of vegetative canopy. Remote Sensing of Environment, 2, 117-125.

Suits, G.H. (1983). Extension of a uniform canopy reflectance model to include row effects. Remote Sensing of Environment, Vol 13, 2, 113-129.

Verhoel, W., & Bunnik, N.J.J. (1976) The sectral directional reflectance of row crops. Delft, Netherlands: NIWARS. Publ., No 35.

Verhoef, W. (1984). Light Scattering by leaf layers with application to canopy reflectance modeling: the SAIL model. Remote Sensing of Environment, 6, 125-184.

Zarco-Tejada, P.J., Berjón, A., López-Lozano, R., Miller, J.R., Martín, P., Cachorro, V., González, M.R. & Frutos, A. (2005). Assessing Vineyard Condition with Hyperspectral Indices: Leaf and Canopy Reflectance Simulation in a Row-Structured Discontinuous Canopy, Remote Sensing of Environment, 99, 271-287.

Zhao, F., Gu, X., Verhoef, W., Wang, Q., Yu, T., Liu; Q., Huang, H., Quin, W., Chen, L. & Zhao, H. (2010). A spectral directional reflectance model of row crops. Remote Sensing of Environment, 114, 265-285.

5. Mapping radiation interception in vineyards using 3D simulation and high resolution airborne imagery

"…Viñedos de Andalucía
sobre la tierra candente,
atravesando lomas y cerros,
largas hileras que se pierden;
cepas geométricamente dispuestas
bajo el sol ardiente.
Paisaje multicolor,
cielo azul, casas blancas,
bellas tonalidades que se eclipsan
con los verdes de las parras…"

José Manuel Monge Alvarez

Chapter 5

Mapping radiation interception in vineyards using 3D simulation and high resolution airborne imagery.

Abstract

Methods for fIPAR estimation in vineyards using high resolution multispectral imagery acquired from an unmanned aerial vehicle (UAV) have been developed in this study. Airborne campaigns provided imagery over a total of 21 study sites from 8 *Vitis vinifera* L. fields using a multispectral sensor for different sun geometries and a wide range of row orientations. Imagery was acquired using a 6-band multispectral camera yielding 15 cm resolution. At the time of the airborne flights, field measurements of fIPAR were conducted with a ceptometer together with structural data to characterize the study sites. Airborne imagery acquisitions were conducted diurnally every two hours from sunrise until midday, collecting data at four times of the day, while fIPAR measurements were performed hourly. Two methodologies are used to estimate fIPAR, using high or medium spatial resolution. In the first one, the high spatial analysis allowed to classify each study plot in three pure components, vegetation, shaded and sunlit soil, the fraction of each component as well as the pure reflectance was used to estimate the fIPAR in each study area. This methodology is named as analysis of component in the image. The accuracy obtained with this methodology is compared with the fIPAR estimated from aggregated reflectance pixels (medium spatial resolution study). The imagery was rescaled to a pixel size of 6 m x 3 m, and the aggregated pixels were used to compute spectral vegetation indices (SVI). Relationships between SVI and fIPAR were established to estimate fIPAR from the imagery. The SVI used for this study was the Normalized Difference Vegetation Index (NDVI). As it was shown in previous chapters, the relationships between indices and fIPAR were affected by solar angles, row orientation and the soil background. Thus the use of radiative transfer models was required, and a modeling approach was conducted to understand the influence of the vineyard architecture and viewing geometry on the canopy reflectance for accurate fIPAR estimation. In this study, a 3-D radiative transfer model based on the 3-D Forest Light Interaction Model (FLIGHT) was used. The fIPAR model simulations conducted with modeling approach was compared against the fIPAR field measurements obtained on each site, yielding a root mean square error RMSE=0.1. The estimation of instantaneous fIPAR using component analysis yielded RMSE=0.08 while spectral indices from the airborne imagery was conducted using scaling-up techniques yielding RMSE=0.12

Keywords: vineyards, fIPAR, radiative transfer models, remote sensing, NDVI, high spatial resolution airborne imagery.

5.1 Introduction

The photosynthetically active radiation (PAR) intercepted by the vineyard is a critical process that determines biomass production and potential yield as well as the quality characteristics in terms of sugar concentration and must and wine colour (Robinson and Lakso, 1991, Dokoozlian and Kliewer, 1995, Poni et al., 1996, Baeza et al., 2010). Solar radiation fluxes have a dominating effect on grapevine physiology acting through photosynthetic, thermal and phytochrome response systems (Smart, 1989). These critical implications of light distribution in viticulture production have been known from the beginning of the 60's (May and Antcliff, 1963; May, 1965). In homogeneous crops, leaf area index (LAI) and vegetation cover fraction have been used in conjunction with light interception as a basis for estimating canopy productivity (Monteith, 1973; Jackson, 1980). However, in heterogeneous stands, where leaves are located within an envelope that is distributed in space according to planting pattern and row orientation, the architecture of the stand must be taken into account for light interception studies as a basis for yield estimation (Mariscal et al., 2000). The interactions between fIPAR in vineyards and architecture have been the focus of several studies (Smart, 1973; Smart, 1985; Mabrouk et al., 1997; Pieri and Gaudillere, 2003; López-Lozano, 2011). As in the case of fruit tree orchards, vineyards are grown in a discontinuous- row-structured architecture that makes their geometrical structure more complex to study than in homogeneous canopies, such as grassland or wheat (Mabrouk and Sinoquet, 1998; Lopez-Lozano et al., 2011). Structural changes such as the row orientation, spacing, pruning, and soil surface management, affect the microclimate of the vineyards, influencing the spatial variability of the

berries as well as the must/wine quality (Pieri, 2010). Due to the large variability found in vineyards, extrapolation of locally-derived relationships between indices and fIPAR should be taken with caution (Acevedo-Opazo et al., 2008). Because of this within-field spatial variability precision viticulture aiming at maximizing grapevine production is showing a growing interest in remote sensing techniques together with the use of canopy models (Hall et al., 2002). The radiative transfer models are needed in these complex canopies to interpret the optical remote sensing spectra which aggregate different scene components, such as sunlit and shaded soil and vegetation areas, as function of canopy architecture and viewing geometry. It was Smart, in 1973, the first one developing a specific model for grapevine to evaluate the effects of variables such as plant shape, size, planting distance or row orientation in relation to the light microclimate. Since then, other models have been formulated where the amount of detail to simulate the vineyard canopy has increased substantially (Riou et al., 1988, Sinoquet and Bonhomme, 1992; Mabrouk et al., 1997, Mabrouk and Sinoquet, 1998; Lebon et al., 2003; Louarn et al., 2008; García de Cortazar, 2009). However, these models do not include canopy reflectance as an output. A review of models including canopy reflectance as output variable may be found in chapter 4 where the evolution of canopy reflectance models from simpler to more physical sophisticated models is shown. This progress, focused on the ability to quantitatively relate canopy reflectance and vegetation canopy attributes, enables monitoring vegetation biophysical parameters by remote sensing (Goel and Grier, 1987, Houborg and Boegh, 2008). Regarding the estimation of intercepted radiation by vegetation, red and near-infrared SVI were used by authors such as Daughtry et al. (1983), Steven et al. (1983), Hatfield et al. (1984; 2008); Asrar et al. (1992); and Moriondo et al. (2007),

among others. In particular, the relation between spectral vegetation indices (SVI) and fIPAR was investigated using radiative transfer models by Huete (1989), Choudhury (1987) or Huemmrich and Goward (1997), showing how the relationships vary with changes in the canopy architecture and in optical properties of the canopy components and the background. However, many of these studies were focused on randomly distributed canopy elements and closed canopy forest areas. Only a limited number of studies have focused on heterogeneous canopies such as the row-structured open-tree canopies, where such random-distribution assumptions may not be valid. The objective of this chapter was to estimate fIPAR in row-structured vineyards using high resolution multispectral remote sensing imagery and radiative transfer models. The high spatial resolution images acquired for this study enabled the discrimination of vegetation, shaded and sunlit soil component. As such, we can obtain their fractional areas as well as the pure reflectance of each component. The high spatial details allow an accurate assessment of FLIGHT's ability to simulate fIPAR and canopy reflectance for this complex canopy architecture. A database including spatial and diurnal variability of fIPAR, as well as, canopy reflectance was collected to achieve these objectives. In this chapter, two different assessment methodologies are used. The first approach exploits the spatial details of the high resolution data to determine fIPAR through scene component analysis. The second method, assumes lower level spatial detail (aggregated pixel analysis) to estimate fIPAR using spectral vegetation indices. As such, we can potentially use the SVI-fIPAR relationships for predictive modelling.

5.2. Materials and Methods

5.2.1. Field data collection

Field data were collected in August-September 2009 in the western area of Ribera del Duero *Appellation d'Origine* (northern Spain). A total of 8 vineyards belonging to a plot network currently monitored by the local government were selected to assure appropriate variability in vegetation cover fraction and row orientation (Figure 4.1, chapter 4). The distance between rows was 3 m with 1.5 m between vines. The field data was determined on 21 sub-areas of 6 m x 3 m located in each of the 8 selected vineyards (Table 4.2, chapter 4). The vineyards under study ranged in canopy structure, soil background, and planting row orientation.

Field sampling was conducted in these areas concurrent with airborne overflights for testing and validating row-structured models. The 3-D radiative transfer model FLIGHT (North, 1996) is used in this study. This model was previously validated for canopy reflectance and vegetation indices in vineyards (chapter 4).

The ground measurements conducted on these selected plots involved measurements of canopy architecture and fraction of intercepted radiation. The interception of solar radiation by the orchard canopies at each time of day was measured with a ceptometer (SunScan Canopy Analysis System, Delta-T Devices Ltd, Cambridge, UK). The measurements were done hourly, starting at the time of the first airborne campaign for imagery acquisition. The ceptometer is composed of two units: (i) a probe, portable instrument of 1-m long, for measuring the transmitted photosynthetically active radiation (PAR) flux beneath the canopy; and (ii) a reference sensor

that measures PAR incident on the canopy. The measurements of transmitted PAR made within the area beneath the 6 m x 3 m of each plot were in a 1 m x 0.5 m grid (Figure 5.1). The measurements were carried out for every study plot assessing the spatial variation of fIPAR. The measurements, repeated every hour from dawn to noon, capture the diurnal variation of the intercepted solar radiation. Figure 5.2 shows the shadow diurnal variation during the day at the airborne imagery (Figure 5.2, left) and as measured with the ceptometer (Figure 5.2, right).

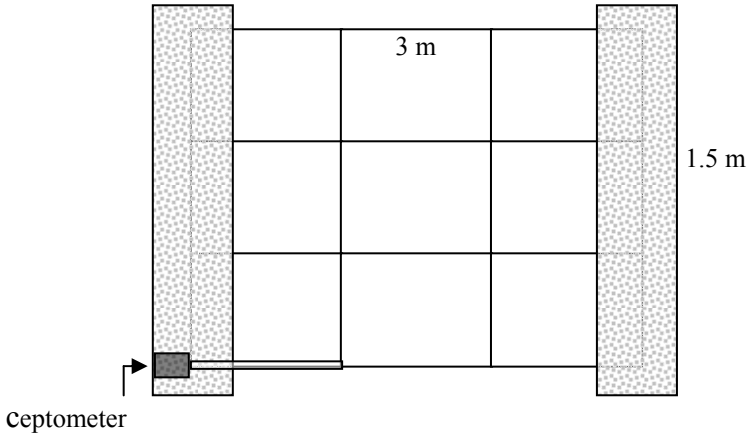

Figure 5.1. Schematic view of the grid (1 m x 0.5 m) used for field measurements made by the ceptometer between the four trees per plot.

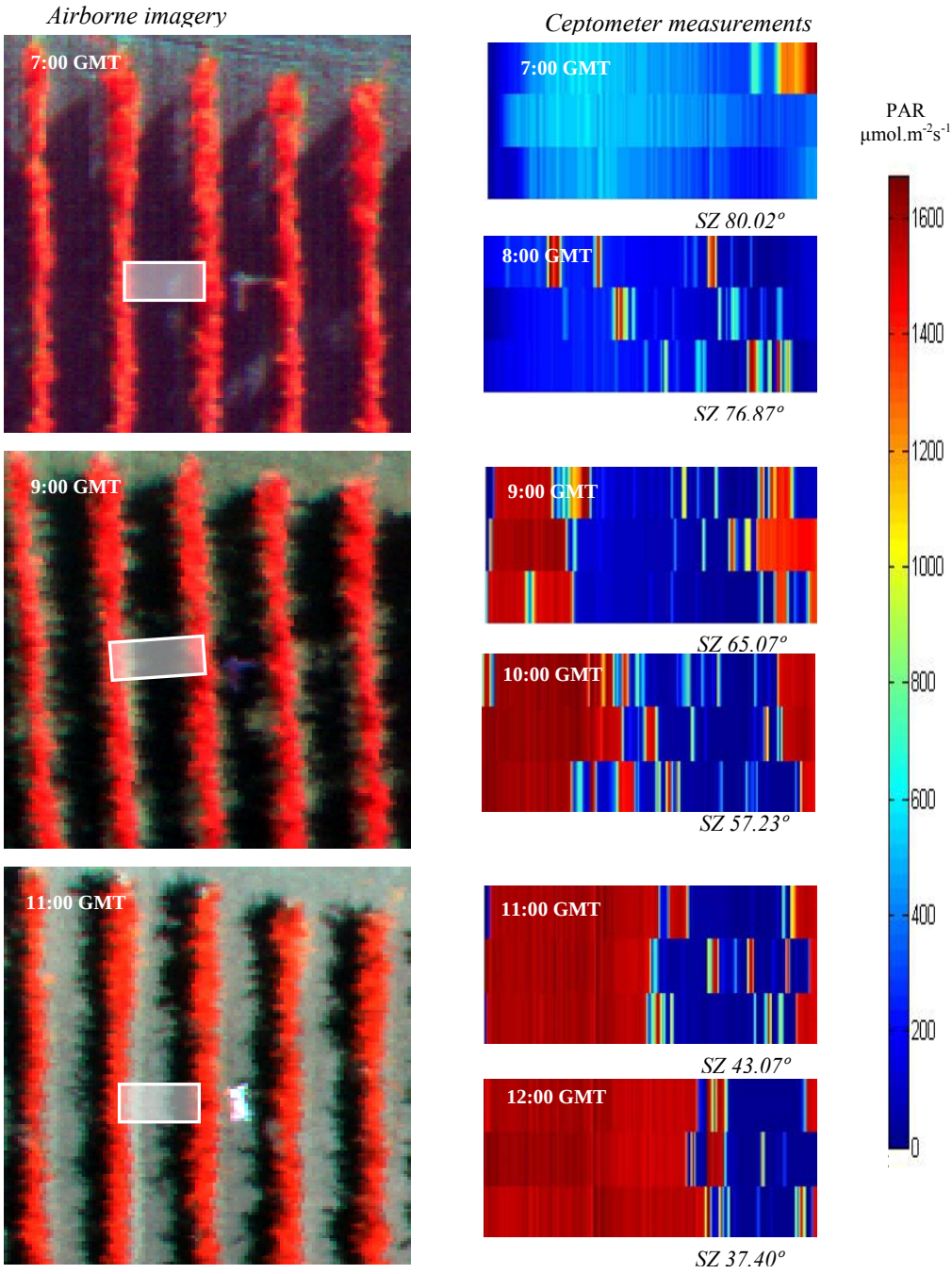

Figure 5.2. Airborne imagery showing one of the study sites at 7.00, 9.00 and 11.00 GMT (2009, 03rd September) (left) and diurnal variation of PAR measured by ceptometer at soil level (area shown is marked area in the airborne image) (right).

Other additional structural and optical parameters were measured to characterize each plot, and used later as input for the canopy model. The leaf optical properties were simulated with PROSPECT leaf radiative transfer model (Jacquemoud and Baret, 1990; Jacquemoud et al., 1996) (Figure 5.3). The inputs required for PROSPECT are shown in Table 5.1. The canopy structural parameters, such as canopy height, visible soil strip and leaf area index (LAI), calculated as in Perez (2002) and explained in chapter 4 were measured in each study plot (mean is shown in Table 4.1). The soil reflectance was measured at each flight time for each location. Sun azimuth and row orientation were both measured in a clockwise direction from north. These data were used as inputs for the model to simulate canopy reflectance and fIPAR, and to validate fIPAR simulations with the measurements taken with the ceptometer in each study plot.

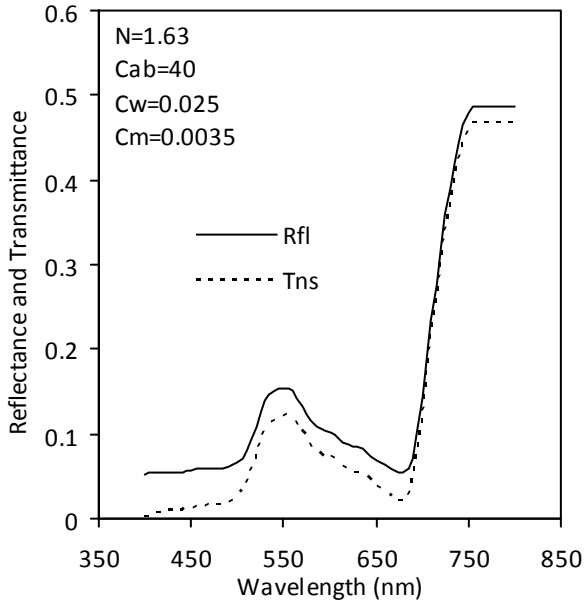

Figure 5.3. Leaf spectral reflectance and transmissivity simulated with PROSPECT.

Table 5.1. Nominal values and range of parameters used for leaf and canopy simulation with PROSPECT and FLIGHT for vine study sites.

	Nominal values and range
PROSPECT **Leaf parameters**	
Chlorophyll a+b C_{ab} *(ug cm^{-2})*	40
Leaf water content, C_w *(cm)*	0.025
Leaf dry matter content, C_m *(g cm^{-2})*	0.0035
Leaf internal structure parameter, *N*	1.62
FLIGHT **Leaf optical and structural parameters**	
Hemispherical reflectance and transmittance of green leaves	PROSPECT simulations
Hemispherical reflectance and transmittance of senescent leaves	Not used
Leaf equivalent radius	0.083 m
Canopy layer and structural parameters	
Leaf area index (LAI)	See Table 4.2
Fractional cover	12-60%
Leaf Angle Distribution Function (LADF)	plagiophile
Fraction of green leaves	1
Fraction of senescent leaves	0
Fraction of bark	0
Number of stands and position coordinates	Not used
Crown shape	Elliptical
Crown height and radius	See Table 4.2
Trunk height and radius	m
Background and viewing imagery geometry	
Solar zenith and azimuth angles	See Table 4.1
Sensor zenith and azimuth angles	Degrees
Soil reflectance	Specific for each site
Soil roughness	0
Aerosol Optical Depth (AOD)	0.15

5.2.2. Airborne campaigns

Airborne campaigns were conducted in 2009 with a narrow-band multispectral camera. Flights were conducted using an unmanned aerial vehicles (UAVs) operated by the *Laboratory for Research Methods in Quantitative Remote Sensing* (QuantaLab, IAS-CSIC, Spain) (Berni *et al.,* 2009b; Zarco-Tejada *et al*., 2008; 2012). This platform was used to fly the multispectral camera over the study sites in 2009. The multispectral sensor flown was a 6-band multispectral camera consisting of 6 independent image

sensors and optics with user-configurable 10 nm full-width at half maximum (FWHM) spectral filters (Berni *et al.,* 2009a; Zarco-Tejada *et al.,* 2009). The image resolution is 2592 x 1944 pixels with 10 bit radiometric resolution, optics focal length of 8.4 mm, and angular field of view (FOV) of 38.04º x 28.53º, yielding 15 cm spatial resolution at 150 m flight altitude. The bandsets selected for this study comprised centre wavelengths located at 515, 530, 570, 670, 700 and 800 nm. The multispectral images acquired over each vineyard field enabled the identification of the study areas used for the leaf sampling and ground structural measurements. The airborne campaign was conducted at 7.00, 9.00, 11.00 and 13.00 GMT. Figure 5.4 shows the multispectral imagery of two study sites with North-South and East-West row orientation at three times of the day. As expect, the percentage of soil shadows change more drastically along the day for NS than for EW row orientation. For identification purposes, each plot was marked in the field using ground control points detectable in the imagery. In chapter 4, the processing required for the multispectral imagery to calculate the spectral reflectance is explained in detail. The multispectral imagery acquired enabled successfully separating pure vine from shaded and sunlit soil reflectance in most cases (Figure 5.5a), obtaining the fraction of each component separately (Figure 5.5b). The high spatial resolution enabled the extraction of the mean reflectance for the spectral bands acquired for vegetation index calculation from the different components identified from each study site (Figure 5.5c).

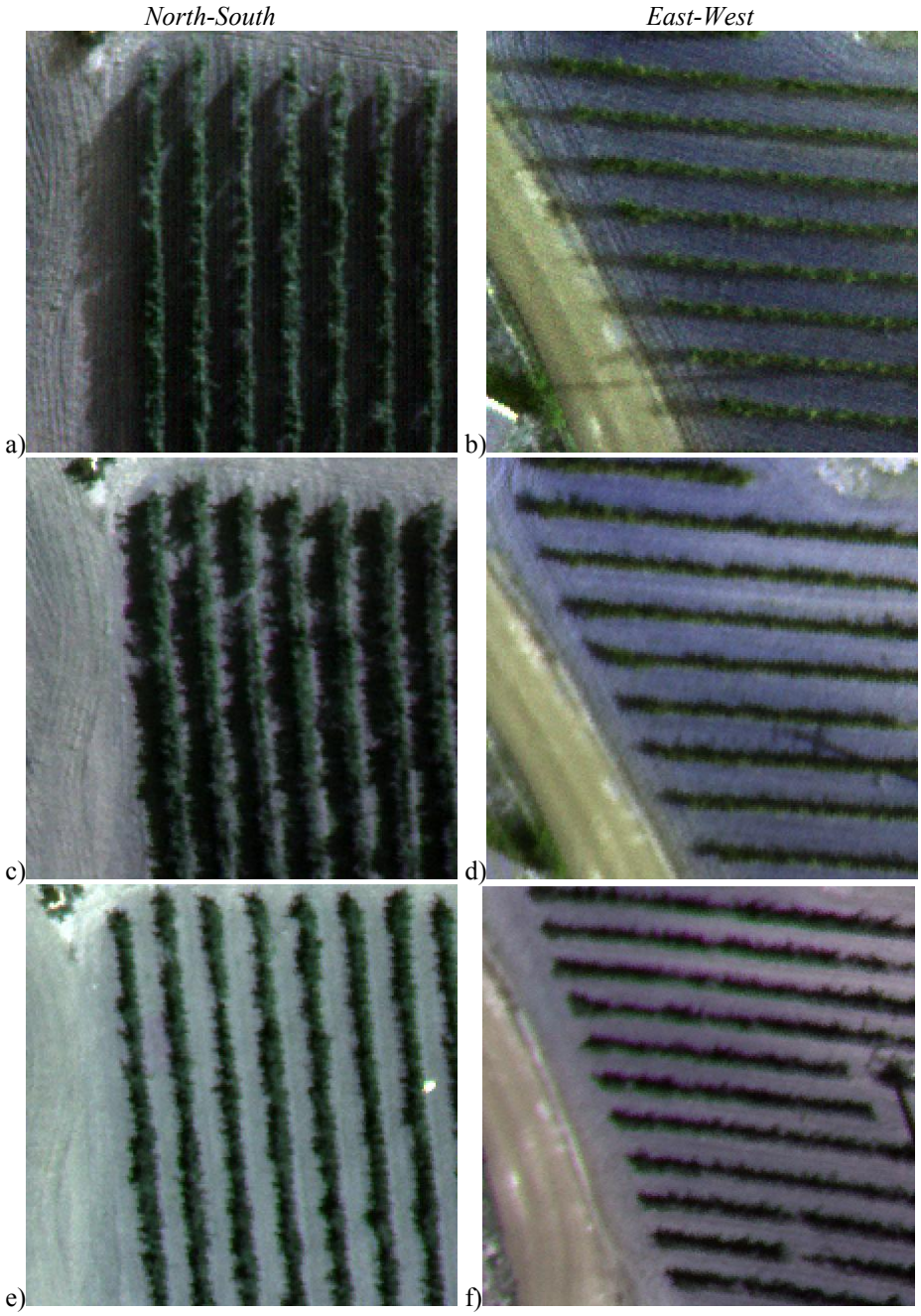

Figure 5.4. Shadows evolution in a N-S study area at 7.00, 9.00 and 11.00 GMT (a, c, e, respectively), and a E-W area at the same times (b, d, f), in the summer of 2009.

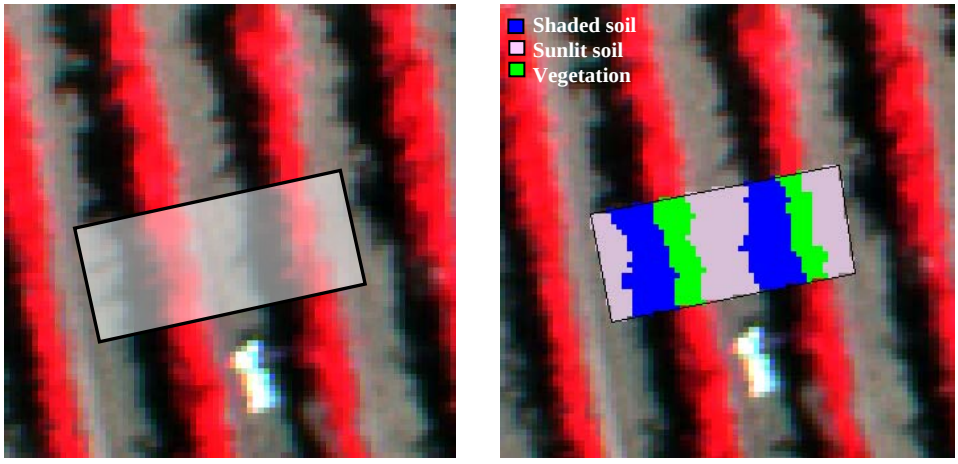

a) b)

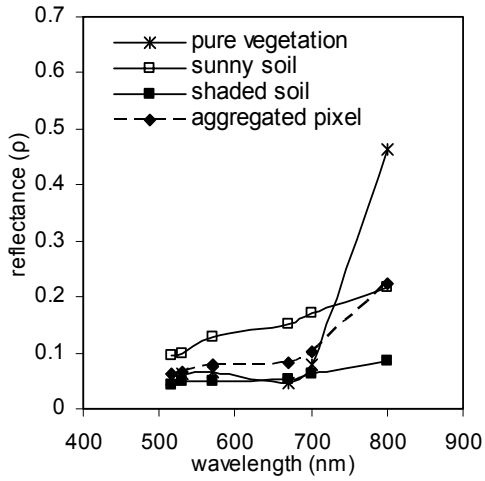

c)

Figure 5.5. Example of multispectral reflectance imagery showing the region of interest, including vegetation, shadows and sunlit and shaded soil (a), and the classified image (b). The pure crown, sunlit and shaded soil and aggregated spectra obtained (c).

5.2.3. fIPAR validation for FLIGHT

A detailed simulation of the land surface bidirectional reflectance was undertaken by radiative transfer models approach. The 3-D Forest Light Interaction Model, (FLIGHT) is based on Monte Carlo ray tracing method as a tool to simulate the radiative transfer in a canopy structure (North, 1996). At the top of canopy, the interaction of radiation within the vegetation depends on the contribution of several components such as leaves, stems, soil background, illumination and view properties of each canopy elements as well as on their number, orientation and location in space (Goel and Thompson, 2000; Koetz et al., 2005). The technique requires sampling the photon free-path within a canopy representation, and the simulation of the scattering event at each iteration. An accurate treatment of the light interception and multiple scattering between foliage elements and the soil boundary is obtained by iteration (North, 2002). The FLIGHT radiative transfer model has been previously applied to row-structured olive orchards (Suárez et al., 2008, and chapter 3) and to peach and orange orchards (chapter 2). In this work, the FLIGHT model was used to simulate vineyard canopy reflectance and fIPAR.

The model allows simulating the effects of row orientation, tree dimensions, soil and leaf optical properties and sun geometry. The simulated orchard is a set of rows and columns referenced by four angles in the coordinate system NSWE-vertical. A tree is positioned at each row-column intersection. The orchard size is dimensioned so that all trees potentially contribute to the interception of radiation.

The model FLIGHT was run with inputs parameters measured in the field. Simulations were done for every single plot whose architectural

characteristics can be found in Table 4.2. Leaf optical properties were obtained with PROSPECT (Figure 5.3) and soil optical properties were obtained from the airborne imagery at each study site. The output fIPAR for FLIGHT was validated at the four different times. Observed (o_i), measurements with the ceptometer, and simulated (p_i) were compared by regression analysis. The root mean square error was calculated as:

$$RMSE = \sqrt{\frac{1}{N}\sum_{i=1}^{i=N}(p_i - o_i)^2} \qquad [5.1]$$

The validation for canopy reflectance in vineyards with FLIGHT model was conducted previously in chapter 4.

The model was used to study the influence of different parameters, such as row orientation, sun position and other architectural properties on canopy reflectance and fIPAR. A detailed study about canopy reflectance in different scenarios appears in chapter 4. The same situations were studied now to analyse the influence of these factors on fIPAR. To show the influence in the relationships between row orientation and fIPAR, FLIGHT was used to simulate different sceneries with the same vegetation cover fraction and different row orientation and varying LAI 0.5, 1 and 2 for three different vegetation cover fractions.

5.2.4. Retrieval of fIPAR using components analysis in the scene and NDVI

5.2.4.1. Component analysis

The high spatial resolution imagery was analyzed to obtain the percentage of each component of the scene, vegetation, shaded and sunlit soil, as well as their reflectances. This information is then used to estimate instantaneous fIPAR. The factors determining the intercepted radiation regime in vegetation canopies are the architecture of the entire canopy, optical properties of vegetation elements and the soil and the spectral composition of the incident radiation field (Wang et al., 2003). The fIPAR for the different study areas is computed as:

$$fIPAR = fr_{shs} \cdot \tau_p = fr_{shs} \cdot \left(1 - \frac{rfl_{PARshs}}{rfl_{PARss}}\right) \quad [5.2]$$

where fr_{shs} is the fraction of shaded soil and τ_p is the vegetation transmisivity in the PAR region (400-700 nm), computed as 1 minus the reflectance of sunlit soil (rfl_{PARss}) divided by reflectance of shaded soil (rfl_{PARshs}).

Each study site is classified into three components, vegetation, shaded and sunlit soil (Figure 5.5b) using a supervised classification methodology. The nadir view does not allow the discrimination of the fraction of shaded soil directly under the vegetation, thereby leading to underestimation in the fIPAR. As a result, a distinction is made between shaded soil visible from above and shaded soil that is hidden as a result of vegetation cover. In this study, it was assumed that the soil under the vegetation was shaded soil, therefore the fr_{shs} was computed as the sum of the fraction of shaded soil seen from above plus the fraction of vegetation.

To check the influence of row orientation and sun geometry in this methodology an analysis with FLIGHT was carried out. The same fraction of vegetation (25%) was simulated at different times of the day to generate difference fraction of shadows, the fIPAR estimated by this methodology was then compared with the output of fIPAR computed by FLIGHT. This methodology was also applied to the different study areas simulated by FLIGHT and fIPAR estimated was compared with the fIPAR obtained with FLIGHT. Additionally the method was validated using the field measurements of fIPAR.

5.2.4.2. Calculation of fIPAR using NDVI. Aggregated pixel analysis.

Several optical indices existing in the literature have been correlated with various vegetation parameters such as LAI, biomass, chlorophyll concentration, and photosynthetic activity, among others. Haboudane et al. (2004) presented a review of studies showing the prediction power of optical indices to canopy parameters. Here, the *Normalized Difference Vegetation Index* (NDVI) (Rouse et al., 1974) was used here to test their relationship with fIPAR.

$$NDVI = \frac{(R_{800} - R_{670})}{(R_{800} + R_{670})} \qquad [5.3]$$

In previous chapters, we demonstrated the good correlation between NDVI and fIPAR for peach, orange and olive orchards. This relationship is also checked here for vineyard fields. Sensitive analysis carried out also previously showed the important effect of row orientation, sun geometry and soil optical properties on NDVI-fIPAR relationships. However, detailed information, such as soil optical properties is not possible to obtain if high spatial resolution is not available. In this chapter, methodology to estimate

fIPAR through predictive relationships is evaluated considering a medium spatial resolution. Thus, predictive algorithms NDVI-fIPAR were calculated under specific canopy assumptions. The predictive algorithms for vineyard orchards were obtained with input parameters fixed according to mean field measurements for each plot: leaf angle distribution, row orientation, and solar position depending on the time of flight. A specific set of input parameters for the models was varied, with a range for the canopy height from 0.6 to 2.0 m; width from 0.2 to 1.0 m, and LAD from 2 to 5. The soil reflectance was extracted from the airborne imagery as mean for all study sites. The soils were calcareous and poor in organic matter, with a medium-weighed texture and an average pH of 8.7. Concentrations of active carbonate (up to 17.6%) and DPTA extractable Fe (1.2 to 7.6 $mg \cdot kg^{-1}$) were highly heterogeneous within the study areas. The high spatial resolution allows extracting the soil reflectance for each study area. However, the medium spatial resolution would not allow it, thus a soil spectra of medium reflectance from the area of study was used.

The aggregated information to obtain the SVI was used considering vegetation, soil and shadows together. The pixel resolution in this approach was 6m x 3m.

The predictive relationships were obtained for three different solar angles corresponding to three flight times. The earlier flight time (*SZ 80.02º, SA 88.40º*) was not used in the study since low zenith angles created a large error in the atmospheric correction of the imagery acquired at that time. This methodology enabled the application of sensor-derived optical indices for predictive algorithms NDVI-fIPAR that are a function of canopy structure, optical properties and the viewing geometry. The modelled relationships

NDVI vs fIPAR obtained for each orchard were then applied to the multispectral airborne imagery reflectance to estimate the instantaneous fIPAR for each flight time at each study site.

Finally, methodologies such as the component analysis and aggregated pixel analysis were applied to the different study areas to obtain maps showing the spatial variation of the instantaneous fIPAR.

5.3. Results

5.3.1. Validation of FLIGHT to simulate fIPAR in vineyards

The validation of modelled fIPAR is shown in Figure 5.6. The comparison between simulations and field data indicated a good performance of the models, with RMSE below 0.1 when three different sun geometries were considered (Figure 5.6a). The same analysis was conducted showing each time independently, with higher errors at 9.00 GMT, with RMSE 0.12 (Figure 5.6b). While the RMSE for 11.00 and 13.00 GMT was 0.07 (Figure 5.6c and Figure 5.6d).

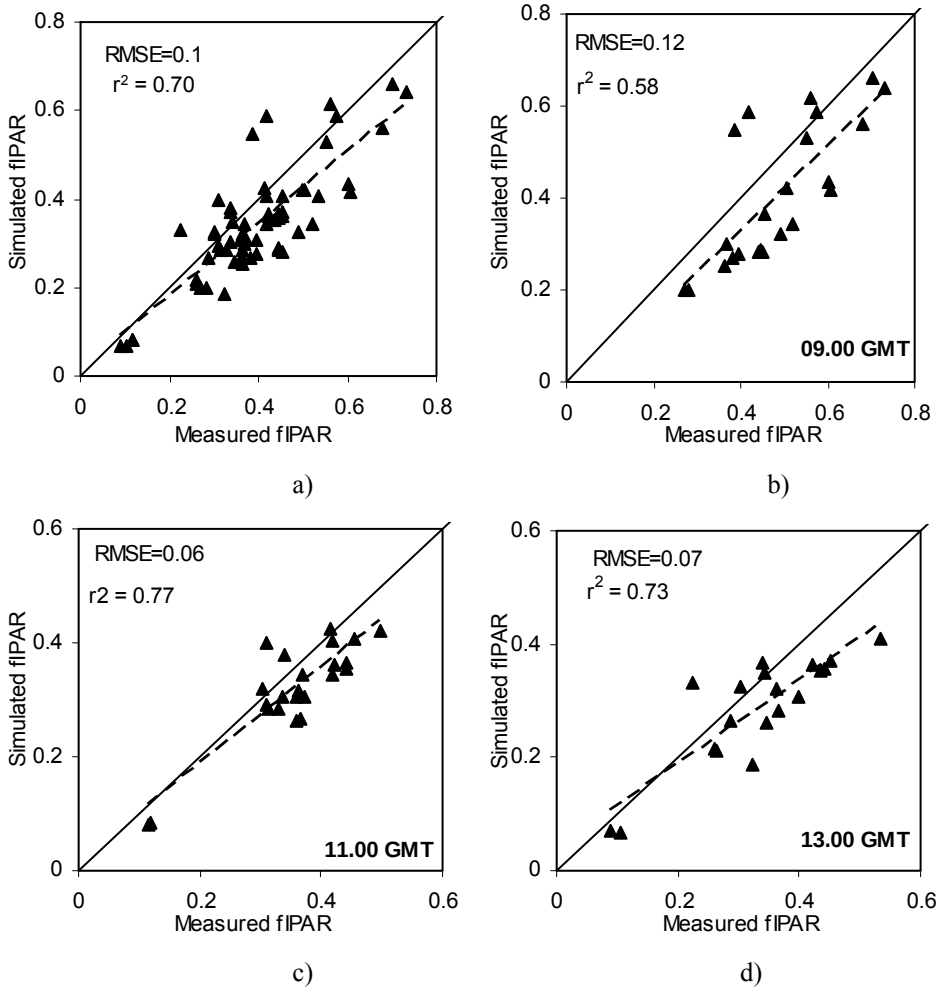

Figure 5.6. Variation of fIPAR measured by the ceptometer versus FLIGHT simulation for all the study plots at three different times (9.00, 11.00 and 13.00 GMT, 03rd September 2009) (a) and for these three times independently, 09.00 GMT (b), 11.00 GMT (c) and 13.00 GMT (d).

The analysis showed previously in chapter 4 with simulations conducted to understand the sensitivity of input parameters on the canopy reflectance and SVI, were now studied here for fIPAR showing the behaviour of fIPAR under different situations. Thus, in a simulation with a North-South row orientation, LAI=1.6, visible soil strip=1.7 m and bright soil, NDVI decreased from 0.8 to 0.42 from early morning to midday, while fIPAR

varied from 0.86 to 0.3. For the East-West row orientation changes in NDVI and fIPAR were negligible during the day, as expected, as changes in percentage of shadows on the soil during the day are minimal (see Figure 5.4).

The relation between fIPAR and row orientation showed that the range of variation for stands with the same vegetation cover fraction as function of row orientation (Figure 5.7) was higher when the vegetation cover fraction was smaller. For a vineyard canopy with LAI=1, the fIPAR varied from 0.5 to 0.55 (vcf=50%) and from 0.25 to 0.5 for vcf=15%. The LAI was varied without modify architecture of the canopy, thus the variation was in the vegetation density. Therefore vineyards with same cover fraction may have large variations in radiation interception.

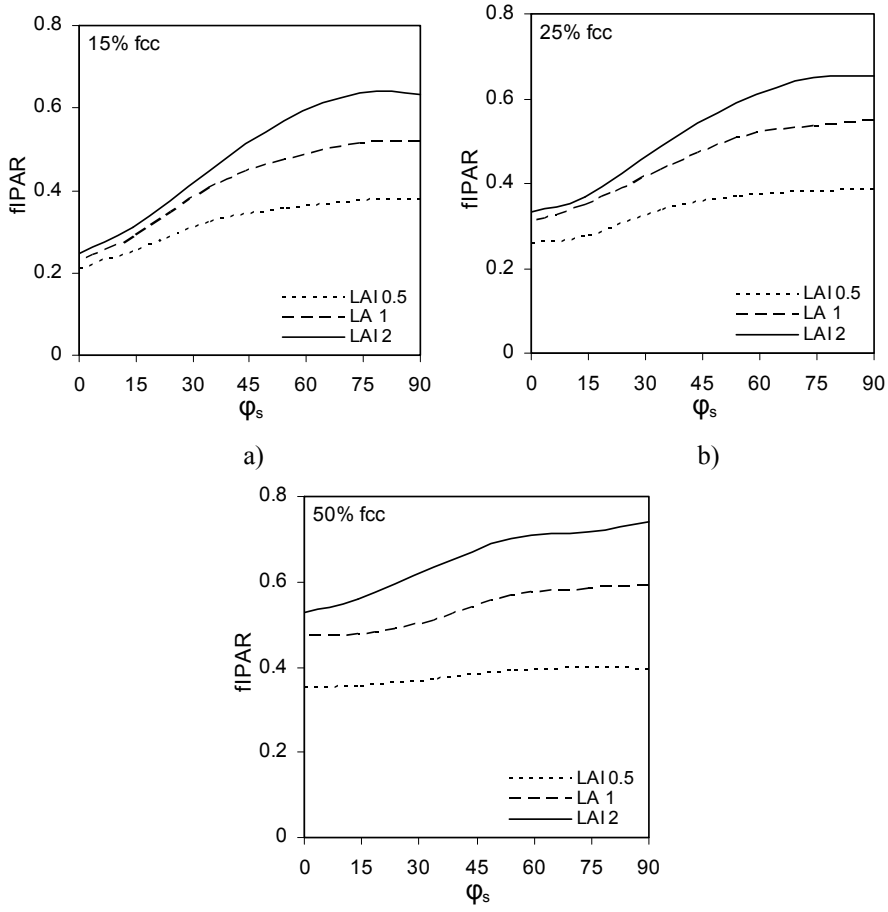

Figure 5.7. Relationships between fIPAR and φ_s (difference between solar azimuth and row orientation) obtained with FLIGHT simulations for vegetation cover fraction of 15% (a) 25% (b) and 50% (c).

The model FLIGHT showed to simulate with adequate accuracy fIPAR in vineyards. The sensitivity analysis of parameter carried out with this model show that fIPAR is highly affected by row orientation and sun geometry.

5.3.2. Using component analysis and NDVI for fIPAR estimation in vineyards

5.3.2.1. Component analysis

Simulations carried out to check equation [5.2] showed that the formula did not work well when the shaded soil percentage is very small and the reflectance of shaded soil is similar to the sunlit soil (Figure 5.8a, estimated $fIPAR_1$). For these situations when the fraction of shaded soil is lower than 0.10 or the relation between reflectance of shaded and sunlit soil higher than 0.5, the fIPAR was assumed to be equal to the sum between vegetation and shaded soil fraction (Figure 5.8a, estimated $fIPAR_2$).

The comparisons between the estimated fIPAR obtained from equation [5.2] applied to the simulated study areas modelled with FLIGHT, and the fIPAR simulated with FLIGHT yielded a RMSE of 0.024 with a correlation coefficient of 0.96.

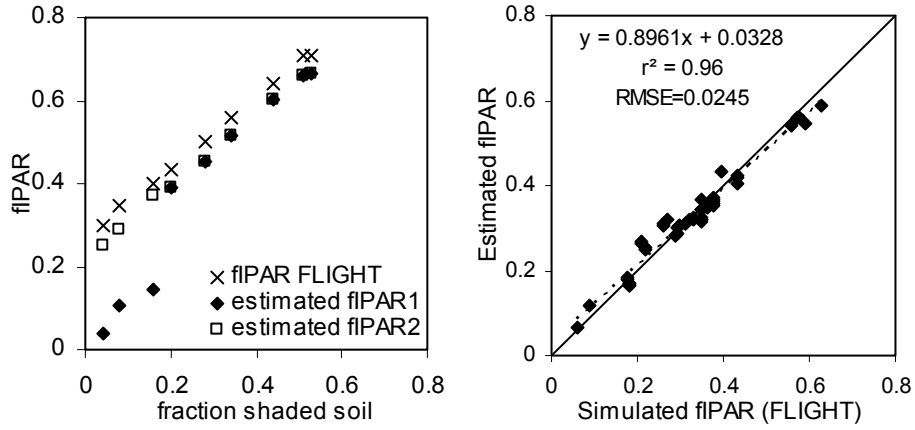

Figure 5.8. Relationships between fIPAR and fraction of shaded soil for the same percentage of vegetation changing φ_s (difference between solar azimuth and row orientation) obtained for FLIGHT, the fIPAR estimated with eq [5.2] (a) . Comparisons between the fIPAR simulated by FLIGHT and fIPAR estimated for simulations of the study areas with component analysis methodology.

This algorithm with these two restrictions was applied to the different study areas at the different times of the day to estimate fIPAR. The estimated fIPAR compared with the field measured fIPAR by ceptometer yielded RMSE of 0.08 (Figure 5.9)

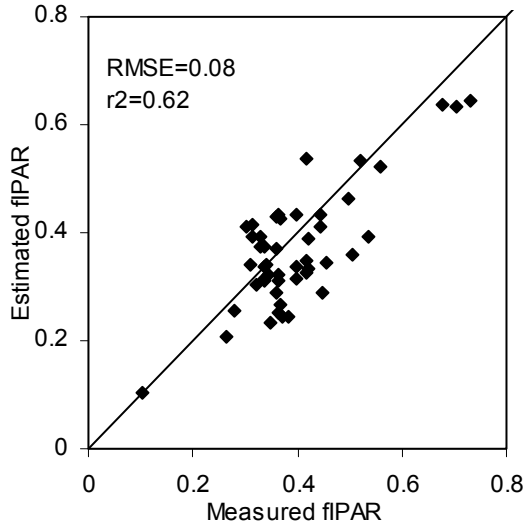

Figure 5.9. Comparison between the fIPAR simulated by FLIGHT and fIPAR estimated for multispectral imagery of the study areas with component analysis methodology.

5.3.2.2. Retrieval of fIPAR with NDVI

The relationships between instantaneous fIPAR and the aggregated spectral vegetation indices (including vegetation, exposed soil and shadows) demonstrated that NDVI yielded better results in the linear regression analysis. As expected, the relationships exhibited a considerable scatter mainly at low zenith angles. As example, Figure 5.10 shows the relation between NDVI obtained from airborne imagery and field fIPAR measured showing to be highly influenced by solar angles, therefore the relation are not applicable in a general way and these indices need to be parameterized using radiative transfer models.

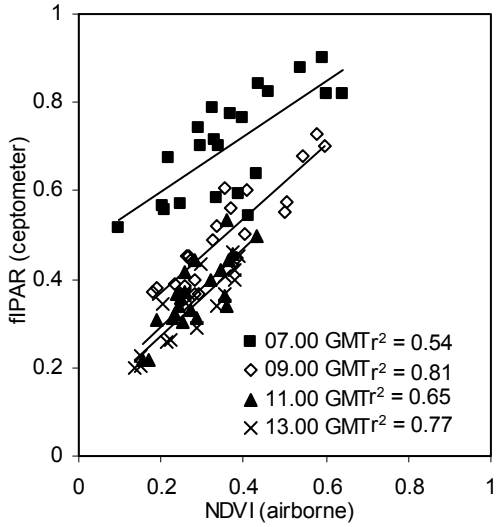

Figure 5.10 Aggregated NDVI computed from high resolution airborne imagery against field-measured intercepted radiation for several study sites acquired at four different times (7.00, 9.00, 11.00 and 13.00 GMT, 03rd September 2009).

The methodology to estimate instantaneous fIPAR through predictive relationships was applied and the results obtained from comparisons between fIPAR estimations and field data measured by ceptometer appear in Table 5.2. Better results were obtained mainly at times when the percentage of shadows are smaller, near midday (Table 5.2). The RMSE was 0.12 without considering sun geometry.

Table 5.2. fIPAR estimations with predictive relationships.

	Time		NDVI
FLIGHT	10.45	RMSE	0.140
		r^2	0.80
	13	RMSE	**0.10**
		r^2	0.76
	14.45	RMSE	**0.12**
		r^2	0.77
	All times together	RMSE	0.12
		r^2	0.75

($p < 0.001$)

A direct application of both methodologies, component analysis with high spatial resolution and predictive relationships with aggregated pixel analysis enabled the mapping of the spatial variation of fIPAR at orchard scale using airborne imagery (Figure 5.11 and Figure 5.12, respectively). Figure 5.13 shows the maps obtained for the same area for both methodologies using medium resolution with a medium soil reflectance (Figure 5.13a) and high spatial resolution (Figure 5.13b). The differences between both methodologies appear in Figure 5.13c, differences of 0.14 are found between them.

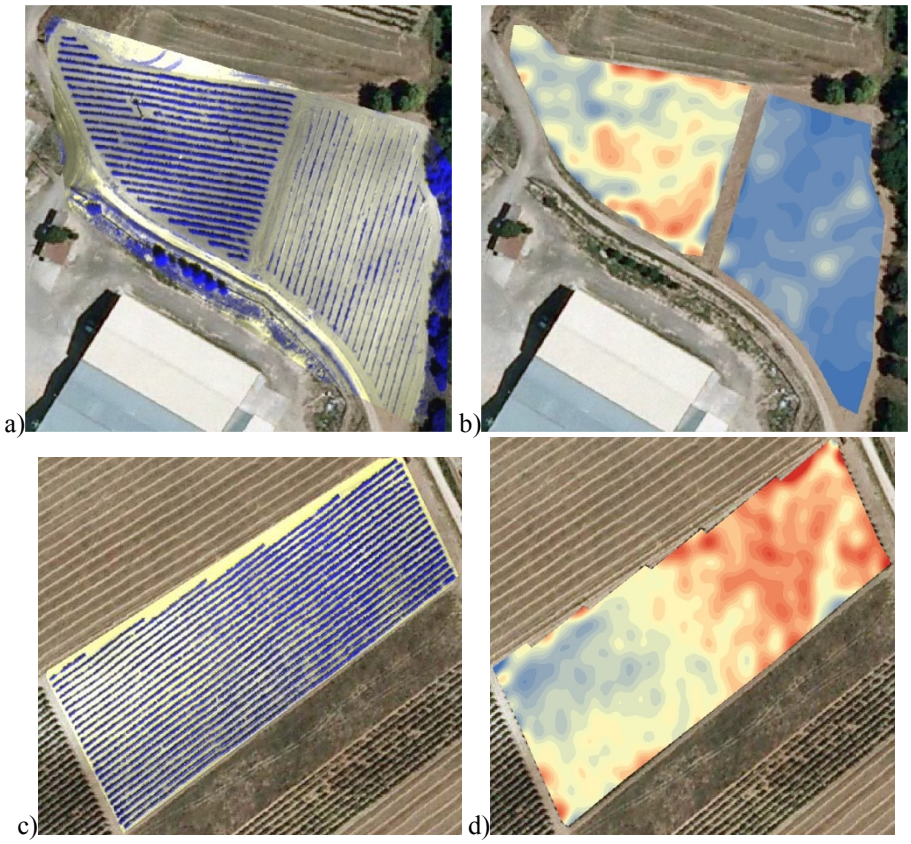

Figure 5.11 Multispectral mosaic of the vineyard (a, c) used to generate a map of fIPAR calculated from high spatial resolution (b, d) using the methodology of component analysis.

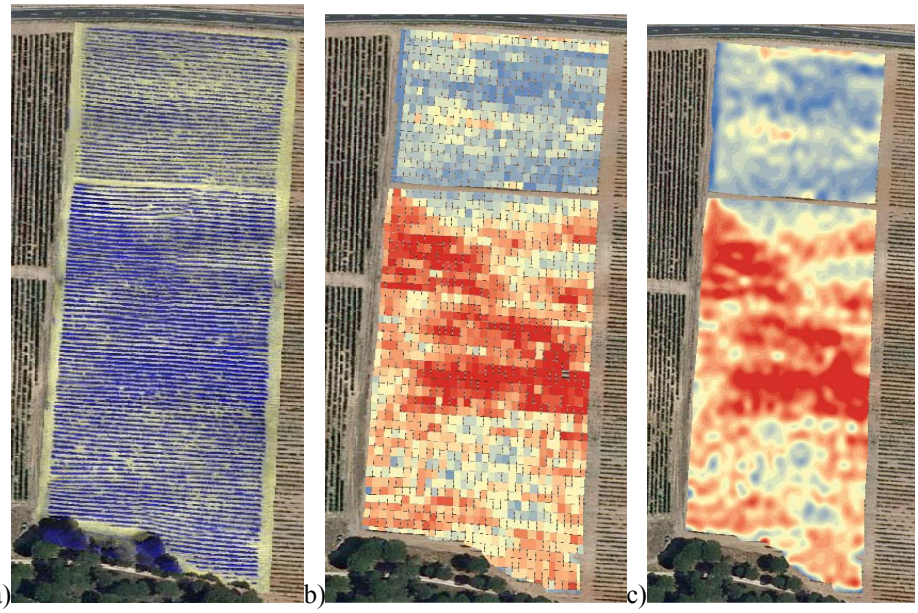

Figure 5.12. Multispectral mosaic of the vineyard (a) used to generate a map of fIPAR calculated from medium spatial resolution (b) using scaling-up with the FLIGHT model and the interpolated map generated (c).

a) b)

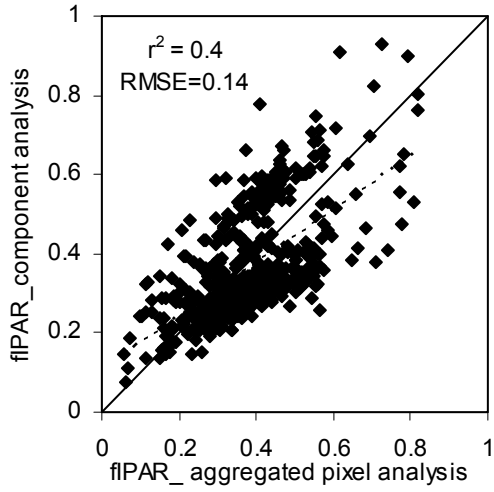

c)

Figure 5.13. Maps of fIPAR calculated from medium spatial resolution (a) using aggregated pixel analysis and high spatial resolution (b) using component analysis. Relationships between fIPAR obtained for both methodologies (c)

5.4. Conclusions

This work investigated methodologies to estimate fIPAR in vineyards using radiative transfer modelling and measurements conducted with ground and remote instruments. Vineyards are grown as canopies that discontinuously cover the ground, leaving free space for crop management. Limited work has been published where field canopy reflectance and fIPAR measurement were compared with simulated scenarios obtained by models. The model used to simulate fIPAR in this study, FLIGHT (North, 1996) was validated against fIPAR field measurements. This study provided a wide database to demonstrate that fIPAR can be simulated with FLIGHT. The model was also used to study the variability of fIPAR for the same vegetation cover fraction under different row orientations. The row orientation and architecture of the canopy is needed to be considered in this kind of row structured orchard to estimate fIPAR. Two methodologies were explored, first exploiting the detailed information obtained by high spatial resolution, and secondly using medium spatial resolution. The high spatial resolution of the multispectral imagery allowed classifying the images in pure components, vegetation, shaded and sunlit soil. The pure reflectance and the fractions of the different components were used to estimate fIPAR. The component analysis methodology yielded an error below 0.08 for comparisons with field fIPAR measurements. Other methodology using aggregated pixel information based on obtaining relationships between vegetation indices and fIPAR was also evaluated. The aggregated pixel does not allow having detail information of soil spectral properties, thus a soil of medium reflectance was used in this case. The potential utility of these indices to estimate fIPAR has been shown in previous chapter and also tested here for vineyards. These relationships are highly influenced by variables,

such as solar angles or background, therefore these indices need to be parameterized using radiative transfer modelling. The aggregated pixel analysis using NDVI-fIPAR relationships yielded RMSE of 0.12 for the estimation of fIPAR. It is concluded that high spatial resolution yielded better results. The medium resolution imagery, unable to get detailed information of the soil variability within the study area, leaded into difference of RMSE=0.14 between both methodologies for one of the study areas selected. Future studies will be focused on obtaining daily fIPAR maps at larger scales.

Acknowledgements

Financial support from the Spanish Ministry of Science and Innovation (MCINN) for the AGL2009-13105, CONSOLIDER CSD2006-67, and AGL2003-01468 projects is gratefully acknowledged, as well as the Junta de Andalucía-Excelencia AGR-595 project co-funded by FEDER (Fondo Europeo de Desarrollo Regional). M.L. Guillén-Climet was supported by a JAE-predoc grant from CSIC, co-funded by the European Social Fund. Gratefully acknowledged are A. Kuusk and J. Praks for sharing the rowMCRM code, P.R.J. North for the FLIGHT code. P. Martin, M.R. Gonzalez, M. Medina, A. Vera, A. Hornero, R. Romero, D. Notario and I. Moorthy are also acknowledged for their scientific and technical support in field and airborne campaigns.

References

Acevedo-Opazo, C., Tisseyre, B., Guillaume, S. & Ojeda, H., (2008). The potential of high spatial resolution information to define within-vineyard zones related to vine water status. Precision Agriculture, 9, 285-302.

Asrar, G., Myneni, R.B. & Choudbhury, B.J., (1992). Spatial Heterogeneity in Vegetation Canopies and Remote Sensing of Absorbed Photosynthetically Active Radiation: A Modelling Study. Remote Sensing of Environment, 41, 85-103.

Baeza,P., Sánchez-De-Miguel,P & Lissarrague, J.R., (2010). Radiation Balance in vineyards. Methodologies and Results in Grapevine Research. S. Delrot et al. (eds.),443 pp.

Berni, J.A.J., Zarco-Tejada, P.J., Suarez, L. & Fereres, E. (2009a). Thermal and Narrow-band Multispectral Remote Sensing for Vegetation Monitoring from an Unmanned Aerial Vehicle. IEEE Transactions on Geoscience and Remote Sensing, 47, (3), 722-738.

Berni, J.A.J., Zarco-Tejada, P.J., Sepulcre-Cantó, G., Fereres, E. & Villalobos, F.J. (2009b). Mapping canopy conductance and CWSI in olive orchards using high resolution thermal remote sensing imagery. Remote Sensing of Environment, 113, 2380-2388.

Choudhury, B.J. (1987). Relationships between vegetation indices, radiation absorption, and net photosynthesis evaluated by a sensitivity analysis, Remote Sensing of Environment, 22, 209-233.

Daughtry, C.S.T., Gallo, K.P., & Bauer, M.E. (1983). Spectral estimates of solar radiation by corn canopies, Agronomy Journal, 75, 527-531.

Dokoozlian, N.K. & Kliewer, W.M., (1995). The light environment within grapevine canopies. II. Influence of leaf area desity on fruit zone light environment and some canopy assessment parameters. Amer. J. Enol. Viticult.46, 219-226.

García de Cortázar, I., Brisson, N., & Gaudillere, J.P., (2009). Performance of several models for predicting budburst date of grapevine (*Vitis vinifera* L.). International Journal of Biometeorology 53, 317-326.

Goel, N.S., & Grier, T., (1986). Estimation of canopy parameters for inhomogeneous vegetation canopies from reflectance data I. Two-dimensional ow canopy. International Journal of Remote Sensing, 7, 665-681.

Goel, N. S., & Thompson, R. L. (2000). A snapshot of canopy reflectance models and a universal model for the radiation regime. Remote Sensing Reviews, 18(2), 197−225.

Haboudane, D., Miller, J.R., Pattey, E., Zarco-Tejada, P.J. & Strachan, I., (2004). Hyperspectral vegetation indices and novel algorithms for predicting green LAI of crop canopies: modeling and validation in the context of precision agriculture.Remote Sensing of Environment, 90(3), 337-352

Hall, A., Lamb, D.W., Holzapfel, B., & Louis, J., (2002). Optical remote sensing applications in viticulture - a review, Australian Journal of Grape and Wine Research, 8, 1, 36-47.

Hatfield, J. L., Asrar, G. & Kanemasu, E. T., (1984).Intercepted Photosynthetically Active Radiation Estimated by Spectral Reflectance. Remote Sensing of environment 14,65-75.

Hatfield, J. L., Gitelson, A. A., Schepers, J. S. & Walthall, C. L., (2008). Application of spectral remote sensing for agronomic decisions. Agronomy journal, 100, 3, 117-131.

Houborg, R. & Boegh, E., (2008). Mapping leaf chlorophyll and leaf area index using inverse and forward canopy reflectance modeling and SPOT reflectance data.

Huete, A.R. (1989). Soil influences in remotely sensed vegetation canopy-spectra. Theory-Applications of Optical Remote Sensing (G.Asrar, Ed.), New York, Willey, 107-141

Huemmrich, K.F. & Goward, S.N., (1997). Vegetation canopy PAR Absorptance and NDVI: An Assessment for Ten Species with SAIL model. Remote Sensing of Environment, 61, 254-269.

Jackson, J.E. (1980). Light Interception and Utilization by Orchard Systems. Horticultural Reviews, 2, 208-267.

Jacquemoud, S. & Baret, F., (1990). Prospect: A model of leaf optical properties spectra. Remote Sensing of Environment, 34, 75-91.

Jacquemoud, S., Ustin, S.L., Verdebout, J., Schmuck, G., Andreoli, G. & Hosgood, B., (1996). Estimating leaf biochemistry using the PROSPECT leaf optical properties model. Remote Sens. Environ. 56:194-202.

Koetz, B., Baret, F., Poilvé, H., & Hill, J. (2005). Use of coupled canopy structure dynamic and radiative transfer models to estimate biophysical canopy characteristics. Remote Sensing of Environment, 95(1), 115−124.

Lebon, E., Dumas, V., Pieri, P. & Schultz, H.R. (2003). Modelling the seasonal dynamics of the soil water balance of vineyards. Functional Plant Biology, 30, 6, 699-710.

Louarn, G., Dauzat, J., Lecoeur, J. & Lebon, E. (2008). Interception and distribution in two grapevine cultivars with different architectures: an original approach based on 3D canopy modelling. Australian Journal of Grape and Wine research, 14, 3, 143-152.

López-Lozano, R., Baret, F., García de Cortázar, I., Lebon, E. & Tisseyre, B. (2011). 2D approximation of realistic 3D vineyard row canopy representation for light interception (fIPAR) and light intensity distribution on leaves (LIDL). Eurpean Journal of Agronomy 35, 171-183.

Mabrouk, H., Sinoquet, H., & Carbonneau, A. (1997). Canopy structure and radiation regime in grapevine.II. Modeling radiation interception and distribution inside the canopy. Vitis, 36, 125-32.

Mabrouk, H. & Sinoquet, H. (1998). Indices of light microclimate and canopy structure of grapevines determined by 3D digitizing and image analysis

Mariscal, M.J., Orgaz, F. & Villalobos, F.J. (2000). Modelling and measurement of radiation interception by olive canopies. Agricultural and Forest Meteorology, 100 (183-197).

May, P. & Antcliff, A.J. (1963). The effect of shading on fruitfulness and yield in sultana. J. Hort. Sci., 38, 85-94.

May, P. (1965). Reducing inflorescence formation by shading individual sultanabuds. Australian J. Agr. Res. 17, 79-80.

Moriondo, M., Maselli, F.& Bindi, M. (2007). A simple model of regional wheat yield based on NDVI data. Europ. J. Agronomy, 26, 266–274.

Monteith,J.L., (1973). Principles of environmental Physics. Edward Arnold Ltd., pp242.

North, P.R.J. (1996). Three-Dimensional Forest Light Interaction Model Using a Monte Carlo Method. IEEE Transaction on Geoscience and Remote Sensing, 34, (4), 946-956.

North, P.R.J. (2002). Estimation of aerosol opacity and land surface bidirectional reflectance from ATSR-2 dual-angle imagery: operational method and validation. *Journal of Geophysical Research* 107.

Pérez, M.A. (2002). Densidad de plantación y riego: Aspectos ecofisiológicos, agronómicos y calidad de la uva en cv. Tempranillo (Vitis vinifera L.). Tesis Doctoral, Dpto. producción vegetal: Fitotecnia. Universidad Politécnica de Madrid. 287 p.

Pieri, P. & Gaudillere, J.P., (2003). Sensitivity to training system parameters and soil surface albedo of solar radiation intercepted by vine rows. Vitis, 42, 77-82.

Pieri, P., (2010). Modelling radiative balance in a row-crop canopy: Row–soil surface net radiation partition. Ecological Modelling, 221,791-801.

Poni, S., Lakso, A.N., Intrieri, C., Rebucci, B. & Filippetti, I., (1996). Laser scanning estimation of relative light interception by canopy components in different grapevine training systems. Vitis 35, 177–182.

Riou, C, Valancogne, C. & Pieri, P., (1988). Un modèle simple d'interception du rayonnement solaire par la vigne - vérification expérimentale. (A simple model for interception of solar radiation by a vineyard: comparison with field data). Agronomie, 9, 5, 441-450.

Robinson, T. & Lakso, A., (1991). Bases of Yield and Production Efficiency in Apple Orchard System. Journal American. Society Horticulture. Science, 116(2): p. 188-194.

Rouse J.W., Haas R.H., Schell J.A., Deering D.W. & Harlan J.C. (1974). Monitoring the vernal advancements and retrogradation of natural vegetation in Nasa/Gsfc final report (ed. MD, U.G.) p. 371.

Sinoquet, H. & Bonhomme, R., (1992). Modeling radiative transfer in mixed and row intercropping systems. Agricultural and Forest Meteorology, 62, 219-240.

Smart, R.E., (1973). Sunlight interception by vineyards. Amer. J. ENol. Viticult., 24, 4, 141-147.

Smart, R.E., (1985). Principles of grapevine canopy microclimate manipulation with implications for yield and quality. A review. Am. J. Enol. Vitic, 36, 230-239.

Smart, R.E., (1989). Solar radiation interception as a guide to design of horticultural planting. II Twenty years experience with grapevines. Acta Hort. (ISHS) 240:87-94.

Steven, M.D., Biscoe, P.V. & Jaggard, K.W., (1983). Estimation of sugar beat productivity from reflection in red and near infrared spectral bands. Int. J. Remote Sens., 4, 325-334.

Suárez, L., Zarco-Tejada, P. J., Sepulcre-Cantó, G., Pérez-Priego, O., Miller, J. R., Jiménez-Muñoz, J. C., & Sobrino, J., (2008). Assessing canopy PRI for water stress detection with diurnal airborne imagery. Remote Sensing of Environment, 112, 560-575.

Wang, Y., Buermann, W., Stenbergb, P., Smolander, H., Häme,T., Tian,Y., Hu, J., Knyazikhin, Y. & Myneni, R., (2003). A new parameterization of canopy spectral response to incident solar radiation: case study with hyperspectral data from pine dominant forest. Remote Sensing of Environment, 85, 304-315.

Zarco-Tejada, P.J., Berni, J.A.J., Suárez, L. & Fereres, E., (2008). A new era in remote sensing of crops with unmanned robots. SPIE Newsroon, doi:10.1117/2.1200812.1438.

Zarco-Tejada, P.J., Berni, J.A.J., Suárez, L., Sepulcre-Cantó, G., Morales, F. & Miller, J.R., (2009). Imaging Chlorophyll Fluorescence from an Airborne Narrow-Band Multispectral Camera for Vegetation Stress Detection, *Remote Sensing of Environment*, 113, 1262-1275.

Zarco-Tejada, P. J., González-Dugo, V., & Berni, J. A. J., (2012). Fluorescence, temperature and narrow-band indices acquired from a UAV platform for water stress detection using a micro-hyperspectral imager and a thermal camera. Remote Sensing of Environment, 117, 322-337.

General discussion

The primary objective of this research was to test the accuracy of the fraction of intercepted photosynthetic active radiation (fIPAR) using high-resolution airborne imagery. Radiative transfer models were used in order to study the link between spectral vegetation indices and instantaneous fIPAR at different sun geometries, vegetation fraction cover, backgrounds, row orientation, and the architecture of the canopy such as in the cases of overlapped and isolated crown and hedgerows.

Different studies have already shown that fIPAR is related to spectral vegetation indices. However, studies focused on row-structure orchards were lacking. Among the vegetation indices tested, the Normalized Difference Vegetation Index (NDVI) yielded consistently the best results for the crop canopies studied in this thesis. An important factor was the understanding of the structural and optical parameters that contribute to the measured reflectance by the multispectral airborne camera. The use of radiative transfer models was needed to understand the aggregation of scene components on these complex canopies, such as sunlit and shaded soil and vegetation proportions. The background soil influenced the aggregated NDVI on row-structured canopies, varying almost 0.2 between darker or brighter soil, while fIPAR was only 0.04. Therefore, the NDVI-fIPAR relationships change as a function of the soil optical properties, due to its large effects on NDVI in these complex open crop canopies. This thesis demonstrates using both experimental and model simulation approaches that previous relationships found for herbaceous or forest canopies between vegetation indices and fIPAR are not valid for row structure orchards. The relationships obtained by Myneni & Williams in 1994 for a heterogeneous

canopy simulated as clumps of leaves randomly distributed were used to estimate fIPAR in an olive orchard yielding a large RMSE=0.24. Nevertheless, the errors decreased to less than 0.1 when accounting for the architecture using physical models.

The orchard systems evaluated in this thesis were peach, citrus, olive and vineyards, proposing for each of them a different methodology to account for their architecture. Peach and orange orchards have overlapped crowns within a planting pattern ranging from 5 m x 3 m and 7 m x 3 m. The olive orchard is presented as isolated trees with a planting pattern of 7 m x 6 m, while vineyards form hedgerows (3 m x 1.5 m). Each crop was characterized by study sites used for structural and optical measurements and fIPAR measurements, showing a wide range in vegetation cover fraction and row orientation. The models were validated for each crop under the specific conditions measured for these plots. The 3D radiative transfer forest light interaction model (FLIGHT) simulated adequately canopy reflectance in peach and citrus orchards, yielding RMSE lower than 0.03 and 0.02 respectively for the visible region and 0.05 for the NIR region. This model is a Monte Carlo radiative transfer model able to simulate different kind of architectures, providing good predictions of the diurnal variability of canopy reflectance. This was in agreement with previous studies, such as Suárez et al., (2008), where FLIGHT was used to simulate olive orchards. The FLIGHT model showed its feasibility for modelling this kind of canopies, as well as for vineyards orchards. Adequate simulations of fIPAR were also performed with RMSE 0.06 for peach, 0.08 for citrus and 0.1 for olive and vineyard orchards.

The capability of two discrete row models, rowMCRM and rowSAIL, to simulate vineyard canopy reflectance was also assessed. The simulation of the canopy reflectance with the rowMCRM yielded closer results to FLIGHT as compared to rowSAIL, obtaining a RMSE = 0.07 for the NIR region. This study emphasizes that these models are computationally simpler and less time consuming than other complex models that need larger number of input parameters.

Two models were used to simulate fIPAR in olive orchards, FLIGHT and a specific model to simulate fIPAR in olive canopies (*ORIM*). The *ORIM* model showed to be more robust than FLIGHT when compared against field fIPAR measurements (RMSE = 0.05).

The field work carried out in this thesis was critical for the correct assessment of the models. The high spatial resolution imagery enabled the evaluation of the canopy reflectance and the influence of the pure optical properties of each component of the scene, as well as the validation process of the models.

The estimation of fIPAR in these row-structured orchards required the development of predictive relationships and model inversion techniques from high spatial resolution airborne imagery. The assessment for these type of canopies was conducted on peach and orange orchards, yielding RMSE lower than 0.1. For olive orchards, the predictive relationships using FLIGHT yielded RMSE of 0.1 as well, while using *ORIM* the RMSE was greater (0.05). The study carried out in vineyards considered wider database than previous chapter. In this case, the fIPAR was measured in a diurnal setting at different study plots for different sun angles. Therefore,

methodologies were studied for different sun geometries, using two different approaches. In the first approach, we used high spatial resolution for a component analysis of the image. Subsequently, the estimation of fIPAR with medium spatial resolution was checked using an aggregated pixel of the image of 6 m x 3 m. For the aggregated pixel analysis, NDVI-fIPAR relationships obtained with FLIGHT were used to estimate fIPAR. As conquence, the soil optical properties are known for component analysis methodology while the aggregated pixel study is assumed a mean soil reflectance for all the study areas. The detailed information about soil optical properties clearly improved the estimation of fIPAR. The best results were obtained for component analysis obtaining a RMSE of 0.08.

The development of remote sensing methods for generating maps of the spatial variability of fIPAR has large potential but still faces many challenges that have been studied in this dissertation. In light of the results, it can be concluded that this study demonstrates the possibility of obtaining the variability of fIPAR at field scale in complex open crop canopies, yielding errors lower than 10%.

Conclusions

1. Modelling methods were investigated to obtain relationships between vegetation indices calculated from airborne imagery and instantaneous fIPAR measured in the field on peach, citrus, olive and vineyards crops.

2. The Normalized Difference Vegetation Index (NDVI) yielded consistently the best results among the vegetation indices tested, yielding high significant relationships ($p<0.001$) and coefficients of determination $r^2>0.85$ for estimating fIPAR on the four crops under study.

3. The NDVI index routinely used in estimating fIPAR in homogeneous crops is not applicable to complex canopies: NDVI-fIPAR relationships obtained in previous studies for homogeneous canopies yielded errors in fIPAR of RMSE=0.24, while methodologies proposed in this thesis specific for heterogeneous orchards yielded errors between 0.05 and 0.1.

4. The simulations conducted with different radiative transfer models demonstrated that NDVI is highly influenced by the background soil properties and the row orientation architecture, both as a function of the sun geometry. Differences in fIPAR higher than 0.2 are obtained as consequence of row orientation while the rest of the parameters yield constant.

5. The radiative transfer models used in this thesis showed to be robust to simulate different row structured canopies and the diurnal changes in canopy reflectance. Either the 3D model FLIGHT used to simulate the four different studied crops, as well as the hybrid models rowMCRM and rowSAIL used to simulate vineyards yielded errors below 0.03 for the visible region and below 0.05 for the NIR.

6. The model FLIGHT used to simulate fIPAR showed to be adequate for all the studied crops with RMSE lower than 0.09. For olive canopies the specific model to simulate fIPAR in olives (*ORIM*) showed better results than FLIGHT with RMSE of 0.05.

7. Work conducted to study fIPAR estimation in row structured canopies focused on predictive relationships and numerical model inversion approaches. Estimations of fIPAR were obtained with errors below to 0.10. In some cases, when model inversion techniques were based on canopy reflectance instead of NDVI the results were slightly improved (RMSE of 0.07).

8. The estimations of fIPAR carried out using the airborne imagery and the 3D RT model FLIGHT in peach and citrus orchards yielded RMSE of 0.08 and 0.09 respectively, when predictive-relationships are used. Similar results (RMSE = 0.08) are obtained for both crops with model inversion techniques based on canopy reflectance used for the inversion. The inversion with NDVI yielded RMSE of 0.12 for peach and 0.10 for citrus orchards.

9. The estimations of fIPAR in olives orchards were conducted with models FLIGHT and a coupled FLIGHT+*ORIM* approach. The results improved with the use of the specific model to estimate fIPAR in olive orchards developed by Mariscal et al. (2000), (RMSE = 0.05), as compared to RMSE=0.1 obtained with FLIGHT only.

10. For vineyards, estimations of fIPAR were carried with component analysis of the image using high spatial resolution and with aggregated pixel using NDVI-fIPAR relationships obtained with FLIGHT. Component

analysis methodology yield RMSE=0.08. The detailed information about soil optical properties clearly improved the estimation of fIPAR.

11. This study demonstrates that obtaining maps of the spatial variability of fIPAR in non-homogeneous canopies is feasible when using remote sensing imagery linked to physical models, yielding errors below RMSE=0.10.

Curriculum Vitae of the author

María Luz Guillén Climent was born on the 4th of August 1982 in Huelva, Spain. In 2005, she obtained a MSc degree in Agricultural Enginering at the University of Cordoba. The Master Thesis on "Unmixing based image fusion for land cover mapping over the Netherlands: A case study Landsat TM and MERIS imagery" was performed at Wageningen University (Netherlands) in 2005. She combined her studies with the assistance at Graphic Engineering and Geomatic Department (September 2004-June 2005).

After her degree, she occupied an agricultural engineer postion at Physic Department of University of Corboba (December 2005- June 2006), working as expert in remote sensing for an European project Interreg III Technolangue. In July 2006, she began to work at Institute for Sustainable Agriculture (IAS-CISC), first to research on the spectral vegetation indices to study stresses in vegetation with thermal sensor and spectrometer, as well as to test the efficiency of biomolecules against nutrient and hydric deficits.

In 2007 she started the PhD programme of "Plant Production, Protection and Improvement" at Agronomy Department of University of Cordoba with a fellowship of Spanish Council for Scientific Research (CSIC) funded through the JAEpredoc programme. The educational activities of PhD programme were supplemented by international courses: Advance land training course by European Space Agengy, ESA (Lisbon, Portugal, 2 to 7 September 2007) and participation at workshops framed in *CONSOLIDER-2006 project* (Lérida, 6 March 2008; Murcia, 4 March 2009) and *Reunion*

Hispano Portuguesa de grupos de investigación en riego y relaciones hídricas en cultivos leñosos (Badajoz, 29 November 2010).

During this period she also performed two research stays abroad at: Geographic Department –Swansea University (October-December 2008, Swansea, United Kingdom) with the objective of working with model to simulate row structured canopies; and Department of Environnement Méditerranéen et Modélisation des Agro-Hydrosystemes (EMMAH-INRA) (February-May 2010, Avignon, France), working on fIPAR modelling on vineyards.

Peer reviewed publications in international journals

Guillén-Climent, M.L., Zarco-Tejada, P.J., Villalobos, F.J., Evaluating hybrid and 3D ray tracing canopy models for vineyard canopy reflectance and vegetation index simulation using high-resolution diurnal airborne imagery (in preparation).

Guillén-Climent, M.L., Zarco-Tejada, P.J., Villalobos, F.J. Estimating radiation interception in an olive orchard using physical models and multispectral airborne imagery, Israel Journal of Plant Sciences, Special issue on VIS-NIR Spectroscopy in Plant Sciences (in press).

Guillén-Climent, M.L., Zarco-Tejada, P.J., Berni, J.A.J., North, P.R.J., Villalobos, F.J..Mapping radiation interception in row-structured orchards using 3D simulation and high resolution airborne imagery acquired from an UAV, Precision Agriculture (in press), DOI: 10.1007/s11119-012-9263-8.

Presentations at conferences published in proceedings

Guillén-Climent, M.L., Zarco-Tejada, P.J., Berni, J.A.J., Villalobos, F.J., 2010.Estimation of radiation interception in row-structured vineyard canopies using discrete radiative transfer models (29 August-3 September 2010, Montpellier)

Guillén-Climent, M.L., Zarco-Tejada, P.J., Berni, J.A.J., Villalobos, F.J., 2009. Validación de un modelo 3D para estimación de radiación interceptada

en cubiertas heterogéneas mediante imágenes de alta resolución espacial (23-29 September, Calatayud).

Guillén-Climent, M.L., Zarco-Tejada, P.J., Berni, J.A.J., Villalobos, F.J., 2008. Estimating radiation interception using high resolution multispectral imagery in open tree orchards (15-19 September 2008, Bologna)